THE EFFECT OF VARIOUS CLAY NANOPARTICLES AND THEIR SYNERGY ON THE PROPERTIES OF POLYLACTIC ACID FOR ADVANCED APPLICATIONS

Maleshoane Mohapi

Dissertation submitted in fulfilment of the requirements for the Degree

Master of Health Sciences in Environmental Health

in the

Department of Life Sciences
Faculty of Health and Environmental Sciences

at the

Central University of Technology, Free State

Supervisor: Prof M.J. Mochane
Co-supervisor: Dr T.C Mokhena

BLOEMFONTEIN

January 2023

DECLARATION OF INDEPENDENT WORK

DECLARATION WITH REGARD TO INDEPENDENT WORK

I, **Maleshoane Mohapi**, student number _____ , do hereby declare that this research project submitted to the Central University of Technology, Free State, for the Master of Health Sciences in Environment, is my own independent work; and it complies with the Code of Academic Integrity as well as other relevant policies, procedures, rules and regulations of the Central University of Technology, Free State; and that it has not been submitted before to any institution by myself or by any other person in fulfilment (or partial fulfilment) of the requirements for the attainment of any qualification.

_____

SIGNATURE OF STUDENT

January 2023

DATE

DEDICATIONS

If it was not of He who created the earth and everything on it, I would not be here. Before everything else, I would like to dedicate this hard-earned work to the Lord, for He provided me with the strength, knowledge, courage, and guidance to do what I thought I could not do.

This work is also dedicated to my parents who have been the source of my inspiration, support, and strength. Their moral, emotional, and spiritual support is recognised. The love they have shown and given me cannot be quantified.

To my one and only brother who has always had my back through everything, this is for you.

This work also goes to all those who stood and supported me throughout this journey.

Lastly, I dedicate this to myself, this was not an easy journey, but I never gave up as I pushed and kept my focus intact. I therefore give myself all the flowers.

ACKNOWLEDGEMENTS

Although this has been the hardest huddle in my studying career so far, it had however opened doors and greater opportunities for me. It has been a remarkable privilege to work with, and be around some great researchers who groomed and shaped me into the person I am now in research. The knowledge they watered me with, and support given to me are remarkably good.

I would like to show my unfiltered gratitude to my main supervisor, Professor M.J Mochane who has walked the ground, and walked by my side from the beginning of this project until the end. He has not only been a true mentor, but he has played a role of a father, and a psychologist in my life. The support, knowledge, motivation, and guidance he has provided, and his continuous believe in me kept me going. My appreciation also goes to my co-supervisor Dr. T.C Mokhena for his efforts, time, input, and guidance in my study. In the midst of all challenges, you both never gave up on me when everything seemed to be going dead wrong. You held my hand and walked with me until I could stand on my own. You remained resolute to the idea that hard work breeds success. I thank you for the selfless leadership you have shown and bestowed in me. Words cannot amount to how grateful I am for all you have done. May you both continue to blossom in research, and may God bless you abundantly.

In addition, I would like to give gratitude to National Research Foundation (NRF), and Central University of Technology for their assistance in funding my studies. This project is a success because of the funds you have provided for me. Likewise to CSIR, I say thank you for allowing me to do my experimental work and analysis at you premises.

Moreover, I would like to extent my gratitude to these individuals.

- My Parents (Enet Mookho Mohapi and Maphatlalatse Johannes Mohapi): If life could offer people a chance to choose their parents; I would choose you again and again. You have been my pillar of strength, guardians of truth, and well of wisdom. You opted for education as a game changer in my life, and I thank you from the bottom of my heart.
- My brother (Modise Mohapi): You have played a huge role in my life, and you always believe in me without a doubt. Your support and cheering during this study did not go unnoticed. I appreciate it.

- To my study partner, Andiswa Kaleni: Yoh “Ngwana” this was never easy for both of us, we would always complain and cry, but we kept our heads up high in the midst of the challenges and pressure we had. We would always console each other and make each other feel better, and it really helped a lot because every time after having a conversation with you, I would feel very calm. Thank you for being a shoulder to cry on, and an amazing study partner.
- To Dr. S.I Magagula: Thank you for your contribution in my research journey.
- To my friends of years: In you I have learnt what friendship is, and what friendship means. We had lost time to spend together because you understood the importance of my schoolwork and supported me immeasurably, and selflessly. When people stand for a good cause, no amount of negativity, despair or torture will tear them apart. I will forever treasure the friendship we have.

ABSTRACT

The study investigates the effect of clay(s) on the properties of the poly (lactic acid) (PLA). Nanocomposites having 3% of clays (*viz.* halloysite, montmorillonite (MMT), and kaolin) were fabricated using melt mixing method. Furthermore, zinc borate was added into the PLA/Clay(s) nanocomposites with the aim of enhancing the properties of nanocomposites. Techniques such as the transmission electron microscopy (TEM), X-ray diffractogram (XRD), thermogravimetric analysis (TGA), rheology, and UL-94 were adopted. TEM was used to investigate the dispersion of the clays within the PLA polymer matrix. The incorporation of the MMT into PLA resulted into an intercalation and exfoliation of the nanoclay within the polymer matrix when compared with kaolin and halloysite clays. As the ZnB was not modified, its nanoparticles were found to be agglomerated into the PLA matrix. Furthermore, the synergy of the other clays with MMT seems to have formed intercalation and exfoliation, which seems to verify that MMT acted as a modifier for other clays within the PLA matrix. It was further observed that the presence of ZnB and clays such as halloysite, and kaolin clays resulted in immiscibility between the nanoparticles and the PLA matrix. According to the XRD, the incorporation of the MMT in the PLA systems acted as a steric hindrance; and as a result, crystallization was restricted, thus causing a reduction in the intact crystalline region. Thermal stability of the tubular halloysite clay-based nanocomposite was found to be higher when compared with the silicate clay-based nanocomposites (*viz.* MMT and kaolin). One can realize that the synergistic effects of the nanoclays showed better thermal stability than all the single clays reinforced PLA matrix. Additionally, the majority of the synergistic nanoparticles were found to have a high thermal stability when compared with single filler-based nanoparticles/polymer composites. Halloysite in the PLA/ZnB system improved the complex viscosity of the system more than all the clays systems and PLA due to a stable and tubular structure of the halloysite. Halloysite, and its synergy with the other clays seemed to dominate in terms of improving the flammability resistance of the PLA matrix with V-0 UL-94 rating. The pollutant removal efficacy was found to be depended on the filler-type. Fillers with stronger interaction with PLA resulted in poor adsorption properties due to limited accessibility to the available active sites.

Keywords: Flame resistance; wastewater treatment; nanocomposites; clay nanoparticles; synergy; zinc borate

RESEARCH OUTPUTS

Published journal articles: Review

1. Mohapi, M., Sefadi, J. S., Mochane, M. J., Magagula, S. I., & Lebelo, K. (2020). Effect of LDHs and Other Clays on Polymer Composite in Adsorptive Removal of Contaminants: A Review. *Crystals*, 10(11), 957.
   DOI:10.3390/cryst10110957

Published book chapters

1. Magagula, S., Mohapi, M., Jafta, N., Mochane, M., Lebelo, K., Setlhare, G.L.N. (2022). Biopolymer-based biodegradable biomaterials for in vivo and in vitro biomedical applications. In: *Polymeric Biomaterials for Healthcare Applications* (pp.165-210) Publisher: ELSEVIER
   DOI: 10.1016/B978-0-323-85233-3.00005-7.
2. Magagula, S., Mohapi, M., Sefadi, J., Mochane, M. (2021). The Production and Applications of Microbial-Derived Polyhydroxybutyrates. In: *Microbial Polymers* (pp.3-43) Publisher: Springer, Singapore
   DOI: 10.1007/978-981-16-0045-6_1.

TABLE OF CONTENTS

LIST OF SYMBOLS AND ABBREVIATIONS

APS	Ammonium perfulfate
ABS	Acrylomitile butadiene styrene
AMLR	Average mass loss rate
BDMHDA	Benzyldimethyl-hexadecylammonium
B34	Bentonite
CED	Cohesive energy density
CS	Chitosan
CEC	Cation exchange capacity
CAPB	Cocamisopropyl betaine
DMHDIM-MMT	Dimethyl-hexadexyl-imidazolium-modified montmorrilonite
E.coli	*Escherichia Coli*
FSM	Fluorinated synthetic mica
FTIR	Fourier transform infrared
hACE2	Human angiotensin-converting enzyme 2
HCL	Hydrogen Chloride
HDTMA	Hexadecyltrimethylammonium bromide
HRR	Heat release rate
HDPE	High density polyethylene
UL-94HB	Horizontal burning test
IFR	Inherent flame retardant
TTI	Time to ignition

Kaol	Kaolinite
LLDPE	Linear low-density polyethylene
LOI	Loss on ignition
MMT	Montmorrilonite
MB	Methylene blue
MnO-Kaol	Modified kaolinite
MLR	Mass loss rate
MA	Maleic anhydride
NC	Natural clay
PVC	Polyvinyl chloride
PHRR	Peak heat release rate
POU	Point of use
PVA	Polyvinyl alcohol
PPA	Polyphosphoric acid
PMMT	Polyphosphoric montmorillonite
PE	Polyethylene
PEO	Poly(ethylene oxide)
PP-g-MA	Polypropylene-graft-maleic anhydride
PLLA	Poly(L-lactic acid)
PDLA	Poly(D-lactic acid)
PDLLA	Poly(D,L-lactic acid)
PLA	Polylactic acid
PBS	Polybutylene Succinate

PHBV	Poly(hydroxyl butyrate-co-hydroxyvalerate)
PGA	Polyglycolic acid
RB	Rhodamine B
ROP	Ring-opening polymerization
SAXS	Small-angle X-ray scattering
SDS	Sodium dodecyl sulfate
SF	Silk fibroin
NaFSM	Sodium Fluorinated synthetic mica
NaMMT	Sodium montmorillonite
C-Si02-OMT	Silica pillared montmorillonite
SEA	Specific extinction area
SPR	Smoke production rate
SEM	Scanning electron microscopy
TGA	Thermogravimetric analysis
THR	Total heat release
TPU	Thermoplastic polyurethane
TEM	Transmission electron microscopy
VPMMA	Virgin poly(methyl methacrylate)
WAXS	Wide angle X-ray scattering
WF	Wood flour
XRD	X-ray diffraction
ZnB	Zinc Borate
ZnONPs	Zinc oxide nanocomposites

LIST OF TABLES

LIST OF FIGURES

CHAPTER 1: General Introduction

1.1 Background introduction

Nanocomposites based on polymer, and inorganic fillers are the new class of nanocomposties, whereby the inorganic filler(s) is(are) dispersed inside the polymer matrix. Various inorganic fillers such as graphene, clays, and carbon nanotubes have been incorporated into polymer matrices to form polymer/inorganic nanocomposites. Polymer/inorganic filler(s) nanocomposites have been the composites of interest due to their lower weight, and lower inorganic filler(s) content within the composites, which make them to be of interest to the industry. Based on their low cost, readily availability, and harmlessness to the environment; inorganic fillers have been incorporated into polymer matrices to form polymer/inorganic nanocomposites for various applications including: (i) Automotive industry, (ii) Water purification, (iii) Building applications, (iv) Flammability resistance, and (iv) Biomedical applications **(Figure 1.1)**.

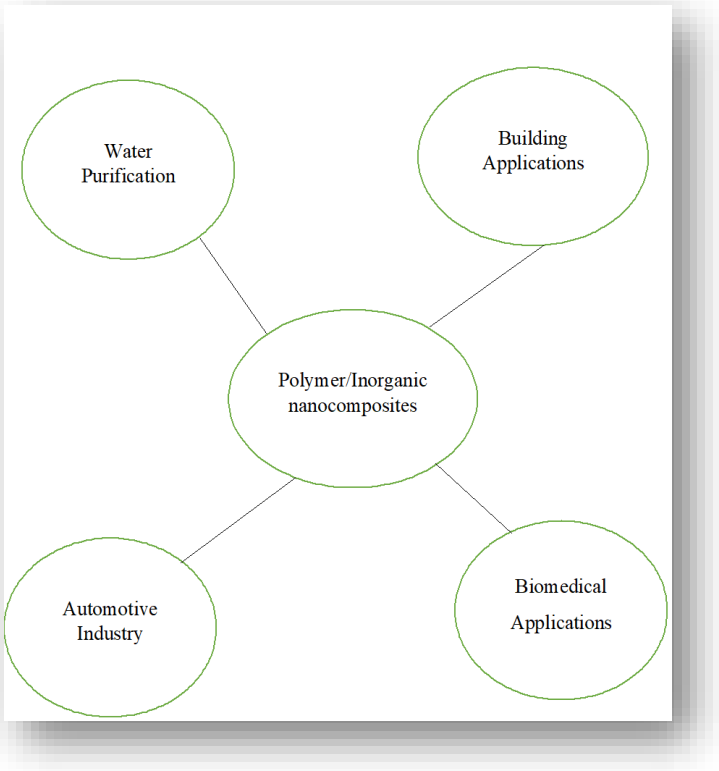

Figure 1.1 Illustration of the polymer/inorganic filler(s) nanocomposites applications

The dispersed inorganic filler(s) in a polymer matrix is(are) expected to enhance the mechanical strength, flame resistance, water treatment, and gas permeability modification. Different polymer matrices have been utilized for the fabrication of polymer/inorganic fillers nanocomposites such as polypropylene (PP) [**1, 2**], low density polyethylene (LDPE) **[3]**, linear low-density polyethylene (LLDPE) **[4,5]**, polylactic acid (PLA) **[6, 7, 8]**, polybutylene succinate (PBS) **[9]**, and poly(hydroxybutyrate-co-hydroxyvalerate)(PHBV) [**10, 11**]. Due to the growing environmental problems regarding an increase in plastic footprint, biopolymers are seen as alternative plastics to replace the non-biodegradable plastics. As a result, various authors have produced different biopolymer/inorganic fillers bionanocomposites for advanced applications. Bionanocomposites are a topic of interest to scientist as they act as an interface amongst various field such as science, nanotechnology, and biology **[12]**. The well-known bionanocomposites emanate from biopolymers such polysaccharides, polypeptides, proteins, and polynuclei [**13**]. The well-known inorganic fillers utilized for fabrication of bionanocomposites include clay minerals, graphite, hydroxyapatite, and metal nanoparticles **[14, 15, 16, 17]**. The term, nanocomposites is referred to in this chapter in various ways such as bioplastics, biocomposites, biohybrids, and/or green composites [**18**]. Amongst the above-mentioned inorganic fillers, clay-based fillers have been incorporated into various biopolymers such as PLA, PHBV, polysaccharides, polyglycolic acid (PGA), and PBS **[19]**. Clay nanofillers became the inorganic filler of choice because it is able to enhance various properties of the biopolymers such as gas barrier, flammability, and mechanical properties of polymers at lower content **[20]**. The clay nanofillers have been utilized in applications such as electronic packaging, electronics, chemical resistance, medical applications, aerospace structures, construction, and coatings **[21]**. Table 1.1 provides an in-depth summary of the clay, and clay-polymer based nanocomposites. Based on Table 1.1, it became clear that the most dominating application of clay involves flame resistance, water purification, and food packaging. Clay materials have been broadly considered as a materials of choice for wastewater treatment since 1960s [**22-24**]. This is because clay shows appealing properties such as high adsorption capacity, high surface area, unique chemical composition with microporous layered structure, and small (nanoscale) sizes. Moreover, clay materials are comprised of hydrous silicates having sharp and fine particles formed in a sheet-like structure [**22**]. They are recognized as the perfect base materials of organic-inorganic composites. Similar to other nanoparticles, the clay particles have few limitations in wastewater treatment such as reuse, recovery, and long-term effect

on health, and environment. In order to address these limitations, clay minerals are usually blended with polymeric materials, which results in polymer/clay nanocomposites. Moreover, the polymeric materials bring additional functional moieties for enhanced adsorption capacity.

Table 1.1: Applications of Clay Nanocomposites

Application	Clay type	Technique/Mechanism	Results	References
Pseudo-antibodies for Covid-19	Na-montmorillonite and palygorskite	Direct binding Sorption simulation (Monte Carlo method)	The interaction of SARS-CoV-2 spike S with clay crystallites resulted in the creation of closely interacting strong van der Waals attraction fields, according to the results of molecular-level simulations. The clay/SARS-CoV-2 configuration had a greater cohesive energy density (CED) due to this van der Waals attraction fields. The presence of clay crystallites was further evidence of SARS-strong CoV-2's affinity for these particles, as compared to the former's affinity for human angiotensin-converting enzyme 2 (hACE2).	[**25**]
Food Packaging	Montmorillonite	Melt compounding	The findings revealed that PP/clay nanocomposites had higher mechanical strengths than pure PP, including greater tensile, flexural, and Izod impact strength. According to the thermal properties, the melting and degradation temperatures rose with the clay concentration. Clay increased	[**26**]

			the gas molecules' movement distance, lowering the permeability of neat PP from 26% to 55%.	
Food Packaging	Halloysite	Twin screw extrusion	Nanocomposites slowed down the ripening process of bananas, firmness of tomatoes, weight loss of strawberries, and aerobic bacterial growth on chickens due to their ethylene scavenging properties, water vapour, and oxygen properties. Incorporation of halloysite boosted these properties. The use of Halloysite nanotubes as natural, nontoxic, and cost-effective nanofillers has therefore been shown to result in potentially multifunctional active food packaging materials with significant food safety benefits.	[**27**]
Water purification	Montmorillonite	Solution mixing	The adsorption capacity of Montmorillonite for the removal of Ag(I) and Cu (II) in an aqueous solution was higher than the other	[**28**]

			adsorbents (such as Activated carbon, red mud etc.)	
Water purification	Montmorillonite (MMT) and Modified MMT (MMT-Na, MMT-K and MMT-Ca)	Solution mixing	MMT-K had the best Hg (II) removal in aqueous medium, followed by MMT-Na and MMT-Ca, implying that monovalent cations are more ideal for obtaining a homoionic mineral phase capable of removing Hg (II) from aqueous medium with superior performance.	[**29**]
Growth performance, internal organs, and blood biochemistry	Nanoclay mineral	Aqueous nanosuspension mixing with feed	The concentrations of clay minerals (1%,1.5% and 2%) all showed enhancement of boiler growing performance, internal organs, and blood biomedical measurements compared to other treatments (such as vaccines and antibodies.	[**30**]
Additives for filtration properties	Bentonite	Solution blending	In terms of filtration control, nano-clay outperformed traditional additives (such as nano titanium, nano copper oxide, nano	[**31**]

alumina) by roughly 5% at a concentration of 6%.

Besides the water purification applications of clay with biopolymers, clay nanoparticles have been utilized as flame retardant fillers for the majority of the biopolymers for advanced applications [**32**]. For an example, Cheng *et al* [**33**] reported the flammability of polylactide with aluminum trihydrate and organoclay. The addition of the Cloisite 30B was found to decrease the heat release rate (HRR) peak, which showed an enhancement in flame resistance of the system. Mokhena and colleagues [**34**] observed that the presence of graphite enhanced the flame retardancy of the PBS matrix, with the flame resistance improving more with the incorporation of both clay and graphite within the PBS matrix. Amongst the fabricated clay/biopolymer bionanocomposites, the PLA polymer is found to be the most attractive biopolymer for fabrication of bionanocomposites since PLA is from the renewable agricultural sources, and can retain its transparency after fabrication. As much as PLA is the polymer of choice in terms of advantages, there are some limitations in relation to poor toughness, highly flammability, low drawability, and limited gas barrier properties. The incorporation of clay nanoplatelets into the PLA matrix have shown to enhance the properties of the PLA matrix. It has however been reported that the synergy of clay and other fillers enhances the flammability resistance of the polymer matrices better than clay alone. In this study, the effect of Zinc borate (ZnB) and clay synergy on the properties of the PLA are reported. The reason ZnB was chosen as a flame-retardant choice to form a synergy with clay is because ZnB has low toxicity, and it also stabilizes up to temperature greater than 290 °C as well as being an excellent smoke suppressant filler [**35, 36**]. The current study reports on the effect of three types of clays i.e., Halloysite, Montmorillonite (MMT), kaolin, and their synergy with Zinc borate on the properties of PLA. Furthermore, the synergy amongst the three types of clays is also reported.

1.2 Research aims

The aim of the study is to investigate the effect of clays (*viz* montmorillonite, halloysite and kaolin), and their synergy on the properties of polylactic acid (PLA). Furthermore, zinc borate was added into the PLA/clay systems in order to analyze the effect of Zinc borate on the flammability properties of the PLA/clays nanocomposites.

1.3 Research objectives

The objectives of this study are presented below.

(i) To study the effect of clay(s) on the flammability properties of PLA

(ii) To investigate the synergy of clays and zinc borate on the flammability properties of PLA

(iii) To investigate the synergy of clays and zinc borate on the thermal stability of PLA

(iv) To investigate the synergy of clays and zinc borate on the crystallinity of PLA

(v) Select clay mineral that will be used as an effective adsorbent

1.4 Thesis organization

The layout of this thesis is as follows:

Chapter 1: Introduction

Chapter 2: Literature Review

Chapter 3: Published review paper - Effect of LDHs and other clays on polymer composite in adsorptive removal of contaminants.

Chapter 4: Materials and methods

Chapter 5: Results and discussion

Chapter 6: Conclusion and future remarks

1.5 References

1. Sharma, S.K., Nayak, S.K. (**2009)**. Surface modified clay/polypropylene (PP) nanocomposites: Effect on physico-mechanical, thermal and morphological properties. *Polymer Degradation and Stability*, 94(1), 132–138.
2. Ma, J., Qi, Z., Hu, Y. (**2001)**. Synthesis and characterization of polypropylene/clay nanocomposites. *Journal of Applied Polymer Science*, 82(14), 3611–3617.
3. Wu, H; Lu, C; Zhang, W; Zhang, X. (**2013)**. Preparation of low-density polyethylene/low-temperature expandable graphite composites with high thermal conductivity by an in situ expansion melt blending process. *Materials & Design*, 52, 621–629.
4. Na, Y., Dai, S., Chen, C. (**2018)**. Direct Synthesis of Polar-Functionalized Linear Low-Density Polyethylene (LLDPE) and Low-Density Polyethylene (LDPE). *Macromolecules*, 51(11), 4040-4048
5. Durmuş, A., Woo, M., Kaşgöz, A., Macosko, C.W., Tsapatsis, M. **(2007)**. Intercalated linear low-density polyethylene (LLDPE)/clay nanocomposites prepared with oxidized polyethylene as a new type compatibilizer: Structural, mechanical and barrier properties. *European Polymer Journal***,** 43(9), 3737–3749.
6. Zhou, Y., Lei, L., Yang, B., Li, J., Ren, J. **(2018)**. Preparation and characterization of polylactic acid (PLA) carbon nanotube nanocomposites. *Polymer Testing*, 68, 34-38.
7. Ilyas, R.A., Sapuan, S.M., Harussani, M.M., Hakimi, M. Y. A. Y., Haziq, M.Z.M., Atikah, M.S.N., Asyraf, M.R.M., Ishak, M.R., Razman, M.R., Nurazzi, N.M., Norrrahim, M.N.F., Abral, H., Asrofi, M. **(2021)**. Polylactic Acid (PLA) Biocomposite: Processing, Additive Manufacturing and Advanced Applications. *Polymers*, 13(8), 1326(1-34).
8. Liao, F., Ju, Y., Dai, X., Cao, Y., Li, J., Wang, X. **(2015)**. A novel efficient polymeric flame retardant for poly (lactic acid) (PLA): Synthesis and its effects on flame retardancy and crystallization of PLA. *Polymer Degradation and Stability*, 120, 251–261.
9. Xu, Y., Xu, J., Liu, D., Guo, B., Xie, X. **(2008)**. Synthesis and characterization of biodegradable poly(butylene succinate-co-propylene succinate)s. 109(3), 1881–1889.
10. Luo, S., Netravali, A.N. **(2003)**. A study of physical and mechanical properties of poly(hydroxybutyrate-co-hydroxyvalerate) during composting. *Polymer degradation and stability*, 80(1), 59–66.
11. Tebaldi, M.L., Maia, A-L-C., Poletto, F., Andrade, F., Soares, D.C.F. **(2019)**. Poly(-3-hydroxybutyrate-co-3-hydroxyvalerate) (PHBV): Current advances in synthesis

methodologies, antitumor applications and biocompatibility. *Journal of Drug Delivery Science and Technology*, 51, 115-126.

12. Tiwari, A. **(2011)**. *Recent Developments in Bio-Nanocomposites for Biomedical Applications.* Nova Science Publishers, Inc., New York, USA, ISBN 978-1-61761-008-0.
13. Nitta, S.K., Numata, K. **(2013)**. Biopolymer-Based Nanoparticles for Drug/Gene Delivery and Tissue Engineering. *International Journal of Molecular Sciences*, 14(1), 1629–1654.
14. Basavegowda, N., Baek, K.-H. **(2021)**. Advances in Functional Biopolymer-Based Nanocomposites for Active Food Packaging Applications. *Polymers*, 13, 4198(1-23).
15. Olivera, N., Rouf, T.B., Bonilla, J.C., Carriazo, J.G., Dianda, N., Kokini, J.L. **(2019)**. Effect of LAPONITE® addition on the mechanical, barrier and surface properties of novel biodegradable kafirin nanocomposite films. *J. Food Eng*. 245, 24–32.
16. Albdiry, M.T., Yousif, B.F. **(2019)**. Toughening of brittle polyester with functionalized halloysite nanocomposites. Compos. *Part B Eng*., 160, 94–109.
17. Lin, Y., Hu, S., Wu, G. **(2019)**. Structure, dynamics, and mechanical properties of polyimide-grafted silica nanocomposites. *J. Phys. Chem. C.*, 123, 6616–6626.
18. Saini, R.K., Bajpai, A.K., Jain, E. **(2017)**. Fundamentals of bionanocomposites.
19. Ruamcharoen, J., Ratana, T., Ruamcharoen, P. **(2014)**. Bentonite as a reinforcing and compatibilizing filler for natural rubber and polystyrene blends in latex stage. *Polymer Engineering & Science*, 54(6), 1436–1443.
20. Bumbudsanpharoke, N., Ko, S. **(2019)**. Nanoclays in Food and Beverage Packaging. Journal of Nanomaterials, 1-13.
21. Harraz, H. **(2016)**. Nano clay and it's applications. Appl. Mineral, 1-56.
22. Awasthi, A.; Jadhao, P.; Kumari, K. **(2019)**. Nano-adsorbent: structure, applications and mechanism for water treatment. *SN Applied Sciences*. 1, 1076,
23. Grim, R.E. **(1962).** Applied Clay Mineralogy. McGraw-Hill, New York, 136, 870-871.
24. Churcman, G.J.; Gates, W.P.; Theng B.K.G.; Yuan, G. **(2006)**. Clay and clay minerals for pollution control. *Developments in Clay Science*. 1, 587-644.
25. Abduljauwad, S.N., Taimur Habib, T., Ahmed, H-u-R. **(2020)**. Nano-clays as Potential Pseudo-antibodies for COVID-19. *Nanoscale Research Letters*, 15, 173(1-12).
26. Choi, R-N., Cheigh, C-I., Lee, S-Y., Chung, M-S. **(2011)**. Preparation and Properties of Polypropylene/Clay Nanocomposites for Food Packaging. *Journal of Food Science*, 76(8), 62-67.
27. Tas, C.E., Hendessi, S., Baysal, M., Unal, S., Cebeci, F.C., Menceloglu, Y.Z., Unal, H. **(2017)**. Halloysite Nanotubes/Polyethylene Nanocomposites for Active Food Packaging

Materials with Ethylene Scavenging and Gas Barrier Properties. *Food Bioprocess Technology*, *10(4), 789-798.*

28. Alandis, N.M., Mekhamer, W., Aldayel, O., Hefne, J.A.A., Alam, M. **(2019)**. Adsorptive Applications of Montmorillonite Clay for the Removal of Ag(I) and Cu(II) from Aqueous Medium. *Journal of Chemistry*,2019, 1-7.
29. Santos, V.C.G.D., Grassi, M.T., Abate, G. **(2015)**. Sorption of Hg(II) by modified K10 montmorillonite: Influence of pH, ionic strength and the treatment with different cations. *Geoderma*, 237–238, 129–136.
30. Al-Beitawia, N.A., Shakerc, M.M., El-Shuraydehb, K.N., Bláha, J. **(2017)**. Effect of nanoclay minerals on growth performance, internal organs and blood biochemistry of broiler chickens compared to vaccines and antibiotics. *Journal of applied animal research*, 45, 1, 543–549.
31. Shakib, J.T. **(2015)**. Nano-clays as additives for controlling filtration properties of water–bentonite suspensions. *J. Petrol. Sci. Eng*.138, 257-264.
32. Abulyazied, D.E., Ene, A. **(2021)**. An Investigative Study on the Progress of Nanoclay-Reinforced Polymers: Preparation, Properties, and Applications: A Review. *Polymers*. 13(24), 4401(1-20).
33. Cheng, K-C., Yu, C-B., Guo, W., Wang, S-F; Chuang, T-H., Lin, Y-H. **(2012)**. Thermal properties and flammability of polylactide nanocomposites with aluminum trihydrate and organoclay. 87(2), 1119–1123.
34. Mokhena, T. C., Sadiku, E. R., Ray, S. S., Mochane, M. J., Motaung, T. E. **(2021)**. The effect of expanded graphite/clay nanoparticles on thermal, rheological, and fire-retardant properties of poly(butylene succinate). *Polymer Composites*, 42(12), 6370-6382.
35. Mustafa, E.Ü., Elif Kaynak, E. **(2019)**. Effect of Zinc Borate on Flammability of PET Woven Fabrics. *Advances in Polymer Technology*, 2019(22), 1–13.
36. Li, J., Ou, Y. **(2019)**. "5. Flame retardation mechanism of other flame retardants". *Theory of Flame Retardation of Polymeric Materials*. Berlin, Boston: De Gruyter, 131-156.

CHAPTER 2: Literature review

2.1 Clay minerals

2.1.1 Sources, types, and their properties

Clay minerals are silicate or phyllosilicate elements consisting of hydrated aluminum silicates with less than 2 microns, and they can be used as natural nanomaterials or as nano sorbents since the launch of nanotechnology [1]. Clay minerals are found in a limited range of geological conditions such as land horizons, continental, marine sediments, geothermal fields, volcanic deposits, and weathered rock formations. The production of clays and clay-based minerals varies depending on the environment. Notably, weathering of rocks and soil is the main source of clays and clay minerals from the Earth's surface today [2]. Clays and clay-derived minerals can be formed by the weather conditions of the pre-existing minerals in the environment. For an example, rock weathering on hills, seabed, or lakebed sediments, deeply buried sediments containing pore water, and rocks in contact with water heated by magma (molten rock) are all sources of pure clay such as bentonite and montmorillonite [2]. The small particle size and unique crystal structure of the clay material give it unique properties, which are beneficial for fabrication of the clay nanocomposites. The properties of clay include cation exchange capacity, wet plasticity, catalytic capacity, swelling, and low permeability [2]. Based on chemical composition and granular morphology, clay minerals are classified into several classes such as kaolinite, halloysite, smectite, illite, and chlorite. The chemical composition of kaolinite is theoretically 39.8% alumina, 46.3% silica, and 13.9% water. Kaolinite is almost white in appearance, soft, with a hardness scale of about 1.5 Mohs [3]. Halloysite, on the other hand, is a two-layered aluminosilicate with a hollow tube structure that occurs naturally. Its exterior diameter ranges from 50 to 70 nm, with a lumen diameter of 10 to 20 nm, depending on the deposit [4]. The smectite class refers to a category of aluminum silicates containing magnesium, sodium, iron, calcium, and lithium. Smectite minerals are dominant in bentonite rocks. The clay mineral smectite has three layers, which includes two tetrahedral sheets of silica that are connected to an octahedral sheet. In description, smectites are often very thin flakes with very small particle sizes, giving them a large surface area. Smectites come in a variety of colours, including white, tan, brown, brownish green, and blue-green [3]. Moreover, chlorite is a form of clay mineral with high iron and magnesium content [5, 6]. Chlorite

clay minerals are well-known in low-temperature prograde metamorphic rocks, retrograde alteration products of ferroan metamorphic minerals, low-temperature biotite alteration products in acid igneous rocks, and hydrothermal alteration products [5, 7]. The other class of the clay-based materials is the illite clays, which include phengite, brammalite, hydrous micas, glauconite, and celadonite. This type of clays are created in temperate regions through weathering of feldspar and mica. Illite clays are the most frequent found clay mineral in marine shales [8]. These classes of nanoclays have been studied, and developed for various applications [9, 10, 11], and they are easily accessible, very inexpensive, and have a low environmental impact. The structure of clay consists of silicate nanoparticles with layered structural units that can lead to the formation of complex/multibranched clay crystals by superposition of these layers [12]. The basic building blocks of clay minerals are tetrahedral silicates, and octahedral hydroxide plates [13]. Octagonal plates are made of aluminum or magnesium in a six-fold combination with the oxygen of a tetrahedron and with hydroxyl. The tetrahedral plates are made up of silicon-oxygen tetrahedral simultaneously with neighbouring tetrahedral that share three angles, while the fourth corner of each tetrahedron is connected to an adjacent octagon through the covalent bond (see Figure 2.1). Figure 2.1 shows the three main types of phyllosilicate, and distinguished by the common 1:1 (TO) layer type, the 2:1 (TOT) layer type, and the 2:1:1 (TOT:O) layer type in the nanoclay material. In a 1:1 (TO) lattice structure, each tetrahedron is connected to an octagon, while in a 2:1 (TOT) lattice structure, each octagon is connected to two tetrahedral plates, and each side is with one sheet. Finally, in the 2:1:1 lattice structure (T-O-T: O), each octahedral plate is adjacent to another octahedron, and it is connected to two tetrahedral plates [10, 14-16]. Table 2.1 shows a detailed summary on the types of clay, and their characteristics. The physicochemical properties of clays, which includes charge surface area, swelling capacity, ion exchange, and density, make the materials convenient for inexpensive remediation of contaminated soils, and aqueous systems.

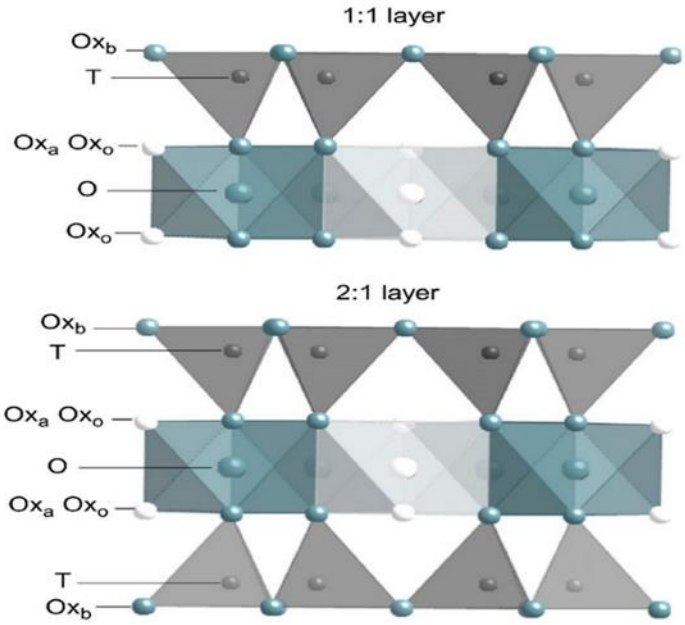

Figure 2.1 Models of 1:1 and in 2:1 layer structures. Oxb, basal oxygen atoms; T, tetrahedral cations; O, octahedral cations; Oxa, apical oxygen atoms; Oxo, octahedral anions (OH, F, Cl) [8].

Table 2.1: Classification of clay minerals and their characteristics

Clay minerals Layer type	Dioctahedral	Trioctahedrals	Characteristics	References.
1:1 (T-O)	**KAOLINITE:** Dickite, kaolinite, nacrite	**SERPENTINE:** Antigorite, amesite, berthierine, cronstedtile, chrysotile, greenalite, lizardite	Non-expansive, no layer charge, and very little isomorphic substitution	[14, 17]
2:1 (T-O-T)	**SMECTITE:** Al: beidellite, Montmorillonite Fe: nontronite **PYROHYLLITE ILLITE, GLAUCONITE**	**SMECTITES:** Mg: hectorite, saponite, stevensite **VERMICULITES**	Highly expansive, low layer charge moderately expansive, intermediate layer charge extensive isomorphic substitution	[15]
2:1 (T-O-T)	**SOFT MICA:** Al: paragonite, muscovite, phengite Fe: celadonite	**MICAS:** Mg-Fe: biotite, phlogopite, lepiodolite. **TALC**	Non-expansive, high layer charge, extensive isomorphic substitution.	[15]

	HARD MICA: Al: clintonite, margarite			
2:1:1 (T-O-T-O)	**CHLORITE** Donbassite	**CHLORITES** Brunsvigite, chamosite, diabantite, penninite	Non-expansive, high layer charge, extensive isomorphic substitution	[10, 16]

2.2 Polylactic acid (PLA) and its properties

Biopolymers are polymeric biomolecules that are generally obtained from living organisms or renewable resources, and in some cases, these polymers may require polymerization, and are therefore considered biodegradable polymers [18]. Generally, biopolymers are decomposable polymers, in a form of waste disposal, CO_2 neutral incineration (with energy recovery), soil decomposition, industrial and household composting, and thermomechanical recycling. The decomposition of biopolymers take place through various organisms (consumption and biodegradation) and anaerobic digestion [19]. Biopolymers can be divided into two types, namely (i) the ones derived from living organisms such as polysaccharides (cellulose, starch), polyesters (PHA) and proteins (soy protein, gelatin, and wheat gluten), and (ii) biopolymers derived from renewable resources but requires polymerization [20]. Polylactic acid is a typical example of the type of biopolymer that is derived from renewable resources; however, it requires polymerization. Biopolymers are currently being used to replace conventional polymeric materials due to their durability, renewability, and most importantly, their environmentally friendly properties. Generally, common biopolymers include poly(α-Hydroxy Esters), poly(p-dioxanone) (PPDO/PDS), poly(Ɛ-caprolactone) (PCL), poly(Trimethylene Carbonate) (PTMC), poly(alkenedicarboxylate), fumarate-based polymers, polyhydroxyalkanoates (PHA), aromatic co-polyesters, polyamides and poly(ester-amide)'s, polyurethanes (PUs), poly (Ortho Esters), polyanhydrides, pseudo poly(Amino Acids), poly(Alkyl Cyanoacrylates), polyphosphazenes, and polyphosphoester. Amongst the above-mentioned biopolymers, PLA has emerged as an alternative biopolymer to replace the traditional petroleum-based plastics in many applications. PLA occupies an important position in the ecological polymers market, and is one of the most promising candidates for future developments [21], and its global production is more than 140,000 tons per year. The production of PLA requires a small amount of energy, thus resulting in reduced greenhouse gas emissions [22]. Poly (lactic acid) or polylactide (PLA) is an industrially obtained biopolymer by polymerization of lactic acid (LA) or ring-opening polymerization of lactic acid (ROP) (ring dimer of lactic acid as an intermediate) [23]. In addition, PLA is not only biocompatible and biodegradable; however, it is also a thermoplastic aliphatic polyester produced from non-renewable natural resources by fermenting polysaccharides. This method allows a complete life cycle to unfold with the biodegradation of the decomposing PLA [23]. PLA is one

of the most frequently used polyesters mainly due to its many favourable properties such as ease of use, relatively good durability, biocompatibility, and biodegradability [19]. Generally, there are two types of enantiomers in PLA, which emanate from the lactic acid (2-hydroxypropionic acid). In this way, the term "polylactic acid" refers to a family of polymers: poly-L-lactic acid (PLLA), poly-D-lactic acid (PDLA), and poly-D,L-lactic acid (PDLLA). In addition, DL-PLA is a syndiotactically alternating D, L-copolymer, or a copolymer having L, and D units. Figure 2.2 below gives more information about D-lactic and L-lactic acids mentioned above.

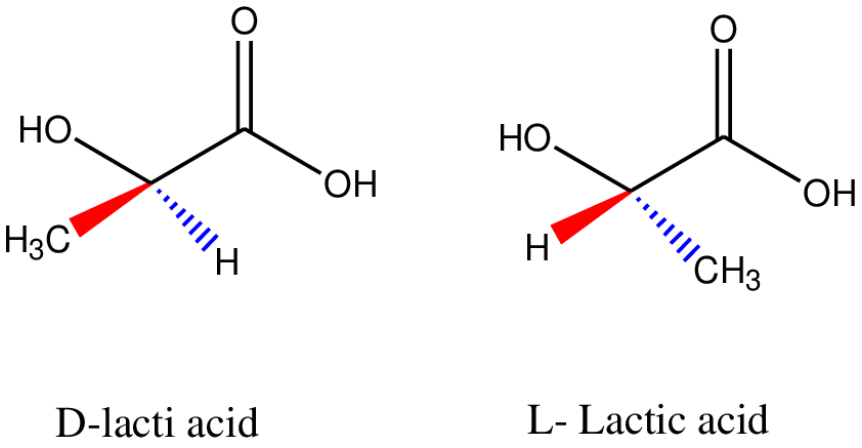

Figure 2.2 Chemical structure of Lactic acid [24]

There are some limitations of PLA, which include brittleness and high cost. There are potential routes to solve these shortcomings, and these include copolymerization, mixing, modifying plasticizing, or additional reinforcing phases (eg, Chitosan (CS), cellulose, and starch) [25]. Table 2.2 shows the advantages and disadvantages of PLA.

Table 2.2: Advantages and disadvantages of PLA

Advantages	Disadvantages	References
The raw material for PLA is derived in nature. In addition, PLA contains ester bonds in its structure and can be easily hydrolyzed. Therefore PLA-based products are completely biodegradable and environmentally friendly.	PLA has low fracture toughness, limiting its widespread application.	[26, 27, 28, 29]
PLA is non-toxic and harmless, so it can be used in food packaging.	It has low heat resistance, and is difficult to apply to heat-resistant products such as home appliances, automobile parts electronic products and food containers.	[26, 27, 28, 29]
Due to its excellent biocompatibility and biodegradability, PLA has been widely used in the medical field for removable surgical attachments, disposable injection devices, and sustained release packages.	Due to the high cost, it is still difficult to widen the applications of PLA.	[26, 27, 28, 29]
Because PLA has excellent tensile strength and elongation at break, it can be highly processed using a variety of common processing methods such as foam molding, injection molding, melt extrusion, vacuum molding and blow film molding, etc.	Even though PLA has good biocompatibility, it does not fully meet all clinical requirements.	[26, 27, 28, 29]
PLA film exhibits excellent oxygen permeability, air permeability, and carbon dioxide permeability. PLA also has excellent antibacterial and mildew.		[26, 27]

PLA is transparent, shiny, and similar to polystyrene film.	[26, 27]

2.3 Preparation and morphology of clay/polymer(s) nanocomposites

Several processing methods including solution blending, melt blending and *in-situ* polymerization method were used for fabrication of polymer-based clay nanocomposites [30, 31] (**See Figure 2.3**). The goal of each preparation method is to achieve a desired uniform dispersion of nanoclays in the pristine polymer matrix. However, there are currently several intriguing perspectives on the applications and use of these techniques. Melt blending is regarded as a significant, industrially viable, and environmentally friendly technique with high economic potential for the preparation of polymer/clay nanocomposites, according to the studies [32, 33, 34]. The *in-situ* polymerization method is a widely used synthesis method because it is an easy method to utilize [35], and it yields a uniform dispersion of the clay filler within a polymer matrix. Both methods necessitate the use of a large amount of organic solvent as well as high viscosity or thermally unstable polymers at high temperatures. When compared to melt blending, the solution-blending technique frequently produces better dispersed clay layers in the polymer matrix [36] due to its low viscosity, and high agitation power. In terms of specific industrial applications, each technique has its own unique significance and limitations.

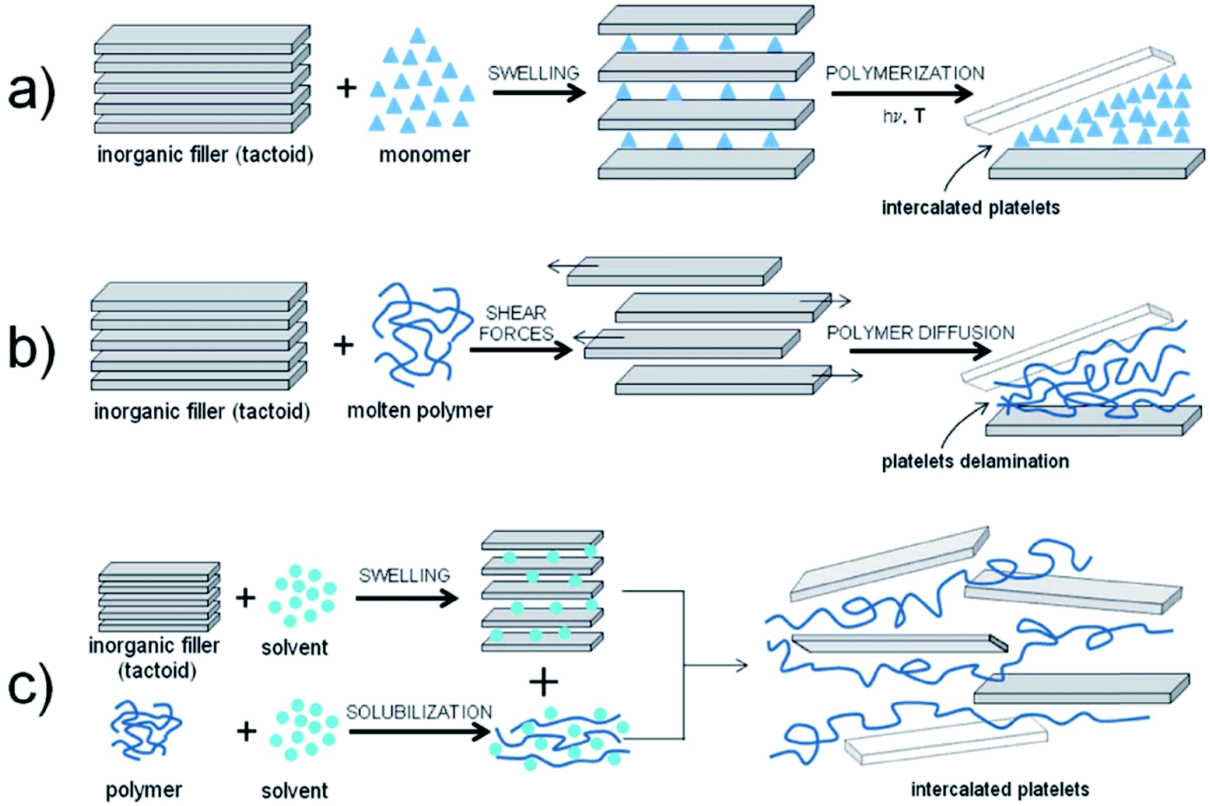

Figure 2.3 Illustration of (a) in-situ polymerization, (b) melt intercalation and (c) solution intercalation [37]

(i) Solution intercalation/mixing

On a laboratory scale, solution intercalation is one of the simple techniques for preparing nanocomposites. Clay platelets are first exfoliated in a solvent that also contains the polymer in this technique. The clay suspension is then mixed with the polymer solution, and the polymer chains intercalate/adsorb on the platelet surface to produce a clay-polymer complex [38, 39]. The last step in the solution mixing method is the evaporation in order to remove the solvent later. The intercalated system retains the nanoscale morphology after the solvent is removed (**Figure 2.3(c)**) [40]. Mansa *et al.* [41] studied the preparation and characterization of novel Clay/PLA nanocomposites using solution mixing. The nanocomposites of mixed morphology were confirmed via the visual observation of dispersion, and intercalation of the clay layers by TEM. Furthermore, three solutions were prepared by dissolving 97mg, 95mg, and 92mg of PLA in 7ml of chloroform. The nanocomposites, montmorillonite SWy-2 (m-SWy-2)/poly(L-Lactide) (PLA), and montmorillonite clay fraction of Braganca material (m-BRN)/poly (L-Lactide) (PLA) contents were prepared respectively. Meanwhile, XRD results of the nanocomposites revealed that the clay was exfoliated within a biopolymer. The fabrication of PLA/clay nanocomposites via a solution intercalation approach was reported by Maharana *et al*. [42], and the nanocomposites showed better mechanical and barrier properties. Krikorian and Pochan [43] reported the effect of different organic modifiers on various clay nanoparticles reinforced polymer nanocomposites. Cloisite-15A, 25A, and 30B at contents of 2, 5, 10, and 15 wt% were modified with dimethyl dihydrogenated tallow quaternary ammonium, dimethyl hydrogenated tallow-2-ethylhexyl ammonium, and methyl tallow-bis-2-hydroxyethyl quaternary ammonium via solvent intercalation, to assess the extent of nanoclay exfoliation in a PLA matrix. Amongst all the investigated clays and organic modifiers, Cloisite 30B with an organic diol in the inter-galleries formed favourable interactions with PLA, and as a result, PLA/Cloisite 30B formed the best nanocomposites.

(ii) Melt intercalation/mixing

Melt intercalation is a commonly utilized method for creating PLA/clay nanocomposites for industrial applications. The method entails mixing organo-modified nanoclay with the polymer and heating the mixture above the melting point of polymer, either under shear or without shear. Polymer chains are forced to diffuse into the clay galleries due to the high temperatures and mechanical forces used, resulting in either intercalated or exfoliated nanostructures depending on the amount of polymer chains that have spread into the silicate layers (**Figure 2b**) [44]. The main advantage of the technique is the specificity for polymer intercalation into clays because there is no solvent in the system to cause competing clay–solvent or polymer–solvent interactions [45]. Most of the PLA/clay nanocomposites that are melt processing normally produce intercalated structures. Paramitha *et al.* [46], demonstrated the preparation of PLA/Clay nanocomposites by melt extrusion technique. Cloisite 15A, and commercial bentonite were employed in that study to design PLA nanocomposites. Nanocomposites were prepared at low clay composition, i.e., 0.5, 1.3, and 5 wt%. XRD spectra revealed a partial exfoliation of nanoclay within polymer. This suggested that the silicate layers were not uniformly dispersed in the nanocomposite. Zaidi *et al.,* [47] investigated the relationship between the structure of polylactide/Cloisite 30B nanocomposites and their rheological, mechanical, and thermal properties. The nanocomposites were prepared by melt intercalation/mixing. The PLA was prepared with 1, 3, and 5 wt% of clay contents. The morphology within PLA matrix indicated a homogenous dispersion of the nanoclays with the PLA matrix as revealed by TEM and WAXS. Zhou *et al.*, [48] then fabricated the PBS/clay nanocomposites via the melt mixing method. The composition of clay incorporated into the PBS matrix was 0.67, 3.4, and 14 vol%. It was observed from the TEM images that the degree of exfoliation reduced with an increase in clay content. The incorporation of 0.67% clays into the matrix dispersed the majority of the clay as individual platelets, and that implies a sign of good exfoliation. Carli *et al.*, [49] reported the effect of clay type on the morphology of PHBV/clay nanocomposites. The two types of clay utilized in their study were montmorillonite and halloysite. The nanocomposites were prepared using a twin screw co-rotating extruder at the temperature range between 150-165 ℃. Interestingly, the authors observed at lower clay content (1wt%), both clays (C-30B), and HNT showed poor dispersion clays with a large agglomeration. There was a more homogenous and a better dispersion of the clay at higher content, i.e., 5 wt%. According to the authors, this behaviour was attributed to a high viscosity and mechanical shear during the mixing process as the clay loading becomes higher.

Elsewhere in the literature [50], PHBV/clay bionanocomposites were fabricated by internal mixer at the temperature of 170 ℃ at 50 rpm for a duration of 10 minutes. The SEM images revealed a homogenous and a well-dispersed vermiculite clay with the PHBV matrix, which may be due to a better interaction between the clay and PHBV. Zaiby *et al.* [51] melt mixed polypropylene with clay in the presence of compatibilizer in the form of polypropylene-graft-maleic anhydride (PP-g-MA) by an internal mixing. Additionally, the XRD diffractograms revealed that the nanocomposite peaks shifted to a lower angle, which confirmed an intercalation of clay layers in the polymer matrix.

(iii) *In-Situ* polymerization

In this method, the polymer and clay are intercalated by selecting appropriate monomers and then polymerizing *in-situ*. Heat or radiation can be used to initiate the polymerization reaction, as can the diffusion of a suitable initiator, or an organic initiator or catalyst fixed inside the interlayer prior to the swelling step. In this case, the monomer is used directly as a solubilizing agent to increase the swelling of the layered silicate. Following the combination of the silicate layers and monomer, subsequent polymerization occurs, thus allowing the formation of polymer chains between the intercalated sheets (**Figure 2.3(a)**) [52]. Sedla'kova' *et al.* [53] demonstrated the preparation of polymer-clay nanocomposites via *in-situ* emulsion polymerization. Notably, chemical modification of sodium montmorillonite (MMT-Na) with a relative coupling agent organically modified clay montmorillonite [2-(acryloyloxy)ethyl]trimethylammonium chloride (MMT-Qs) was employed for the synthesis of hybrids. The researchers used sodium dodecyl sulfate (SDS), and ammonium persulfate (APS) as surfactant and initiator in an *in-situ* seeded emulsion polymerization of hydrophobic vinyl monomers like butyl methacrylate and styrene. Intercalation was observed by TEM, WAXS, and SAXS analyses; which showed that the poly(butyl methacrylate) (PBMA)/montmorillonite [2-(acryloyloxy)ethyl]trimethylammonium chloride (MMT-Qs) nanocomposites exhibited a better dispersion of disordered clay platelets in polymer matrix film than that of hydrophilic MMT-Na for both used clays.

Table 2.3: Comparison between solution mixing and melt blending techniques on Biopolymer/Clay nanocomposite

Polymer	Clay	Processing method	Observed morphology	References
Thermoplastic polyurethane (TPU)	Organoclay (Cloisite 30B)	Melt blending and solution mixing	XRD, SEM, and TEM methods were used to characterize the microstructures of the samples. The amount of organoclay in the composition varied between 2 and 8 Wt%, and 10 Wt% TPU was prepared. The results showed that the organoclay layers in the melt blending sample had better dispersion, exfoliated, and semi-exfoliated structure than the solution mixing counter parts.	[54]
Polyethylene (HDPE)	Organclay (Cloisite 20A)	Melt compounding and solution mixing	XRD, DSC, SEM, and POM were used to investigate the properties of polymer/clay nanocomposites to determine the exfoliation/intercalation of the preparation procedure. Six composite formulations were created using organoclay concentrations of 5, 10, and 15% by weight. As a result, they were labelled HDPE 5, HDPE 10, HDPE 15, HDPE-g-MA 5, HDPE-g-MA 10, and HDPE-g-MA 15. The presence of poorly dispersed, micro-sized, yet intercalated clay particles was discovered in solution-blended composites, whereas nanocomposites prepared in the melt under shear stress had the most extensive dispersion of nanometric clay particles, and the highest levels of exfoliation.	[55]
Acrylonitrile-butadiene	Dimethyl-hexadecyl-imidazolium-	Melt blending and solution sonification	XRD, TEM, mechanical testing, DMA, TGA, and fluorescence spectroscopy (FS) were used to investigate the structural property relationship of the composites. TEM revealed that a mixed	[56]

styrene (ABS) thermoplastic	modified Montmorillonite (DMHDIM-MMT)		intercalated/exfoliated structure was obtained using both the melt blending and solution processes; and FS revealed that the solution sonification sample had more homogeneous dispersion.	
Poly (ethylene oxide) (PEO)	Na-Montmorillonite and organo-modified bentonite (B34)	Solution intercalation and melt intercalation	X-ray diffraction and Fourier transform infrared spectroscopy were used to compare the nanocomposites. The gallery size of solution intercalation hybrids in both the PEO/MMT and PEO/B34 systems increased with PEO content until it reached a plateau at 15%. Regardless of PEO concentration however, the gallery size of melt intercalated PEO/MMT and PEO/B34 hybrids remained constant. When solution intercalated samples were compared to melt intercalated samples, FTIR revealed no differences in spectrum.	[57]

2.4 The effect of clay-nanocomposites for water purification (modified and unmodified clay)

The entry of harmful compounds either through synthetic or natural origin into the environment (pesticides, hydrocarbons, heavy metals, dyes, detergents, and others) is a concerning indicator of environmental deterioration. The removal of these harmful substances from wastewater before it is discharged into aquatic ecosystems has become critical, and the development of effective methods for water pollution remediation has been a major focus for environmental research. Advanced oxidation, ion exchange, membrane filtration, ozonation, and adsorption are major technologies with variable degrees of efficiency [58, 59] in terms of water purification. Due to the ease of use however, cheap investment costs, and better accessibility to various adsorbents; adsorption is regarded as the most successful technology for the treatment of contaminated water [59, 60, 61]. Many studies are being conducted to find new low-cost, more stable, safer, environmentally friendly, and efficient adsorbents for pollutant removal from water in batch mode procedures [59, 60, 62]. Among these adsorbents, clays are a possible adsorption material because of their good features such as large surface area, cation exchange capacity (CEC), swelling, microporosity, layered structure, nano-size, and reduced cost compared to other adsorbents such as activated carbon. Moreover, clays are suited for large-scale applications because of their outstanding stability and safety [59, 63]. Relatedly, bentonite, montmotmorillonite, and attapulgite are the most extensively utilized and effective clay minerals for heavy metal removal sorption in water [64, 65]. These are effective for adsorbing various heavy metals in soil, water, wastewater, sludge, and synthetically contaminated solutions. Other clays for contaminants removal include kaolinite, halloysite, and many more. Several studies [66-87] employed these various clays to remove pollutants from water. Wahab *et al*.[66], investigated the removal of heavy metals from an aqueous solution using Silk/Bentonite clay. In their study, the heavy metal ions that were investigated included lead, cadmium, mercury, chromium, and zinc. The bentonite clay was modified with bombyx mori silk cocoons (Silk-fibroin (SF)). This modification was done because SF/Clay composites yielded a mixture of random coils and beta sheets. The presence of B-sheets of SF on SF/Clay composites provided more available amino acid groups to be required to bind with metals than in SF or clay alone. Strong hydrogen bond of SF after modification with clay resulted in better arrangement of metal ion binding. Furthermore, the authors studied the effect of adsorbent dose on

adsorption efficiency of heavy metal ions removal, and various concentrations of heavy metal salts were taken while the range of SF/Bentonite adsorbent was 0.01-0.15mg. It was observed that when the amount of the adsorbent is increased, adsorption efficiency also increases due to a greater surface area and enhanced adsorption sites or greater availability of exchangeable sites to adsorb metal ions. The authors further observed that the temperature had an effect on the adsorption efficiency with the adsorption efficiency being maximum at a lower temperature, while higher temperature showed desorption due to high mobility of adsorbate. The pH also played an important role in adsorption efficiency because it affected the surface properties of the adsorbent. An increased in pH of the solution caused a decrease in heavy metal ions; therefore, an optimized pH of 5 removed metal ions from the solution better. The study showed that bigger than 90% of heavy metal ions removal was achieved by using 0.05g of SF/Clay composites for lower initial metal ion concentration (1-30ppm) in a solution. Elsewhere in the literature, Sheikhanova *et al*. [67] used bentonite polymer reinforced polymer composite to purify water. Bentonite (BT) clay in that study was modified with polyethylene glycol (PEG) to adsorb heavy metals ions such as lead (Pb(II)), and Cadmium (Cd(II)) from the water. PEG is polar substance which is miscible in water and compatible with aqueous clay mineral suspensions and interacts at the molecular level; hence, it was used to modify the bentonite clay in this study. The authors prepared the composites BT-PEG by dispersing 20g of BT in 100ml of 0.1, 1.0, 2.0, and 5.0% of PEG solutions. The PEG concentration and sorbent dose for the removal of Pb (II), and Cd (II) was studied at 25 ℃. The amount of metal ions adsorption was found to rise as the polymer concentration in the BT-PEG material increased. This was found to be based on higher polymer concentration ions adsorbed onto the sorbent surface not only on the mechanism of physical sorption but also due to functional groups of PEG. The authors likewise studied the effect of pH at pH values of 2 to 6. At pH values of 3 to 5, the adsorption capacity of Cd(II) was higher than of Pb(II), however, at pH 6 the adsorption capacity was the same for both metal ions. Adsorption Isotherms was further done using the Freundlich isotherm model, which showed maximum adsorption of 22mg $g^{-}1$ for lead, and 18mg $g^{-}1$ for cadmium by modified sorbent (BT-PEG). The study showed that BT-PEG composite was a highly effective sorbent for the extraction of lead and cadmium ions from wastewater. Moreover, Stanly *et al*. [68] studied the purification of water using modified Montmorillonite clay and its polyvinyl alcohol (PVA) nanohybrid. In that study, the authors modified montmorillonite with polyphosphoric acid (PAA) to form a polyphosphoric acid montmorillonite (PMMT) composite to adsorb cationic dyes such as methylene blue (MB), rhodamine B (RB), and anionic dye rose bengal. The authors analyzed dye

adsorption and kinetic studies of modified montmorillonite (MMT) using Methylene Blue dye. Adsorption of MB on MMT clay and PMMT clay were carried out at 10 mg L^{-1} MB/water solution for 1 hour. The capacity of 99.99 mgg^{-1} (99.99%) of MB was adsorbed onto PMMT from the solution, and the capacity of 87.65 mgg¯1 (87.65%) of MB was adsorbed onto MMT. The high adsorption on modified montmorillonite was because the negative charges on the adsorbate surface increased after modification, which boosted the attraction with cationic adsorption capability. The modification resulted in increased surface area and improved pore volume, both of which were beneficial for adsorption metals. The authors further investigated the adsorption isotherm, which provided insight into the adsorbate-adsorbent relationship. Freundlich and Langmuir models were utilized in that study. In addition, data were obtained from 30mg L¯1 concentration of MB, RB, and rose bengal. The adsorption capacity of PMMT clay was up to 293.9mgg¯1 for MB, 244.77mgg¯1 for RB, and 296.13mgg¯1 for anionic clay rose bengal. More than 90% of dyes were adsorbed within 10 minutes, with a very small increase after those 10 minutes. The availability of high surface area and pores of PMMT played a positive role in the adsorption of the above dyes. The authors also analyzed the dye adsorption of PVA (Polyvinyl Alcohol)/Clay composites. PVA was employed to aid in the recycling and recovery of clay powder following adsorption in this case. PVA also demonstrated a higher water affinity, with a 7 percent adsorption capacity. MMT, PMMT, and PVA (0.1w/v percent) were synthesized and compared for their adsorption capabilities. For 24 hours, 100 mg of PVA/PMMT and PVA/MMT were maintained in 10ml of 200mgL^{-1} of MB solution. The adsorption capacity of PVA/PMMT was superior when compared with PVA alone. As a result, the composites were made in two distinct concentrations of 0.1w/v percent and 0.5w/v percent, with the adsorption capacity increasing as the percentage of PVA/PMMT increased. Evidently, PVA composite with 0.5 w/v percent PMMT eliminated 99.99 percent of dye (in 30 mgL^{-1} dye solution). Consequently, PMMT was able to remove 90% of organic pollutants in just 10 minutes, and PVA/PMMT nanocomposite had a stronger adsorption capability for removing 99 percent of MB than RB and Rose Bengal dye. Moreover, Zhao *et al*. [69] conducted a study on the comparison of the two clays halloysite and kaolin nanotubule for efficient water purification. Both the clays were not purified and modified. The water pollutants that were tested included cationic and anionic dyes, namely cationic (+) rhodamine 6G, and anionic (-) chrome azurol S. Dye adsorption experiment was carried out in a 1ml of dye solution and 2 mg adsorbent clay. The authors studied the adsorption properties of halloysite and kaolin using aqueous dye contents of 0-0.5wt%. According to the Langmuir model, 43.6 mgg^{-1} of Rhodamine 6G, and 38.7 mgg^{-1} of Chrome azurol S were adsorbed

onto halloysite, while 21.4 mgg^{-1} of rhodamine 6G, and 36.7 mgg^{-1} of chrome azurol S were adsorbed onto kaolin. It was therefore observed that halloysite had better adsorption efficiency for both dyes when compared with kaolin. This is because the halloysite's vast surface area provided more dye adsorption sites as well as the fact that both the negative outer surface and the positive inner surface were exposed to the solution, and thereby permitting adsorption of both positive and negative molecules. Some studies [70, 71] have also showed that due to dual electrostatic attraction between charged dyes, and halloysite nanotubules external or internal surfaces, it efficiently removes both positive and negative dyes. The authors further studied the effect of temperature and adsorption dose on the removal efficiency of dyes. Removal efficiencies increase from 51.4% to 89.0% for rhodamine 6G, and from 43.9% to 72.8% for chrome azurol S with an increase of halloysite amount from 1.0mg to 15.0mg per 1.0ml of dye solution. Temperature also played an important role as the adsorption capacity of rhodamine 6G on halloysite increased from 43.6 to 51.8 mg/g with increased temperature from 20℃ to 60℃ (10.5kj/mol); however, a decrease from 38.7 to 22.8 mgg^{-1} (28.3kg/mol) for chrome azurol S. The effect of pH was also studied by the authors. Dye adsorption was studied at a pH range from 3 to 12. The optimum rhodamine 6G adsorption was found at pH of 8, while chrome azurol S adsorption capacity decreased with an increased pH. The overall dye removal efficiency was found to be over 99.9% after 5 reused cycles of halloysite for anionic (-) chrome azurol S, and 95% for cationic (+) rhodamine 6G. Alandis *et al.* [72] investigated the ability of montmorillonite clay (Saudi clay) for the removal of Ag (I), and Cu (II) in an aqueous solution. The authors studied the effect of clay mass by changing the amount of clay from 1.0 to 5g/50ml while other parameters were kept constant (i.e., pH at 6, metal concentration at 500mg/l, temperature at 298K, and time at 1hour), for clay mass of 0.1g to 5.0g the adsorption of Ag (I) increased from 14.2 to 82.6 and Cu (II) from 0.02 to 80%. The adsorption capacity increased with an increase in the amount of clay. It was found that the effect of pH also played an important role on the adsorbent amount of the metals onto clay surface as the adsorbed amount of Cu (II) onto clay increased from 33.3mg (pH=2) and 49.87mg (pH=8). For Ag(I) however, the pH weakly influenced the adsorbent onto the clay surface. The authors also compared the effects of Saudi clay and other adsorbents such as activated carbon, shells of wheat, red mud, etc., on the adsorption of Ag (I), and Cu (II); and it was found that Saudi clay had a higher adsorption capacity for Ag (I), and Cu (II) than other adsorbents. The overall results showed that Saudi clay can effectively remove Ag (I), and Cu (II) from an aqueous solution. Samad *et al*. [73] also studied the potential of synthesized zinc oxide clay tablets on purification of water. The clay in this study (silty clay) was modified with zinc

oxide nanoparticles (ZnONPs), and thereafter the composite zinc oxide clay (ZnO-Clay) was molded into a tablet to purify water from the point of use (POU). The tablet was used to remove Cd (II), Co (II), Ni (II), and Pb (II) from the synthetic wastewater system by contact time of 0.5, 1, 1.5, 2, 3, 4, 24, 48, and 72 hours. It was observed that Pb (II) was adsorbed on the tablets rapidly, and in the first hour; more than 90% removal of Pb (II) was noted, and after 4 hours; almost all the Pb (II) was removed from the system (98.8%). Similarly, Co (II) exhibited high adsorption efficiency, with the removal of Co (II) being achieved in 4 hours (96.5 percentage removal). Furthermore, in 4 hours, 98.6 percent of Ni (II) was adsorption on the tablet. The removal of Cd (II) by the ZnONPs-clay tablets was a relatively slow process. For an example, in 2.5 hours; 80% removal Cd (II) ions was observed. Furthermore, even after 4 hours; the removal of Cd (II) was found to be around 89.9% and with the removal reaching 94% after 3 days for Cd (II). Overall, it has been observed that the porous ZnONPs-clay tablet has strong potential for eradication of metal ions from contaminated aqueous media, by accumulating them around itself and thereby decontaminating the waste and water systems. The authors further studied the antibacterial activity of the tablet against *Escherichia Coli (E.Coli).*The antibacterial efficiency was seen by the inhibition zone made around the tablet, and it was shown that the concentration of 40% of ZnO-Clay tablet had a greater inhibition zone of 15mm, and concentration of 10%-30% of the tablet had 5-11.3mm inhibition zone. The greater the inhibition zone, the better the antibacterial efficiency of the tablet. The study showed that the ZnO-Clay tablet was effective in disinfecting and decontaminating water from POU. It is evident from different studies that modified and unmodified clay nanocomposites have a positive effect on water due to their capabilities of removing various unwanted contaminants in wastewater. Investigation on the removal of hexavalent chromium from an aqueous solution using an eco-friendly natural clay was done by Ashour *et al* [74]. The clay in the study was modified with hydrogen chloride (HCl). HCL was added for clay regeneration and successive utilization. The natural clay (NC) montmorillonite, and modified HCL-Montmorillonite heated at 600°C (MC600) were therefore tested for the removal of chromium (IV) in an aqueous solution. The authors investigated the effect of the initial concentration of chromium on the adsorption capacity ranged from 10mg/l to 80mg/l using clay contents of 0.1g. The results showed that an increase in chromium concentration in both adsorbents (NC and MC) indicated a significant improvement in adsorption capacity which was from 1.1 mgg^{-1} to 4.0 mgg^{-1} with a chromium increase of 10-80mg/l. Removal efficiency however decreased due to a limited number of active sites on the adsorbent to adsorb the increased number of chromium molecules. Contact time also played a key role in the adsorption of chromium, which

showed that the adsorption rate of chromium on both clays increased with an increase in contact time. The authors further investigated the effect of the adsorbent dose, which was carried out at contents of 4.5 mgg^{-1} and 7.0 mgg^{-1}, corresponding to 0.5g/l of NC and MC600, and which emphasized that an increase in clay content decreases the adsorption capacity to 2.0 for NC, and 2.6 mgg^{-1} for MC600 due to a decrease in available adsorption active sites and surface area when the dose of the clay is increased. The effect of pH was also examined as it controls the surface charge of the clay minerals. The pH on chromium solution was initially evaluated at pH ranges of 2.0 to 8.0; therefore, pH of 2.0 to 5.0 showed an increase in adsorption capacity, which reached 4.5mg/g for NC, and 7.0 mgg^{-1} for MC600. An increase of pH above 5 however showed a decrease in adsorption capacity. This decrease was explained by positively charged surfaces of clay surrounded by excess H^+ in the solution at lower pH, and the deprotonation mechanism of active groups activated at higher pH. Furthermore, at high solution pH, chromium ions interact chemically with OH_2 ions present in aqueous media, thus resulting in metal ion hydrolysis, which can lead to chromium precipitation in the form of hydroxide speciation. As a result, at high pH, overall adsorption capacity is reduced [75, 76]. Essentially, the study showed that 66% of chromium was removed within 90 minutes with an adsorption capacity of 10.0mg on NC, and 7.0mg on MC600. Unuabonah *et al.* [77] also used a hybrid clay (HYCA) to treat water. Kaolin clay was used and also modified with Carica papaya seeds, and 0.1M of sodium chloride (NaCl) for the removal of heavy metal ions, cadmium (Cd(II)), nickel (Ni(II), and lead (Pb(II)). The authors only studied the effect of HYCA adsorption on heavy metal ions in an aqueous solution at an initial metal concentration of 1mg/l with 2g of HYCA adsorbent. The results showed that the hybrid clay reduced ≤4ug/l of Cd(II), ≤7ug/l of Ni(II), and ≤20ug/l of Pb(II) in 5 hours, at a flow rate of ≈7ml/min, which were within the permissible limit for heavy metals in water according to the World Health Organisation except for Pb(II). The study therefore suggests that HYCA can be used to remove organic contaminants and Pb from wastewater. Xi *et al.* [78] also used unmodified-organoclays, halloysite, bentonite, and kaolinite which, were modified with surfactant hexadecyltrimethylammonium bromide (HDTMA) to adsorb nitrate in water. In that study, 100mg/l of nitrate solution was used to compare the sorption capacity of the organoclays mentioned above. Natural bentonite and kaolinite did not remove any nitrate ions from the solution; however, halloysite removed 0.54mg of nitrate ions per gram of clay. The modified clays showed improved removal capacities of 12.03mg of bentonite at 2-cation exchange capacity (CEC) of HDTMA, and 14.76mg of bentonite at 4-cation exchange capacity (CEC) of HDTMA. The modified halloysite, and kaolinite however removed 1.78mg and 1.5mg at

2-cation exchange capacity of HDTMA, and 1.93mg for both clays at 4-cation exchange capacity of HDTMA, which was lower in comparison to the removal of nitrate by modified bentonite. The improved removal difference was due to the difference of CEC on modified clays, which was 66.67meq/100g for bentonite, 9.78meq/100g for kaolinite, and 10meq/100g for halloysite. The study therefore showed that modified clay can remove nitrate efficiently than unmodified clay and that among the modified clays, modified bentonite had better adsorption capacity. Ghafar *et al*. [79], investigated the removal of contaminants from water using a natural and zwitterionic surfactant-modified clay. The natural clay (NC) consisted of quartz and kaolinite were modified by cocamisopropyl betaine (CAPB) to enhance the clay efficiency for removal contaminants. These clays were used to remove lead (Pb(II)), and reactive yellow 160 dye (RY160) from the water. The authors compared the adsorption efficiency of NC and CAPB-NC, of which NC showed inefficient adsorption of RY160 dye, which was 2 mgg^{-1}; and CAPB-NC showed an enhanced adsorption efficiency of 12mg/g. The adsorption of Pb(II) on both clays however showed great adsorption efficiency of 40mg/g of Pb(II) adsorption onto CAPB-NC, and 43 mgg^{-1} of Pb(II) adsorbed onto NC. The effect of contact time of RY160 adsorption on CAPB-NC, and Pb(II) on NC was also studied. Adsorption of RY160 was rapid and reached equilibrium within 20 mins, which indicated strong interaction between the modified clay and the dye. The adsorption of Pb(II) happened in three stages: quick adsorption in the first 5 mins, along with slower adsorption up to 45 mins, and lastly, equilibrium was reached within 60 mins. The pH results also showed that the adsorption interaction between RY160 and CAPB-NC was strong and favoured at pH=2, and resulted in multiple layers; while Pb(II) adsorption on NC occurred via monolayer formation, and was favoured at pH=6.2. Based on the results, it can be concluded that the natural clay and modified clay efficiently remove RY160 dye and lead from the aqueous solution. In another study, adsorption of Cd(II) by raw, and modified clay in an aqueous solution was investigated by Sari *et al* [80]. Manganese oxide (MnO_2) modified kaolinite (MnO-Kaol), and raw kaolinite (Kaol) were used to remove cadmium (Cd(II)) ions from wastewater. MnO_2 modified adsorbents were used because of their recent attraction and noticeability of increasing the ability of surface area of silica-based adsorbents, loading ability at large amounts of silica-based surfaces, and ionization at low pH [81, 82]. The concentration of adsorbents was carried out at 1-40g/l, while Cd(II) solution was diluted at concentrations from 10-40mg/l. In that study, the authors investigated the effect of the concentration of the adsorbent on Cd(II) at an initial concentration of 10mg/l, pH of 5, contact time of 30 mins, and temperature of 20 °C. The outcome showed that an increase in the adsorbent concentration of up to 4g/l increased the

sorption efficiency due to the increased number of adsorption sites per unit mass, and depending on adsorbent concentration, thus allowing for relatively high adsorption, while high adsorbent concentration causes particle aggregation, and a decrease in total specific surface area, and thereby resulting in a decrease in total specific surface area. Resultantly, a decrease in adsorption efficiency was observed. For further experiments, the ideal concentration of MnO-Kaol was determined to be 4 g L^{-1}. Furthermore, the effect of pH was studied at ranges of 2-8, which showed an increase in removal efficiency at a maximum value of (95–86%) at pH 5–7 range, hence pH 5 was selected as the optimum pH. Evaluation of the effect of contact time and the temperature was also done, and contact time ranges were 5 to 60 mins, and the initial adsorption of Cd(II) onto MnO-Kaol was rapid as cadmium ions and clay interaction reached equilibrium in less than 30 minutes, hence the optimum contact time was 30 mins. Additionally, the temperature was optimum at 20℃ because at ranges of 20-50℃, the adsorption efficiency decreased from 95% to 83%. Lastly, from the Langmuir model, the sorption capacities of Cd(II) onto Kaol and MnO-Kaol were found to be 14.11 and 36.47 mgg^{-1} respectively. The overall conclusion based on the results then showed that the modified clay removed the cadmium from the water solution better than unmodified clay. The effect of clay in water purification depends on several factors such as pH, clay mineral type and its dosage, temperature, modification, and the extent of the contaminant. Most studies have proved that modified clays are more efficient in water treatment than natural clays as the adsorption capacity is increased when there is modification due to an increase in adsorption sites. In Table 2.4, other studies are summarized as pertained to modified and unmodified clay nanocomposites for the removal of contaminants in water.

Table 2.4: Summary of other studies on modified and unmodified clay nanocomposites effects on water purification.

Composite	Contaminants	Operating variables	Effectiveness of the composites	References
Montmorillonite modified with micelles of benzyldimethylhexadecylammonium (BDMHDA)	Tetracycline and sulfonamide antibiotics	Adsorption Isotherms	BDMHDA micelle-clay complexes (1%w/w) removed 96-99.9% of antibiotics from water solution containing 5mg/L to 50mg/l of pharmaceuticals	[83]
Chitosan/Clay (Ch/Clay, Ch/ANPs/Clay, Ch/AgNPs/Clay)	Copper (II)	Contact time, adsorbent dose, pH, temperature	The adsorption efficiency of Cu(II) ions by Ch/AgNPs/Clay and Ch/AuNPs/Clay was bigger than that of individual Ch/Clay composites, the metal nanocomposites enhanced the adsorption character of the composites.	[84]
Silimanite, quartz, and mullite modified with rice husk-Na_2CO_3	Escherichia Coli (E.Coli), nitrate, phosphate, arsenic, and lead	pH, adsorbent dose, contact time and, adsorption isotherm	The removal rate of E.Coli was up to log 4, and reduction efficiency for phosphate was from 27.33%-76%, and 10.67%-46% for nitrate; and adsorption isotherm for lead and arsenic was found to be better using Langmuir than Freundlich models.	[85]
Bentonite clay	Cd(II), Pb(II) and Cr(III)	Working regime (static and dynamic)	Removal efficiencies of up to 97.82% in the case of Cd(II), 100% in the case of Pb(II), and 80.77% in the case of Cr(III)	[86]

			were reached in the dynamic (3D shaker) regime. Also, to achieve an efficient removal (>98%) of Cd ions, wastewaters containing were used. The bentonite clay proved to be efficient in the removal of heavy metal ions.	
Kaolinite, Montmorillonite and Nontronite	Arsenate (As(V)) and Arsenite (As(III))	pH, adsorption kinetic, adsorption isotherm	The maximum sorption was achieved at pH 5.0 and pH 7.0 for As(V) and As(III) respectively. Kinetic experiments demonstrated that a pseudo-second-order model accurately represented the sorption of As(V) and As(III) on all clay minerals. Nontronite minerals (NAU-1 and NAU-2) absorbed more As than the other minerals investigated.	[87]

2.5 Flammability of clay nanocomposites

Various clay nanoparticles have been added into different polymer matrices in order to enhance the flammability resistance of the polymers. In most cases, it has been reported that the clay nanoparticles were most effective at lower contents, i.e., 1 to 5% since there is a better dispersion of the clay at lower contents. Pandey *et al*. [88] examined the impact of clay loading on the flammability of poly(methyl methacrylate) (PMMA) at clay concentration of 5%. The nanocomposites were fabricated by utilizing the commercially modified nanoclays like cloisite 30B (C30A), and cloisite 93A (C93A) as well as modified nanoclays in the form of OTAB-Na-MMT (Quaternary ammonium salt modified Na-MMT). The flammability characteristics of the nanocomposites have been examined using techniques such as cone calorimeters, and the horizontal burning test (UL-94HB). In comparison to the virgin poly(methyl methacrylate) (VPMMA), the nanocomposite systems demonstrated a greater burning rate, and shorter average burning times, which suggests that they burn quickly. Furthermore, the authors observed that none of the nanocomposites drip during the test, which is notably different from VPMMA, which was found to heavily drips. According to the cone calorimeters, nanocomposites are more fire resistant than virgin PMMA. Elsewhere in the literature, Morgan *et al*. [89] compared the flammability properties of fluorinated synthetic mica (FSM) clays, and natural montmorillonite (MMT) clays incorporated in polystyrene. The performance of the nanocomposites' flammability was investigated using cone calorimetry. The non-treated inorganic FSM nanocomposites showed lower heat release rate (HRR) values. Both sodium fluorinated synthetic mica (NaFSM) and sodium montmorillonite (NaMMT) nanocomposites exhibited a similar behavior, with just a little decrease in HRR. The nanocomposites were found to burn very slow according to the UL-94. The flammability properties of Polypropylene/organo-montmorilonite (PP/OMMT) nanocomposites were reported by Szustakiewicz *et al*. [90] at a heat flux of 50 kW/m^2,and 35 kW/m^2. The flame behaviour of the nanocomposites (PP/OMMT), and Polypropylene/organo-montmorrilonite/ commercial flame retardant (PP/OMMT/FR) were investigated at heat flux of 50 kW/m^2. Both nanocomposties exhibited longer time to ignition (TTI) than pure PP. The maxima of HRR in PP/organoclay/FR composites were both roughly 50% lower. Moreover, the HRR and mass loss rate (MLR) values for nanocomposites that were burned at a heat flux of 35 kW/m^2 were little different from those of clean PP. After the addition of FR, the cone calorimeter experiments revealed a reduction in the HRR,

and MLR in both heat flux. The flammability properties of the composites fabricated with maleated polypropylene, and silica pillared montmorillonite were reported by Zue, and co-workers [91]. In order to evaluate the flammability performance of several PP composite formulations, a microscale combustion calorimeter (MCC) was used. The heat release capacity (HRC) value of the PP/PP-g-MA/OMT nanocomposite was reported to be 1872 J/g.k, which was significantly higher than the PP/PP-g-MA *viz* 997 J/g.k. There was a 33% reduction in the HRC peak of the PP/PP-g-MA/C-SiO_2-OMT nanocomposite when compared with PP/PP-g-MA/OMT nanocomposite. The main reason for such an observation is the possibility that more pyrolytic gaseous products were delayed or absorbed by Silica pillared montmorillonite (C-SiO_2-OMT) than by organically modified montmorillonite (OMT), and thereby resulting in less volatilization into the (MCC) combustor to be oxidized, as sample PP/PPg-MA/C-SiO_2-OMT exhibited lower total heat release (THR) value than that of PP/PPg- MA/OMT. Furthermore, Zhang *et al*. [92] studied the flammability resistance of the polyethylene (PE)-clay nanocomposites. Clays such as cloisite 6A, 20A, or 25A were used in the study. The peak heat release rate (PHRR), heat release rate (HRR), specific extinction area (SEA), and mass loss rate (MLR) were cone calorimetry measures used to determine flammability. According to the cone calorimetric data, all PE-clay nanocomposites had PHRRs that are 30 to 40% lower than those of pure PE. The SEA values remained unaltered from virgin PE, which supported the fact that the clay's presence does not result in more smoke being produced. The preparation and flammability characteristics of polyethylene/clay nanocomposites by melt intercalation technique from Na+ montmorillonite was reported by Wang *et al* [93]. The HDPE/5 wt% MMT nanocomposite peak HHR was lower than the HDPE peak. This is to be expected since the clay platelets acted as a heat barrier, and thereby enhancing the flammability resistance by reducing the HRR peak.

2.6. Flammability behaviour of Zinc Borate

Zinc borate (ZnB) is a flame retardant and smoke suppressant, and it can increase flame retardancy by enhancing char production and char quality when used with several intumescent flame-retardant systems [94-97]. Several studies have been conducted to investigate the effect of zinc borate on polymers and its synergistic behaviour with other nanoparticles. The effect of zinc borate on the flame resistance of polypropylene (PP) composites was investigated by Feng *et al* [98]. Two techniques were used, i.e., limiting oxygen index (LOI), and UL-94. The 20% inherent flame

retardant (IFR) and various ZnB loadings were used for the LOI values, and UL rating of the PP/IFR composites. The PP, PP/1%ZnB, and PP/IFR had LOI values of 17.0%, 17.5%, and 27.1% respectively. The LOI value of the PP/IFR composite was 27.1%, which satisfied the requirements of UL-94 V-0. The findings demonstrated that the LOI values first rose sharply as the amount of ZnB in the PP/IFR composites increased, but these values marginally fell with loadings of more than 2% ZnB. The findings clearly explain that the content of ZnB played a key role in the flammability properties of the composites, with the optimum content being 2%. The LOI value of the PP/IFR composite achieved a maximum value of 32.2% when the ZnB loading was 2%, thus passing the UL-94 V-0 rating. As much as 2% was however found to be the optimum content, it was observed that the LOI value still approached V-0 grade with a higher LOI value than that of the PP/IFR composite at 4% ZnB concentration, despite a minor decrease to 31.9%. The results of the LOI and UL-94 ratings showed that a suitable amount of ZnB could enhance the flame-retardant performance of PP/IFR, and clearly exhibit a synergistic effect between ZnB and IFR; whereas a higher loading of ZnB would degrade the balance between the function of foaming and charring in PP/IFR composites [99]. Fang *et al.* [100] reported on the effect of zinc borate on the flammability properties of wood flour (WF)/polyvinyl chloride (PVC) composites. It was reported that ZnB did little to increase the flame resistance of WF-PVC; however, it did an excellent job of suppressing smoke in the WF-PVC composite. Elsewhere in the literature, the ability of zinc borate to retard flame on polyurethane was studied by Yildiz *et al* [101]. The polyurethane composites were fabricated by adding flame retardant filler in the form of zinc borate into the matrix. It was proven that even with a 0.5 weight percent of zinc borate, the burning time of polyurethane was significantly (160%) improved. This demonstrated how crucial zinc borate is to a flame resistance product formation. Qian *et al.* [102] reported the flammability behaviour of the composites fabricated from vinyl acetate, double hydroxides, and zinc borate (EVA/LDHs/ZnB). The LOI value of the ethylene layered double hydroxide (ELDH)(1) (50% of LDHs) was found to increase quickly from 17.0%, i.e., pure EVA to 26.8% for ELDH2-ELDH6. Interestingly, the LOI value of the composites marginally decreased as ZnB quantity increases. The reduction in the LOI values was associated with a decrease in the content of the LDHs within the synergy system, which happened to be more effective as a heat barrier than the counter part in the form of zinc borate (ZnB). The mechanism of flame retardancy for LDHs is such that the LDHs as a flame-retardant filler would breakdown in the presence of heat, and thereby producing both CO_2 and H_2O. Obviously, the H_2O would act as a heat suppressant, and as a result it would enhance the flammability resistance. It was noticed that

the EVA/LDHs/ZnB composites need to have a reasonable amount of ZnB (5%) in order to pass the UL-94 V-0 test, according to the UL-94 results. Zinc borate (ZnB) as a flame-retardant material is therefore capable of acting as an anti-dripping in the polymer composites. In the UL-94 test, pure EVA, and ELDH1-ELDH4 with insufficient ZnB dripped quite a lot. When enough ZnB was however added in the polymer matrix, the polymer's melting viscosity would increase, thus favouring the UL-94 test with V-0 rating. It is well documented that a viscous system is resistant to the release of volatile materials, and in turn enhances the flammability resistance [102]. Moreover, flame retardancy of the unsaturated polyester composites with modified ammonium polyphosphate, montmorillonite, and zinc borate was investigated by Jiang *et al* [103]. The results showed that the MMT had the barrier effect to stop the transmission of heat and flammable volatiles during the thermal degradation process of the unsaturated polyester resin (UPR) composite. The barrier function as a preventer of the UPR composite from being fully burned. When ZnB was added, the carbon's compact structure was improved, thus allowing for the easy release of water at higher temperatures as well as the production of boric acid, which helped to promote the creation of the pyrolysis layer. He *et al.* [104] used cone calorimetry to investigate the synergistic effect of organo-sepiolite (OSEP) and zinc borate on the fire retardancy of polypropylene. The parameters collected from the cone calorimeter includes the heat release rate (HRR), peak heat release rate (PHRR), average mass loss rate (AMLR), total heat release, smoke production rate (SPR), and fire performance index (FPI). The HRR peak of PP was recorded to be 2086 kW/m^2. Nonetheless, with 3%, 5%, and 10% loading of the OSEP, the PHRR for PP/OSEP composites reduced by 34%, 42%, and 66% respectively. The PHRR was further reduced when 3% ZnB was introduced to the PP/OSEP system; and the reductions were 46%, 51%, and 71% at 3%, 5%, and 10% OSEP loading respectively. The PHRR was reduced by 57%, 62%, and 73% at 3%, 5%; and 10% OSEP loading respectively when 5% ZnB was introduced into the PP/OSEP system. Relatedly, the PHRR was reduced by 68%, 70%, and 78% at 3%, 5%, and 10% OSEP loading respectively when 10% ZnB was added to the PP/OSEP system, which represented a notable improvement over the PP/OSEP system. The outcome showed that adding ZnB to the PP/OSEP system has a considerable impact on improving the flame resistance of the PP/OSEP composites. Furthermore, similar study was done by *Tai et al.* [105] on iron-montmorillonite and zinc borate as synergistic agents in the flame-retardant of the glass fiber reinforced polyamide 6 (GFPA6) composites in combination with melamine polyphosphate (MPP). It has been demonstrated that GFPA6 with 28 weight percent MPP, and 2 weight percent of either ZnB or Fe-OMT can obtain a UL-94 V0 rating, and display

superior flame retardancy than GFPA6 with 30 weight percent of MPP alone. Furthermore, Wang *et al.* [106] employed cone calorimetry to study the flame retardancy of polypropylene (nano) composites containing LDH and zinc borate. When the LDH is loaded by 3, 5, and 10 weight percent in the PP/organo-LDH nanocomposites, the PHRR falls by 2, 18, and 21% respectively. The reduction was ascribed to an effective char formation by LDH at nanoscale, which is able to prevent heat from entering the system, and preventing the volatiles from leaving the system, and resultantly enhances the flammability resistance.

2.7 References

1. Schaming, D.; Remita, H. **(2015)**. Nanotechnology: From the ancient time to nowadays. *Found. Chem*. 17, 187–205.
2. Mana, S.C.A., Hanafiah, M.M., Chowdhury A.J.K. **(2017)**. Environmental characteristics of clay and clay-based minerals. *Geology, Ecology, and Landscapes*, 1:3, 155-161.
3. Murray, H.H. **(1991)**. Overview - clay mineral applications. In: H.H. Murray (Editor), Some Applications of Selected Clay Minerals. *Appl. Clay Sci*, 5, 379-3.
4. Lazzara, G., Cavallaro, G., Panchal, A., Fakhrullin, R., Stavitskaya, A., Vinokurov, V., Lvov, Y. **(2018)**. An assembly of organic-inorganic composites using halloysite clay nanotubes. *Current Opinion in Colloid & Interface Science*, 35, 42–50.
5. Worden, R.H., Griffiths, J., Wooldridge, L.J. **(2020)**. Chlorite in sandstones. *Earth-Science Reviews*, 204, 103105(1-101).
6. Deer, W.A., Howie, R.A., Zussman, J. **(2013)**. *An introduction to the rock-forming minerals*, 3rd edition. The MIneralogical Society, London, 498 pp
7. Deer, W.A., Howie, R.A., Zussman, J. **(2013)**. Chlorite Group: Clinochlore (Mg)10Al2[Al2Si6O20](OH)16 - Chamosite (Fe2+)10Al2[Al2Si6O20](OH)16. In: W.A. Deer, R.A. Howie, J. Zussman (Editors), *An Introduction to the Rock-Forming Minerals*. Mineralogical Society of Great Britain and Ireland, 1-506.
8. Dayal, A.M., Mani, D. **(2017)**. *Expoloration Techniques. In Book: Shale Gas: Exploration and Environmental and Economic Impacts*. Elsevier, 65-93.
9. Müller, K., Bugnicourt, E., Latorre, M., Jorda, M., Echegoyen Sanz, Y., Lagaron, J.M., Miesbauer, O., Bianchin, A., Hankin, S., Bölz, U., *et al*. **(2017)**. Review on the processing and properties of polymer nanocomposites and nanocoatings and their applications in the packaging, automotive and solar energy fields. *Nanomaterials*. 7, 74.
10. Guo, F., Aryana, S., Han, Y., Jiao, Y. **(2018)**. A review of the synthesis and applications of polymer–nanoclay composites. *Appl. Sci*., 8, 1696.
11. Nasir, A., Masood, F., Yasin, T., Hameed, A. **(2019)**. Progress in polymeric nanocomposite membranes for wastewater treatment: Preparation, properties and applications. *J. Ind. Eng. Chem*., 79, 29–40.

12. Usmani, M.A., Khan, I., Ahmad, N., Bhat, A.H., Sharma, D.K., Rather, J.A., Hassan, S.I. **(2016)**. Modification of Nanoclay Systems: An Approach to Explore Various Applications. In *Nanoclay Reinforced Polymer Composites*; Springer: Singapore, 3, 57–83.
13. Uddin, M.K. **(2017)**. A review on the adsorption of heavy metals by clay minerals, with special focus on the past decade. *Chem. Eng. J.*, 308, 438–462.
14. Jlassi, K., Krupa, I., Chehimi, M.M. **(2017)**. Overview: Clay preparation, properties, modification. In *Clay-Polymer Nanocomposites*; Elsevier: Amsterdam, The Netherlands, 1–28.
15. Ghadiri, M., Chrzanowski, W., Rohanizadeh, R. **(2015)**. Biomedical applications of cationic clay minerals. *RSC Adv.*, 5, 29467–29481.
16. Lázaro, B.B. **(2015)**. Halloysite and kaolinite: Two clay minerals with geological and technological importance. *J. Acad. Exact Phys. Chem. Nat. Sci. Zaragoza*, 70, 7–38.
17. Awasthi, A., Jadhao, P., Kumari, K. **(2019).** Clay nano-adsorbent: Structures, applications and mechanism for water treatment. *SN Appl. Sci.*, 1, 1076.
18. Mahbuba Rahman, M., Hasan, M.R. **(2019)**. *Synthetic Biopolymers*. Springer Nature
19. Ilyas, R.A., Sapuan, S.M. **(2020)**. The preparation methods and processing of natural fibre bio-polymer composites. *Current Organic Synthesis*, 16, 1068–70.
20. Kian, L.K., Saba, N., Jawaid, M., Sultan, M.T.H. **(2019)**. A review on processing techniques of bast fibers nanocellulose and its polylactic acid (PLA) nanocomposites. *International Journal of Biological Macromolecules*, 121, 1314–28.
21. Nasir, A.; Masood, F.; Yasin, T.; Hameed, A. **(2019)**. Progress in polymeric nanocomposite membranes for wastewater treatment: Preparation, properties and applications. *J. Ind. Eng. Chem.*, 79, 29–40.
22. Murariu, M., Philippe Dubois, P. **(2016)**. PLA composites: From production to properties. *Advanced Drug Delivery Reviews*, 107, 17–46.
23. Siakeng, R., Jawaid, M., Ariffin, H., Sapuan S.M., Asim, M., Saba, N. **(2018)**. Natural Fiber Reinforced Polylactic Acid Composites: A Review. *Polymer Composites*, 40(2), 446-463.
24. Farazin, A., Mohammadimehr, M. **(2021)**. Effect of different parameters on the tensile properties of printed Polylactic acid samples by FDM: experimental design tested with MDs simulation. *The International Journal of Advanced Manufacturing Technology*.118(1), 103-118.

25. Moataz, A., Elsawya., Kimc K-H., Parkc J-W., Deepb, A. **(2017)**. Hydrolytic degradation of polylactic acid (PLA) and its composites. *Renewable and Sustainable Energy Reviews*, 79, 1346–1352.

26. Gong, X., Pan, L., Tang, CY., Chen, L., Li, C., Wu, C., Law, W.C., Wang, X., Tsui, C.P., Xie, X. **(2016)**. Investigating the crystallization behavior of poly(lactic acid) using CdSe/ZnS quantum dots as heterogeneous nucleating agents. *Composites Part B*, 91, 103–10.

27. Granda, L.A., Espinach, F.X., Tarres, Q., Méndez, J.A., Delgado-Aguilar, M., Mutjé, P. **(2016)**. Towards a good interphase between bleached kraft softwood fibers and poly (lactic) acid. *Composites Part B*, 99, 514–20.

28. Scaffaro, R., Lopresti, F., Botta, L., Maio, A. **(2016)**. Mechanical behavior of polylactic acid/ polycaprolactone porous layered functional composites. *Composites Part B*, 98, 70–7.

29. Khan, B.A., Chevali, V.S., Na, H., Zhu, J., Warner, P., Wang, H. **(2016)**. Processing and properties of antibacterial silver nanoparticle-loaded hemp hurd/poly(lactic acid) biocomposites. *Composites Part B*, 100, 10–8.

30. Salavagione, H.J., Diez-Pascual, A.M., Lázaro, E., Vera, S., Gomez-Fatou, M.A. **(2014)**. Chemical sensors based on polymer composites with carbon nanotubes and graphene: The role of the polymer. J. Mater. *Chem. A.*, 2, 14289–14328.

31. Bhattacharya, M. **(2016)**. Polymer nanocomposites—A comparison between carbon nanotubes, graphene, and clay as nanofillers. *Materials*, 9, 262.

32. Wang, J., Wang, Z., Vieira, C.L., Wolfson, J.M., Pingtian, G., Huang, S. **(2019)**. Review on the treatment of organic pollutants in water by ultrasonic technology. *Ultrason. Sonochemistry, 55, 273-278.*

33. Madhumitha, G., Fowsiya, J., Mohana Roopan, S., Thakur, V.K. **(2018)**. Recent advances in starch–clay nanocomposites. *Int. J. Polym. Anal. Charact*., 23, 331–345.

34. Cui, Y., Kumar, S., Kona, B.R., van Houcke, D. **(2015)**. Gas barrier properties of polymer/clay nanocomposites. *RSC Adv*., 5, 63669–63690.

35. Hammad, S., Noby, H., Elkady, M.F., El-Shazly, A.H. **(2018)**. In-situ of polyaniline/polypyrrole copolymer using different techniques. *Mater. Sci. Eng*., 290, 012001.

36. Guo, F., Aryana, S., Han, Y., Jiao, Y. **(2018)**. A review of the synthesis and applications of polymer–nanoclay composites. *Appl. Sci*., 8, 1696.

37. Unalan, I.U., Cerri, G., Marcuzzo, E., Cozzolino, C.A., Farris, S. **(2014)**. Nanocomposite films and coatings using inorganic nanobuilding blocks (NBB): Current applications and future opportunities in the food packaging sector. *RSC Adv.*, 4, 29393–29428.

38. Singha, S., Hedenqvist, M.S. **(2020)**. A Review on Barrier Properties of Poly (Lactic Acid)/Clay Nanocomposites. *Polymers*, 12(5), 1095.

39. Cui, Y., Kumar, S., Rao Kona, B., Van Houcke, D. **(2015)**. Gas barrier properties of polymer/clay nanocomposites. *RSC Adv*., 5, 63669–63690.

40. Sangeetha, K., Vinodhini P.A., Sudha, P.N. **(2019)**. *Clay Based Biopolymer Nanocomposites and Their Applications in Environmental and Biomedical Fields*. Springer.

41. Mansa, R., Huang, C-T., Quintela, A., Rocha, F., Detellier, C. **(2015)**. Preparation and characterization of novel clay/PLA nanocomposites. *Applied Clay Science*, 115, 87-96.

42. Maharana, T., Mohanty, B., Negi, Y.S. **(2009)**. Melt-solid polycondensation of lactic acid and its biodegradability. *Prog. Polym. Sci*., 34, 99–124.

43. Krikorian, V., Pochan, D.J. **(2003)**. Poly (L-Lactic Acid)/Layered Silicate Nanocomposite: Fabrication, Characterization, and Properties. *Chem. Mater*., 15, 4317–4324.

44. Sinha R.S., Okamoto, M. **(2003)**. Polymer/layered silicate nanocomposites: A review from preparation to processing. *Prog. Polym. Sci*., 28, 1539–1641.

45. Pavlidou, S., Papaspyrides, C.D. **(2008)**. A review on polymer-layered silicate nanocomposites. *Prog. Polym. Sci*., 33, 1119–1198.

46. Paramitha, T., Wonoputri, V., Sitompul, D.S.D., Lee, H.W., Sitompul, J.P. **(2020)**. Properties of clays reinforced PLA nanocomposites by melt extrusion technique. *Malaysian Journal of Fundamental and Applied Sciences*, 16, 4, 453-457.

47. Zaidi, L., Bruzaud, S., Bourmaud, A., Me´de´ric, P., Kaci, M., Grohens, Y. **(2010)**. Relationship Between Structure and Rheological, Mechanical and Thermal Properties of Polylactide/Cloisite 30B Nanocomposites. *Journal of Applied Polymer Science*, 116, 1357–1365.

48. Zhou, S.Y., Chen, J.B., Li, X.J., Ji, X., Zhong, G.J., Li, Z.M. **(2016)**. Innovative enhancement of gas barrier properties of biodegradable poly(butylene succinate) nanocomposite films by introducing confined crystals. *RSC Advances*, 6, 4, 2530–2536.

49. Carli, L.N., Crespo, J.S., Mauler, R.S. **(2011)**. PHBV nanocomposites based on organomodified montmorillonite and halloysite: The effect of clay type on the morphology and thermal and mechanical properties. *Applied Science and Manufacturing*, 42(11) ,1601-1608.

50. Reis, d-C., Cristino, D., Morais, L., de Carvalho, A.C., Alves, L.H., Tatianny S., Barbosa, R. **(2016)**. Assessment of the Morphology and Interaction of PHBV/Clay Bionanocomposites: Uses as Food Packaging. *Macromolecular Symposia*, 367, 1, 113–118.

51. Zaiby, R., Yogi, A S., Ariadne, L J., Onny, U. **(2018)**. Polypropylene/clay nanocomposites prepared in an internal mixer: optimization of processing conditions to improve flexural modulus. *IOP Conference Series: Materials Science and Engineering*, 432(1), 1-6.

52. Zanetti, M.; Lomakin, S.; Camino, G. **(2000)**. Polymer layered silicate nanocomposites. *Macromol Mater Eng*., 279(1), 1–9.

53. Sedla´kova´, Z., Plesˇtil, J., Baldrian, J., Sˇlouf, M., Holub, P. **(2009)**. Polymer-clay nanocomposites prepared via in situ emulsion polymerization. *Polym. Bull*, 63, 365–384.

54. Ercan, N., Durmus, A., Kas¸go¨z, A. **(2015)**. Comparing of melt blending and solution mixing methods on the physical properties of thermoplastic polyurethane/organoclay nanocomposite films. *Journal of Thermoplastic Composite Materials*, 1–21.

55. Tanasa, M., Zanoaga, M. **(2014)**. Study of properties of some polyethylene-clay nanocomposites: influence of preparation method on the degree of clay intercalation/exfoliation. *Chemistry Journal of Moldova. General, Industrial and Ecological Chemistry*, 9(1), 106-111.

56. Modesti1, M., Besco, S., Lorenzetti, A., Zammarano, M., V. Causin, V., Marega, C., Gilman, J.W., Fox, D.M., Trulove, P.C., De Long, H.C., Maupin, P.H. **(2008)**. Imidazolium-modified clay-based ABS nanocomposites: a comparison between melt-blending and solution-sonication processes. *Polym. Adv. Technol.*, 19, 1576–1583.

57. Shen, Z., Simon, G.P., Cheng, Y-B. **(2002)**. Comparison of solution intercalation and melt intercalation of polymer-clay nanocomposites. *Polymer*, 43, 4251-4260.

58. Tarpani, R.R.Z.; Azapagic, A. **(2018)**. Life cycle environmental impacts of advanced wastewater treatment techniques for removal of pharmaceuticals and personal care products (PPCPs). *J. Environ. Manag*., 215, 258–272.

59. Orta, M-D-M., Martin, J., Santos, J.L., Aparicio, I., Medina-Carraco, S., Alonso, E. **(2020)**. Biopolymer-clay nanocomposites as novel and eco-friendly adsorbents for environmental remediation. *Applied Clay Science*, 198, 105838.

60. Sophia, A.C., Lima, E.C. **(2018)**. Removal of emerging contaminants from the environment by adsorption. *Ecotoxicol. Environ. Saf*., 150, 1–17.

61. Tran, V.S., Ngo, H.H., Guo, W., Zhang, J., Liang, S., Ton-That, C., Zhang, X. **(2015)**. Typical low-cost biosorbents for adsorptive removal of specific organic pollutants from water. Bioresour. *Technol*., 2015, 182, 353–363.

62. Bhat, A.H., Rehman, W.U., Khan, I.U., Khan, I., Ahmad, S., Ayoub, M., Usmani, M.A. **(2018)**. Nanocomposite membrane for environmental remediation. In: Jawaid, M., Khan, M.M. (Eds.), *Polymer-based Nanocomposites for Energy and Environmental Applications*. Elsevier, U.K, 15, 407–440.

63. Awad, A.M., Shaikh, S.M.R., Jalab, R., Gulied, M.H., Nasser, M.S., Benamor, A., Adham, S. **(2019)**. Adsorption of organic pollutants by natural modified clays: a comprehensive review. *Sep. Purif. Technol*., 228, 115719.

64. Zhang, G., Lin, Y., Wang, M. **(2011)**. Remediation of copper polluted red soils with clay materials. *J. Environ. Sci*., 23 (3), 461–467.

65. Otunola, B.O., Ololade, O.O. **(2020)**. A review on the application of clay minerals as heavy metal adsorbents for remediation purposes. *Environmental Technology & Innovation*, 18, 100692.

66. Wahab, N., Saeed, M., Ibrahim, M., Munir, A., Saleem, M., Zahra, M., Waseem, A. **(2019)**. Synthesis, Characterization, and Application of Silk/Bentonite Clay Composite for heavy Metal removal From Aqueous Solution. *Front. Chem*., 7, 654.

67. Seilkhanova, G., Imangaliyeva, A.N., Mastai, Y., Bakhym, A.B. **(2019)**. Bentonite polymer composite for water purification. *Bull. Mater. Sci*., 42, 60.

68. Stanly, S., Jelmy, E.J., John, H. **(2020)**. Studies on Modified Montmorillonite Clay and Its PVA Nanohybrid for Water Purification. *Journal of Polymers and the Environment*, 28(9), 2433-2443.

69. Zhao, Y., Abdullayev, E., Vasiliev, A., Lvov, Y. **(2013)**. Halloysite nanotubule clay for efficient water purification. *Journal of Colloid and Interface Science*, 406, 121–129.

70. Abdullayev, E., Lvov, Y. (2010). Clay nanotubes for corrosion inhibitor encapsulation: release control with end stoppers. *Journal of Materials Chemistry*, 20(32), 6681-6687.

71. Lee, S.Y., S.J. Kim, S.J., **(2002)**. Adsorption of naphthalene by HDTMA modified kaolinite and halloysite. *Appl. Clay Sci.*, 22(1-2), 55-63.

72. Alandis, N, M., Mekhamer, W., Aldayel, O., Hefne, J.A.A., Alam, M. **(2019)**. Adsorptive Applications of Montmorillonite Clay for the Removal of Ag(I) and Cu(II) from Aqueous medium. *Journal of Chemistry*.1-7.

73. Samad, A., Din, M.I., Ahmed, M. **(2020)**. Synthesis of zinc oxide nanoparticles impregnated clay tablets and their potential applications as point of use water purification intervention. *Desalination and Water Treatment*, 181, 251–257.

74. Ashour, E.A., Tony, M.A. **(2020)**. Eco-friendly removal of hexavalent chromium from aqueous solution using natural clay mineral: activation and modification effects. *SN Applied Sciences*, 2, 2042.

75. Kim, D-H., Yang, J-S., Baek, K. **(2012)**. Adsorption characteristics of As(III) and As(V) on alum sludge from water purification facilities. *Sep Sci Technol*., 47, 2211–2217

76. Tony, M.A., Lin, L.S. **(2022)**. Attenuation of organics contamination in polymers processing effluent using iron-based sludge: process optimization and oxidation mechanism. *Environmental Technology, 43(5), 718-727.*

77. Unuabonah, E.I., Günter, C., Weber, J., Lubahn, S., Taubert, A. 2013. Hybrid Clay: A New Highly Efficient Adsorbent for Water Treatment. *ACS Sustainable Chemistry & Engineering*, 1(8), 966-973.

78. Xi, Y., Mallavaraptants, M., Naidu, R. **(2010)**. Preparation, characterization of surfactants modified clay minerals and nitrate adsorption. *Applied Clay Science*, 48, 92–96.

79. Ghafar, H.H.A., Radwan, E.K., El-Wakeel, S.T. **(2020)**. Removal of Hazardous Contaminants from Water by Natural and Zwitterionic Surfactant-modified Clay. ACS omega, 5(12), 6834-6845.

80. Sari, A., Tuzen, M. **(2014)**. Cd(II) adsorption from aqueous solution by raw and modified kaolinite. *Applied Clay Science*, 88-89, 63–72.

81. Eren, E., Afsin, B., Onal, Y. **(2009)**. Removal of lead ions by acid activated and manganese oxide-coated bentonite. *J. Hazard Mater*., 161 (2–3), 677–685.

82. Khraisheh, M.A.M., Al-Deges, Y.S., Mcminn, W.A.M. **(2004)**. Remediation of wastewater containing heavy metals using raw and modified diatomite. *Chem. Eng. J*., 99, 177–184.

83. Polubesova, T., Zadaka, D., Groisman, L., Nir, S. **(2006)**. Water remediation by micelle-clay system: Case study for tetracycline and sulfonamide antibiotics. *Water Research*, 40, 2369– 2374.

84. Azzam, E.M.S., Eshaq, Gh., Rabie, A.M., Bakr, A.A., Abd-Elaal, A.A., El-Metwally, A.E., Tawfik, S.M. **(2016)**. Preparation and Characterization of Chitosan-Clay Nanocomposites for the Removal of Cu (II) from Aqueous Solution. *International Journal of Biological Macromolecules*,89, 507-517.

85. Ihekweme, G.O., Obianyo, I.I., Anosike-Francis, E.N., Anyakora, V.N., Odusanya, O.S., Onwualu, A.P. **(2021)**. Expanded clay aggregates multifunctionality for water purification: Disinfection and adsorption studies. *Cogent Engineering*, 8:1, 1883232.

86. Bedelean, H., Maicaneaunu, A., Burca, S., Stanca, M. **(2009)**. Removal of heavy metal ions from wastewaters using natural clays. *Clay Minerals*, 44, 487–495.

87. Ghorbanzadeha, N., Jungb, W., Halajniac, A., Lakzianc, A., Kabrab, A.K., Jeonb, B-H. **(2015)**. Removal of arsenate and arsenite from aqueous solution by adsorption on clay minerals. *Geosystem Engineering*, 18(6), 302-311.

88. Pandey, P., Dayanidhi, A., Mohanty, S., Nayak, S. K. **(2013)**. Effect of clay loading on flammability of poly(methyl methacrylate)/clay nanocomposites. *Journal of Thermoplastic Composite Materials*, 26(5), 663–679.

89. Morgan, A.B., Chu, L-L., Harris, J.D**. (2005)**. A flammability performance comparison between synthetic and natural clays in polystyrene nanocomposites. *Fire and Materials:An International Journal*, 29(4), 213–229.

90. Szustakiewicz, K., Kiersnowski, A., Gazińska, M., Bujnowicz, K., Pigłowski, J. **(2011).** Flammability, structure and mechanical properties of PP/OMMT nanocomposites. *Polymer degradation and stability*, 96(3), 291–294.

91. Zhu, F., Liu, D., Cai, G., Tan, X., Wang, J., Lu, H., Wilkie, C.A. **(2014)**. Thermal stability and flammability performance of polypropylene composites with silica pillared montmorillonites. *Polymers for Advanced Technologies*, 25(2), 211–216.

92. Zhang, J., Wilkie, C. A. **(2003)**. Preparation and flammability properties of polyethylene–clay nanocomposites. *Polymer Degradation and Stability*, 80(1), 163–169.

93. Wang, S., Hu, Y., Zhongkai, Q., Wang, Z., Chen, Z., Fan, W. **(2003)**. Preparation and flammability properties of polyethylene/clay nanocomposites by melt intercalation method from Na+ montmorillonite. *Material Letters*, 57(18), 2675–2678.

94. Tugba, Orhan T., Isitman, N.A., Hacaloglu, J., Kaynak, C. **(2011)**. Thermal degradation mechanisms of aluminium phosphinate, melamine polyphosphate and zinc borate in poly(methyl methacrylate). *Polym Degrad Stab*., 96(10): 1780-1787.

95. Shen, K.K., Kochesfahani, S, Jouffret, F. **(2008)**. Zinc borates as multifunctional polymer additives. *Polym Adv Technol*., 19(6): 469-474.

96. Braun, U., Schartel, B., Fichera, M.A., Jager, C. **(2007)**. Flame retardancy mechanisms of aluminium phosphinate in combination with melamine polyphosphate and zinc borate in glass-fibre reinforced polyamide 6, 6. *Polym Degrad Stab*., 92(8): 1528-1545.

97. Wu, Z.P., Hu, Y.C., Shu, W.Y. **(2010)**. Effect of Ultrafine Zinc Borate on the Smoke Suppression and Toxicity Reduction of a Low-Density Polyethylene/Intumescent Flame-Retardant System. *J App Polym Sci*., 117(1): 443-449.

98. Feng, C., Zhang, Y., Liang, D., Liu, S., Chi, Z., Xu, J. **(2015)**. Influence of zinc borate on the flame retardancy and thermal stability of intumescent flame retardant polypropylene composites. *Journal of Analytical and Applied Pyrolysis*. 115, 224-232.

99. Dogan M, Yilmaz A, Bayramli E. **(2010)**. Synergistic effect of boron containing substances on flame retardancy and thermal stability of intumescent polypropylene composites. *Polym Degrad Stab*., 95(12): 2584-2588.

100. Fang, Y., Wang, Q., Guo, C., Song, Y., Paul A.C. **(2013)**. Effect of zinc borate and wood flour on thermal degradation and fire retardancy of Polyvinyl chloride (PVC) composites. *Journal of Analytical and Applied Pyrolysis*, 100, 230–236.

101. Yıldız, B., Seydibeyoğlu, M. Ö., Güner, F.S. **(2009)**. Polyurethane–zinc borate composites with high oxidative stability and flame retardancy. *Polymer Degradation and Stability*, 94(7), 1072-1075.

102. Qian, Y., Zhou, S., Chen, X. **(2017)**. Flammability and thermal degradation behavior of ethylene-vinyl acetate/layered double hydroxides/zinc borate composites. *Polymers for Advanced Technologies*, 28(3), 353-361.

103. Jiang, M., Zhang, Y., Yu, Y., Zhang, Q., Huang, B., Chen, Z., Chen, Tingting; Jiang, J. **(2018)**. Flame retardancy of unsaturated polyester composites with modified ammonium polyphosphate, montmorillonite, and zinc borate. *Journal of Applied Polymer Science*, 47180.

104. He, M., Cao, W. C., Wang, L. J., Wilkie, C. A. **(2013)**. Synergistic effects of organo-sepiolite and zinc borate on the fire retardancy of polypropylene. *Polymers for Advanced Technologies*, 24(12), 1081–1088.

105. Tai, Q., Yuen, R.K.K., Yang, W., Qiao, Z., Song, L., Hu, Y. **(2012)**. Iron-montmorillonite and zinc borate as synergistic agents in flame-retardant glass fiber reinforced polyamide 6 composites in combination with melamine polyphosphate. *Composite Part A: Applied Science and Manufacturing*, 43(3), 415–422.

106. Wang, L., He, X., Lu, H., Feng, J., Xie, X., Su, S., Wilkie, C.A. **(2011)**. Flame retardancy of polypropylene (nano)composites containing LDH and zinc borate. Polymer for advanced technologies, 22(7), 1131–1138.

CHAPTER 3: Published paper - Effect of LDHs and other clays on polymer composite in adsorptive removal of contaminants

M. Mohapi[1], J.S Sefadi[2], M.J. Mochane[1], S.I. Magagula[1] and K. Lebelo[1]

[1]Department of Life Sciences, Central University of Technology, Free State, Private Bag X20539, South Africa

[2]Department of Physical and Earth Sciences, Sol Plaatje University, Kimberley, 8301, South Africa

***** Correspondence:Correspondence:jeremia.sefadi@spu.ac.za(J.S.S.), mochane.jonas@gmail.com or mmochane@cut.ac.za (M.J.M.);

Crystals 2020, 10(11), 957; https://doi.org/10.3390/cryst10110957

Abstract: Recently, the development of a unique class of layered silicate nanomaterials has attracted considerable interest for treatment of wastewater. Clean water is an essential commodity for healthier life, agriculture, and a safe environment at large. Layered double hydroxides (LDHs) and other clay hybrids are emerging as potential nanostructured adsorbents for water purification. These LDH hybrids are referred to as hydrotalcite-based materials or anionic clays and promising multifunctional two-dimensional (2D) nanomaterials. They are used in many applications including photocatalysis, energy storage, nanocomposites, adsorption, diffusion and water purification. The adsorption and diffusion capacities of various toxic contaminants heavy metal ions and dyes on different unmodified and modified LDH-samples are discussed comparatively with other types of nanoclays acting as adsorbents. This review focuses on the preparation methods, comparison of adsorption and diffusion capacities of LDH-hybrids and other nanoclay materials for the treatment of various contaminants such as heavy metal ions and dyes.

Keywords: Layered double hydroxides (LDHs); other nanoclays; organically modified LDH; water purification; adsorption; adsorption interaction; diffusion

3.1. INTRODUCTION

A reliable, affordable, sustainable, and easily accessible clean water supply chain for many societies in the entire world is an essential component for healthier life and safe environment. However, due to limited economical resources or lack of infrastructure, millions of poor and vulnerable people including children die annually from diseases caused by an inadequate water supply, poor water quality, sanitation, and hygiene. Recently, many countries and communities experienced the global challenge/phenomenon known as “Coronavirus (COVID-19) or COV2 infections”, which required a frequent washing of hands with clean water and soap or hand sanitizer to avoid or curb the spread (flatten the curve). These key risk aspects or factors adversely impact on food security, livelihood diversities and learning opportunities for poor and most susceptible households across the world. According to the World Health Organization (WHO), almost 1.7 million people lost their lives because of water pollution, and four billion cases of diverse health issues were reported every year due to water borne diseases [1]. Table 1 represents various types of water contaminants, their sources and negative effects. To improve access to quality and safe drinking water, sanitation, and hygiene (WASH), there must be value-added infrastructure investment in dealing with and managing the freshwater ecosystems and sanitation facilities on a local level in many developing countries. The improved WASH is thus fundamental to poverty reduction, promotion of equality, and support for socioeconomic development under the sustainable development goals (SDGs) [2,3]. The most essential requirements for clean water supply chain is a proper material with high degree of separation capacity, low cost, porosity, and reusability [4–7]. Nanotechnology presents a set of opportunities to develop nanomaterials for effective water purification systems. Optimization of the properties like hydrophilicity, hydrophobicity, porosity, mechanical strength and dispersibility [8–10] is the best option to treat wastewater. Due to their high surface area, high chemical reactivity, adsorption capabilities, excellent mechanical strength and cost-effectiveness, nanomaterials have a huge potential to effectively purify water in numerous ways [8,10–12] by removing various contaminants. This can be done by using different purifiers with different pore sizes such as: microfiltration (MF), ultrafiltration (UF), nanofiltration (NF) and reverse osmosis (RO) (Figure 1). However, the main stumbling block associated with addition of 2D nanomaterials is the aggregation or agglomeration that restricts their effective use in many industrial applications. This daunting aggregation or agglomeration challenge of nanomaterials can be minimized by (i) transforming 2D nanomaterials into nanocomposites and (ii) surface modification of 2D nanomaterials, owing to their

excellent interfacial interaction between the surface of 2D nanomaterials and polymer matrices. Surface modification of nanomaterials (SMNs), compared to unmodified nanomaterials, has attracted a considerable interest in science communities.

Table 3.1. List of different water pollutants with their sources and adverse effects.

Water pollutants	Sources of pollutants	Effects of pollutants	Refs
Pathogens	Viruses and bacteria	Causes water borne diseases which can affect anyone. Those at high risk are infants, younger children, the elderly and patients with underlying illnesses (diabetes, chronic diseases of heart disease and kidney).	[14]
Agricultural Pollutants	Agricultural chemicals	Directly affect the fresh water resources and can cause health-related problems contributing to blue baby syndrome leading to the death in infants.	[15]
Sediments and suspended solids	Land cultivation, demolition, mining operations	Affect water quality and bring about toxicity on fish life and involve reduced oxygen transfer at the gills, reduced ability to clear sediment from the gills, and diminished bloodstream.	[16]
Inorganic pollutants	Metals compounds, trace elements, inorganic salts, heavy metals, mineral acids	Cause several human health –related problems on the flora and fauna of the Earth system such as abnormal growth, high risk of cancer, diabetes and obesity.	[17]
Organic pollutants	Detergents, insecticides, herbicides	They are resistant to degradation and tend to bioaccumulate within the food chain. Cause various negative health issues including cancer, immune system	[18]

		suppression, decrements in cognitive and neurobehavioral function, and at least some of them increase the risk of chronic diseases, such as hypertension, cardiovascular disease, and diabetes.	
Industrial pollutants	Municipal pollutant water	Cause air, water and land pollution leading to many environmental problems, illnesses and loss of life.	[19]
Radioactive pollutants	Different Isotopes	Exposure to high levels of radiation causes acute health problems like bones, teeth, skin burns and cancer as well as cardiovascular disease.	[20]
Nutrients pollutants	Plant debris, fertilizer.	Cause serious environmental and human health issues which influence the socio-economic issues. Causes algae to grow and expand higher than ecosystems can handle.	[21]
Macroscopic pollutants	Marine debris	Macroscopic pollutants are non-biodegradable materials which cause garbage wastes and plastic pollution.	[22]
Sewage and contaminated water	Domestic wastewater	Causes the quality of the water to worsen, water borne diseases and affects aquatic ecosystems.	[23]

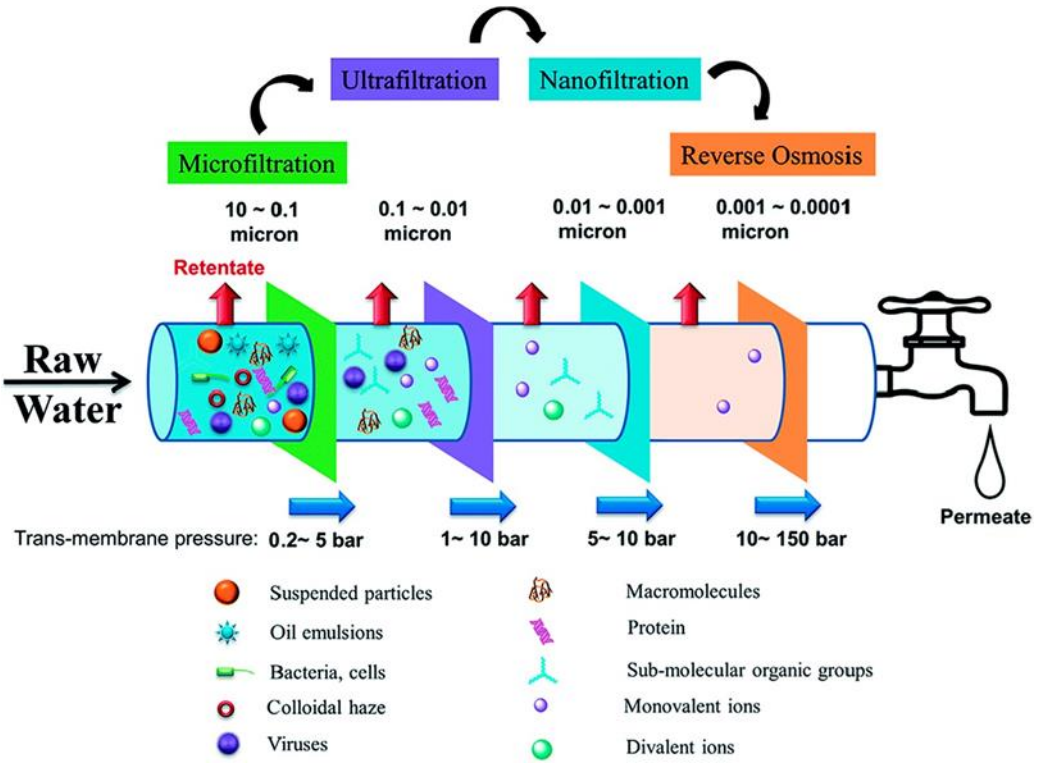

Figure 3.1. Trans-membrane pressure processes for water treatment technologies with different pore sizes. Reproduced with permission from Reference [13]. Copyrights 2018, Elsevier Science Ltd

Nanocomposites are multi-phasic materials, in which at least one of the phases shows dimensions in the nano range of 10–100 nm [24,25]. Currently, these materials have emerged as alternatives to overcome deficiencies of different engineering materials and are said to be the 21st century materials, due to their design uniqueness and property combinations which are different from conventional composites. Nanocomposite materials can be classified according to their primary phase (matrix) and secondary phase (reinforcing filler) [26,27]. Among different nanocomposites, polymer-based nanocomposites (PNCs) have become a noticeable field of current research interest and innovation development. PNCs have a lot of advantageous multifunctional properties such as film forming ability, dimensional variability, and activated functionalities [8,28]. Generally, the properties of PNCs are strongly related to the type of polymer matrix and the extent of dispersion of nanomaterials incorporated into the polymer matrix, as well as interfacial interactions between the polymer and nanomaterials [29–31]. The improved interfacial interactions of the nanomaterials with pure polymer change the overall morphology leading to synergistic effects in the nanocomposite properties. The accomplished properties are much better than the individual constituents. Finally, the properties of the PNCs are directly dependent on the volume fraction of nanomaterials, aspect ratio, alignment in matrix and other geometrical factors [32,33]. The main challenges in the development of superior PNCs are (i) the selection of appropriate nanomaterials that possess specific interfacial interaction, (ii) compatibility of nanomaterials with polymer matrix and (iii) suitable processing method to evenly disperse and dispense these nanoparticles within a polymer matrix. The impact of polymer nanocomposites (PNCs) in wastewater treatment can be recognized by an uninterrupted rise in publications over the past ten years. This is contrary to the less extensively instigated environmental impacts of nanomaterials in polymer nanocomposites in water purification (Figure 3.2).

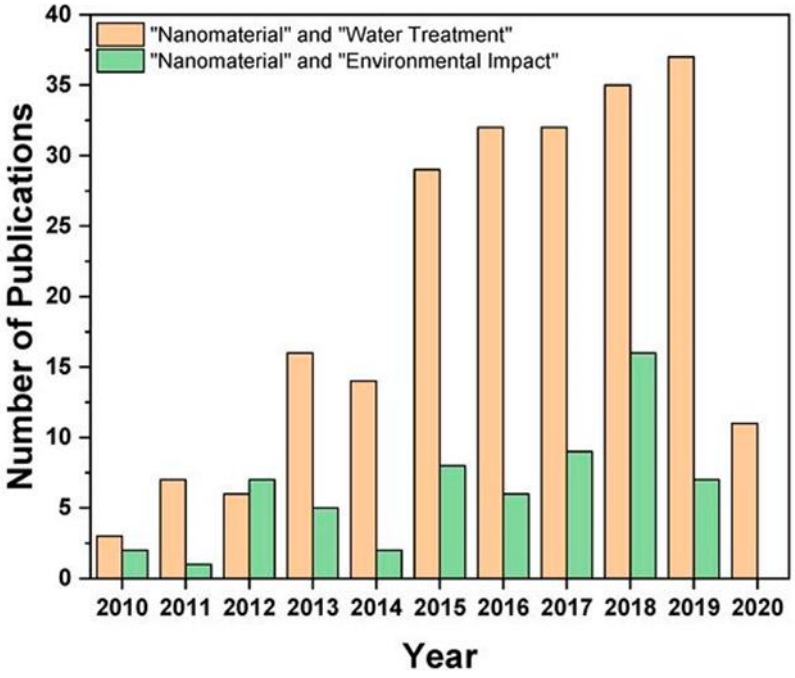

Figure 3.2. Number of publications in polymer nanocomposites (PNCs) and water treatment. Reproduced with permission from Reference [34]. Open Access 2020, MDPI Water.

In this review, we focus on the comparison of 2D nanomaterials such as layered double hydroxides (LDHs) and other nanoclays in polymer-based nanocomposites (PNCs), their preparation methods and multifunctional properties and their use for water purification. The primary goal is to highlight an optimal efficiency of LDHs and other nanoclays adsorption capacities and recent progress of nanomaterials in decontamination ability of various pollutants with selectivity including practical and potential applications.

3.2. Comparison of other nanoclays and LDHs crystal structures

3.2.1. Other nanoclays crystal structure

Nanoclays (NCs) are a broad class of naturally occurring inorganic minerals optimized for use in polymer-clay nanocomposites for water purification and environmental protection. NCs are versatile and two-dimensional (2D) building blocks for multifunctional material systems with several property enhancements targeted for many applications. Based on their chemical composition and particle morphology, clay minerals are categorized into many classes such as smectite, chlorite,

kaolinite, illite and halloysite. Nanoclays have been studied and developed for various applications [29,31,35] and are abundantly available, very cheap and low environmental impact. Clay minerals are members of the phyllosilicate or sheet clay silicates consisting of hydrated alumina–silicates and can be used as natural nanomaterials or nano-absorbent since the dawn of nanotechnology [36]. Nanoclays are nanoparticles of layered mineral silicates with layered structural units that can lead to the formation complex/multifaceted clay crystallites by stacking these layers [37]. The basic building blocks of clay minerals are tetrahedral silicates and octahedral hydroxide sheets [38]. Octahedral sheets consist of aluminum or magnesium in a six-fold coordination with oxygen from a tetrahedral sheet and with hydroxyl (Figure 3.3). Tetrahedral sheets consist of silicon–oxygen tetrahedra concomitant to neighboring tetrahedral sharing three corners, while the fourth corner of each tetrahedron sheet is connected to an adjacent octahedral sheet via a covalent bond.

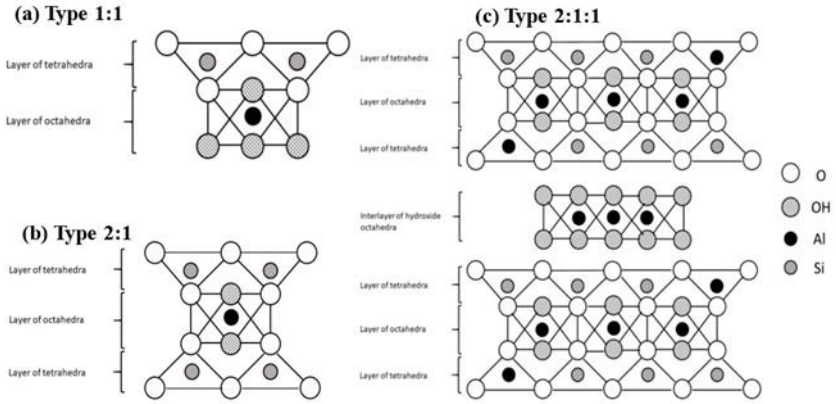

Figure 3.3. The layer phyllosilicate structures: (a) Type 1:1; (b) Type 2:1; and (c) Type 2:1:1. Reproduced with permission from Reference [39]. Open Access 2019, MDPI Animals.

The arrangements of these sheets influence a number of contributing factors in clay silicates. Based on their mineralogical composition, there are nearly thirty different types of nanoclays used in various applications [40,41]. Table 3.2 depicts three major types of phyllosilicates which are distinguished as 1:1 layer type (T-O), 2:1 layer type (T-O-T) and 2:1:1 layer type (T-O-T:O) common in nanoclay materials. In 1:1 lattice structures (T-O), each tetrahedral is connected to one octahedral sheet, while in 2:1 lattice structures (T-O-T), each octahedral sheet is connected to two tetrahedral sheets, one sheet on each side. Lastly, in 2:1:1 lattice structures (T-O-T:O), each

octahedral sheet is adjacent to another octahedral sheet and connected to two tetrahedral sheets [31,42–44].

Table 3.2. Classification of clay minerals and their characteristics.

Clay minerals group	Layer type ratio	Characteristics	Ref.
Rectorite, kaolinite, Halloysite, Chyrsotile.	1:1 (T-O) Dioctahedral	Non-expansive, no layer charge & very little isomorphic substitution.	[41,42]
Smectite Vermiculite	2:1 (T-O-T) dioctahedral Trioctahedral	Highly expansive, low layer charge moderately expansive, Intermediate layer charge. extensive isomorphic substitution.	[43]
Pyrophylite talc, mica, brittle mica.	2:1 (T-O-T) dioctahedral Trioctahedral	Non-expansive, high layer charge, extensive isomorphic substitution.	[43]
Chlorite	2:1:1 (T-O-T-O) dioctahedral Trioctahedral Di, Trioctahedral	Non-expansive, high layer charge, extensive isomorphic substitution.	[44,45]

Halloysite nanoclay is an aluminosilicate nanotube naturally occurring clay material with the average dimensions of 15 nm × 1000 nm [45]. This halloysite nanoclay has (1:1-layer type) and the hollow tube structure is primarily utilized in medical applications, food packaging industry and rheology modification [46]. The most commonly used nanoclay in materials applications is plate-like montmorillonite (MMT) material. This MMT has approximately 1 nm of aluminosilicate layers which are surface coated with metal cations in a multilayer stacks of ~10 µm. Depending on surface modification of the clay layers, MMT can be dispersed in a polymer matrix to form polymer-clay nanocomposites with applications such as, flame-resistance, solidifying agents, water purification and gas permeability modification. MMT clay layers with 2:1 layered silicates of T-O have high cation exchange capacity (CEC) on the siloxane surface that can interact well with different substances like organic or biological molecules [47,48]. The MMT nanoclay stacks have attracted a lot of interest because of outsized surface area, swelling behavior and high cation exchange capacity [49,50]. Unlike MMTs, halloysite materials are easily dispersed in many polymers showing no exfoliation due to scarcity of OH groups on their surfaces. In addition, these tube-like nanoclays are excellent nanomaterials for numerous chemical molecules [51]. Therefore, the modified clays are used as effective reinforcing phase for polymers to improve their mechanical and thermal properties. Nanoclays acting as carriers continuously and constantly released some active molecules such as flame-retardants, antioxidants, anticorrosion and antimicrobial agents [52,53]. In recent years, the research and development of novel polymer/nanoclay composites for water purification has attracted a lot of attention in the field of material chemistry [54]. Rigid nanoclay like layered double hydroxides (LDHs) must be used as an effective reinforcing filler to polymer structures and impede the polymer chains free movement adjacent to the filler [29–31,54].

3.2.2. Layered double hydroxides (LDHs) crystal structure

Layered double hydroxides (LDHs) also known as hydrotalcite (HT)-like materials are a class of synthetic two-dimensional (2D) nanostructured anionic clays with a highly tunable brucite [Mg(OH)2]-like layered crystal structure (Figure 3.4). These inorganic materials contain layers of positively charged metal hydroxides with multivalent anions for neutrality. The LDHs are generally represented by formula

$$[M2+ 1-X M3+ X (OH)2] X+ [A n-]X/n mH2O \quad (1)$$

In this formula, M2+ and M3+ represent the divalent and trivalent layer cations, respectively. An− is the exchangeable anion such as OH− , F − , NO− 3 , Cl− , CO2− 3 and/or SO2− 4 . Reasonably stable LDH phases are often observed only when the value of x varies in the range 0.22–0.33 resulting in M2+/M3+ molar ratios of 2:1 to 4:1 [55–59]. If x is more than 0.33, then an increased number of neighboring M3+ containing octahedra leads to the formation of M(OH)3. If x is less than 0.2, then an increased number of neighboring M2+ containing octahedra in the brucite-like sheets resulted in the precipitation of M(OH)2. However, these limits of the value of x must be regarded as the maximum interval, which can be narrower depending on the composition of the LDH.

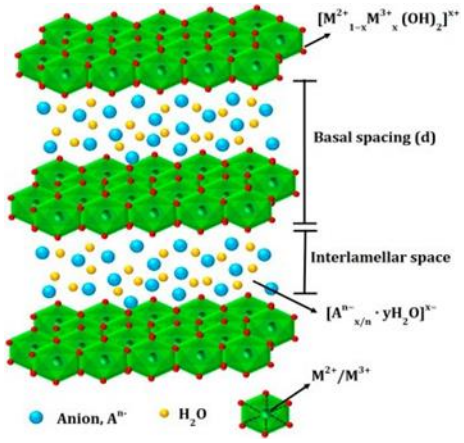

Figure 3.4. Structure of layered double hydroxide (LDH). Reproduced with permission from Reference [60]. Copyrights 2018, Elsevier Science Ltd.

As result, a large class of isostructural materials, which can be well-thought-out complementary to aluminosilicate clays, with useful physical and chemical properties can be achieved. This can be carried out by changing the nature of the metal cations, the molar ratios of divalent/trivalent cations, and the types of interlayer anions. These compounds are composed of positively charged brucite-type octahedral sheets, interchanging with interlayers containing carbonate anions in the natural mineral or other exchangeable anions in the synthetic hydrotalcite (HT)-like materials, along with water molecules. The hydrogen bonding associated with the interlamellar water molecules serves as a driving force for the stacking of the clay layers (see Figure 3.4).

3.2.3 An overview of preparation methods of LDHs

In the last few decades, a number of studies associated with the synthesis of LDH have been reported and some are easy and simple to process for many industrial applications. Various kinds of low cost, environmentally and eco-friendly LDHs can be synthesized by using fundamental methods of choice. These commonly used methods include co-precipitation; ion exchange; reconstruction; sonochemical method; hydrothermal/solvochemical method; sol–gel method; induced hydrolysis method; and urea method [57,59–65].

3.2.3.1 Co-precipitation method

Co-precipitation method is also referred to as a large-scale and direct technique typically utilized for the synthesis of LDH platelets with different divalent and trivalent cations (M2+ and M3+) coupled with many inorganic anions (Cl^- , NO^-_3 , CO^{2-}_3) and organic molecules/outsized biomolecules [57]. In this co-precipitation method, a dropwise addition of alkali solution into the divalent and trivalent layer cations/mixed metal salts containing solution in a proper ratio resulted in formation of LDH as shown in Figure 3.5. During this method, a pH emerged as a very crucial factor which negatively influences both the structural and chemical properties of LDH component to a larger extent. In a dropwise addition, the pH of the reaction mixture is maintained constantly at the range of 8–10 and purged at N_2 atmosphere in an attempt to achieve high chemical homogeneity in LDH [61]. The resulting solution mixture is allowed to stay for a long period of time in order to obtain a reproducible and well-crystallized LDH structural material. The obtained precipitate is collected by filtration, washed thoroughly with deionized water and dried in an oven overnight. The underpinning principle of co-precipitation is based on a simple, economical and industrially feasible technique utilized for the synthesis of metal oxide materials in solution. This led to the brucite-like layers' formation, which uniformly dispersed metallic cations and inorganic anions.

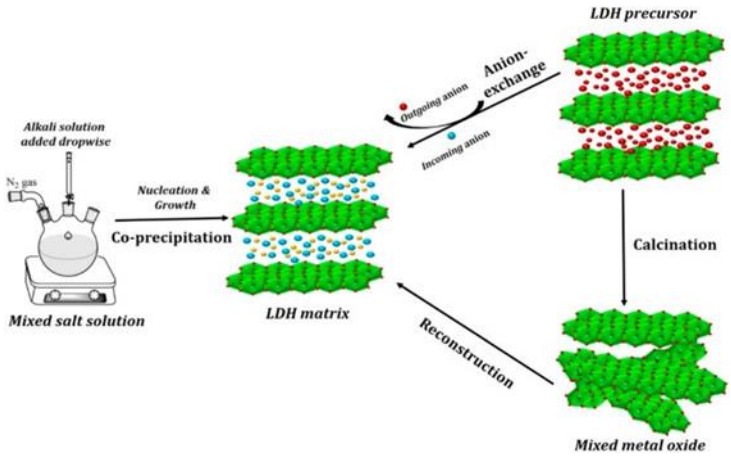

Figure 3.5 Schematic representation of co-precipitation, ion exchange and reconstruction methods LDH. Reproduced with permission from Reference [59]. Copyrights 2018, Elsevier Science Ltd.

3.2.3.2 Ion exchange method

Anion-exchange method is better for the incorporation of layered silicates into a solution containing anions species ready for exchange as compared to other methods. The ion exchange method (Figure 3.5) is based on the exchange of anions in interlayer space with other anionic species. In this method, the precursor LDH is suspended in an aqueous solution containing the anionic species to be exchanged. The suspension is then stirred constantly for several hours at room temperature. The solid precipitate is then collected by filtration, washed several times with deionized water and dried in an oven overnight. Furthermore, the interlamellar region can also contain water molecules and is referred to as internal water dominant region where water molecules are organized by the inorganic layers via hydrogen bonding. The high anion exchange capacity of LDH matrix-like compounds produces their interlayer ion exchange by outgoing anions and incoming useful anions, easily accomplished and reflected in LDH precursor product formation [62] (Figure 3.5).

3.2.3.3 Reconstruction method

As shown in Figure 3.5, this reconstruction method is a well-known regeneration or memory effect method of LDH. According to this method, the layered structure of brucite-like LDH with

carbonate anion is used as a precursor during hydration and calcination due to its behavioral pattern. The reconstruction method is based on the memory effect or regeneration which is one of the unique properties of LDHs. In first step, the calcination of LDHs is performed at a particular temperature to obtain mixed metal oxides (Figure 3.5) and then subjected to rehydration in aqueous solution with the anion to be intercalated [63]. The solid precipitate is collected by filtration, washed several times with deionized water and dried in an oven overnight. The structural recovery, however, depends upon some experimental conditions such as, calcination temperature, duration and rate of heating. The reconstruction method is useful mainly in the preparation of large organic anions intercalated LDH [63,64].

3.2.3.4 Sonochemical method

In sonochemical method, LDHs are prepared by co-precipitation method followed by sonochemical treatment. In first step, the co-precipitation method is performed to the latter as explained fully under Section 2.3.1 above. In the second step after successful completion of mixing, the resultant solution is subjected to ultrasound irradiation at a given time and temperature. The solid precipitate is filtered, washed thoroughly with deionized water and put in an oven overnight for further drying. This sonochemical method is best described as a synthetic and high intensity ultrasonic/three-fold acoustic cavitation phenomenon which assist in improving the crystallinity of LDH phases [61,65]. When the solution mixture is subjected to ultrasonic irradiation, rapid movement of the fluid leads to three-fold acoustic cavitation phenomenon (Figure 3.6) in which microbubbles undergo nucleation formation, growth and implosive collapse [65]. The formation of microbubbles produced a distinctive hot spot due to the compressional heating induced by collapsing of bubble and therefore yields the bubble with extremely high temperature, pressure and cooling rates [66].

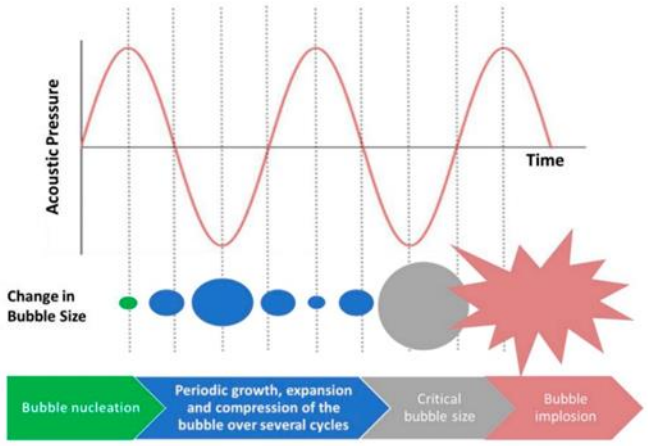

Figure 3.6 Schematic representation of three-fold acoustic cavitation phenomenon. Reproduced with permission from Reference [67]. Open Access 2020, MDPI Energies.

3.2.3.5 Hydrothermal/Solvothermal method

The hydrothermal synthesis method illustrated in Figure 3.7a,b is similar to the co-precipitation method. In this method, two solutions containing M2+ and M3+ metal salts are added dropwise to another solution containing base under vigorous stirring at room temperature. Thus, the suspension is transferred into a Teflon-lined autoclave and heated at higher temperature (100–180 ◦C) for many hours (10–48 h) based on the metal ions [68]. The pH of the supernatant solution is in the threshold range of 8–10. The solid precipitate is collected by centrifugation washed thoroughly with deionized water and ethanol and dried in an oven overnight. The hydrothermal method is useful for synthesis of highly crystalline LDHs with uniform morphology compared to co-precipitation technique [69]. Solvothermal method is a synthesis method where a chemical reaction takes place in a closed solvent system at elevated temperatures above the boiling point and standard pressures. In a typical solvothermal synthesis, the amount of organic solvent such as glycerol or alcohol is used in a non-aqueous solution at somewhat high temperatures, while hydrothermal method refers to synthesis via chemical reactions in aqueous solution just above boiling point of water in a closed vessel. Many scientists realized the importance of preparing inorganic nanomaterials using hydrothermal and solvothermal reactions, upon which effective syntheses of novel high-technology and green materials would be established. The main reason for this remarkable and milestone achievement in preparing nanomaterials is the easy of processing which

include low temperature process, low energy consumption, no harm to the environment and more importantly high degree of crystallinity of the material can easily be produced [68,69]

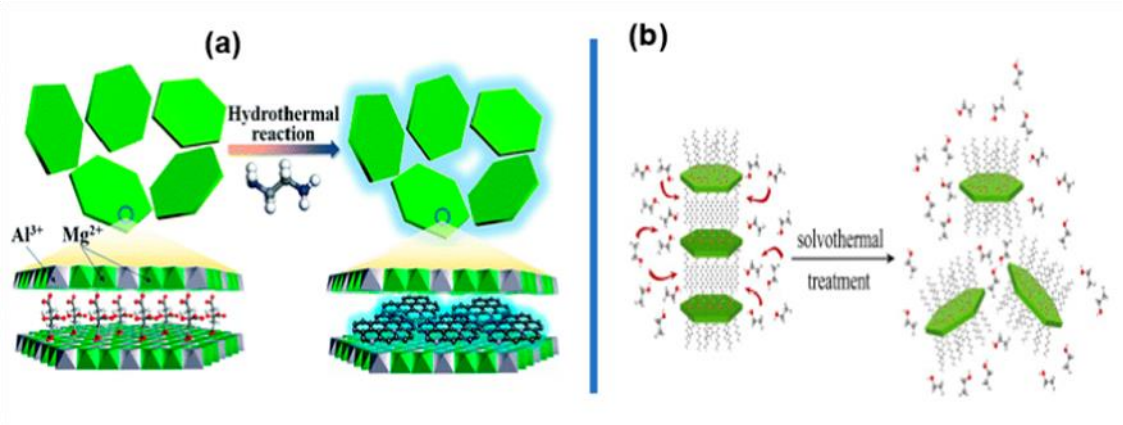

Figure 3.7 Schematic representation of (a) hydrothermal method, (b) solvothermal treatment of layered double hydroxide (LDH). Reproduced with permission from Reference [70,71]. Copyrights 2017 & 2019, RSC & Elsevier

3.2.3.6 Adsorption and layer-by-layer method

In this case, adsorption (Figure 3.8a) can be referred to as the adhesion of divalent and trivalent ions (M2+ and M3+) from a liquid or dissolved solid to surface of the LDH adsorbent. This creates a film of the adsorbate over the surface in many processes such as chemical, physical, biological and natural systems and widely used in various industrial applications [72]. The adsorption process may occur through weak van der Waals forces (physisorption) or covalent bonding (chemisorption) and also may occur due to electrostatic attraction between the adsorbate and surface of the adsorbent. It is a surface phenomenon most widely adopted in wastewater treatment for removal of various organic contaminants from aqueous solution.

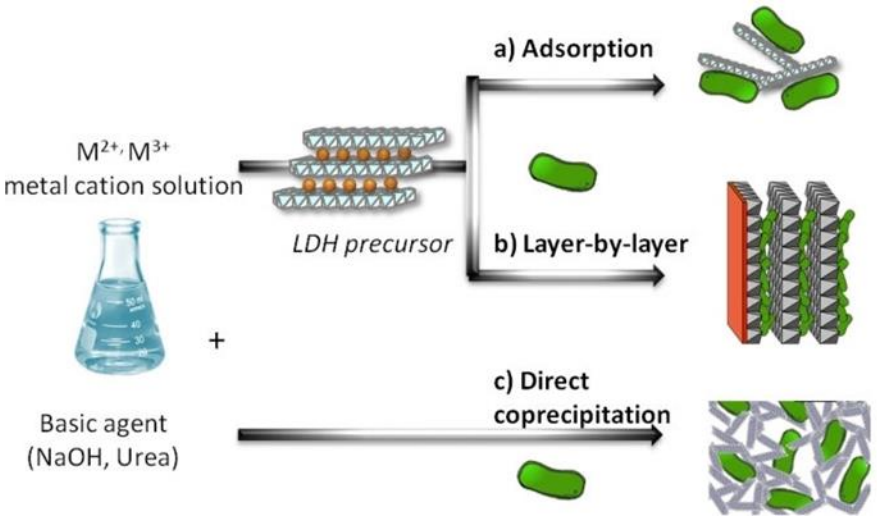

Figure 3.8 Schematic representation of (a) adsorption method, (b) layer-by-layer deposition, (c) direct co-precipitation method of layered double hydroxide (LDH). Reproduced with permission from Reference [73]. Copyrights 2018, John Wiley and Sons.

Layer-by-layer (LBL) assembly (Figure 3.8b) is a universal method for coating substrates with polymers, colloids, biomolecules, and even cells. This presents superior control and versatility when compared to other thin film deposition techniques in certain research and industrial applications. The LBL technique is known to support electrostatic interactions between positively charged layers and negatively-charged molecules and leads to nanostructured thin films [74]. This LBL deposition technique has three types of methods known as (i) the dipping layer-by-layer deposition technique (dipping-LBL); (ii) spray layer-by-layer deposition method (spray-LBL) and (iii) spin layer-by-layer deposition method (spin-LBL) method. Dipping-LBL is executed by chronologically adsorbing opposite charged materials onto a substrate via enthalpic and entropic driving forces [75]. In this method, the time depends on both the diffusion and adsorption of molecules, solutions or suspensions. Spray-LBL is a deposition technique where divalent and trivalent solutions are sprayed onto a vertical substrate, and the layer is formed after completion of drying in an oven overnight [58]. In spin-LBL method, the solutions or suspensions are deposited on a substrate attached to a spin coater, and the rotation speed generates a high centrifugal force. Thus, high rotational speed with high airflow rate at the surface leads to fast

drying times of the liquid which in turn quickly and easily produce very uniform layers or thin films. In both spray-LBL and spin-LBL methods, the total time does not depend on the diffusion of molecular species. The co-precipitation method shown in Figure 3.8c has already been previously explained in Section 2.3.1.

3.2.3.7 Sol-gel method

The sol-gel method is a low-cost, simple preparation method and efficient wet-chemical method of high-purity metal oxide materials from LDH precursors through hydrolysis and condensation processes [76]. In this method (Figure 3.9), the mixed salt solution of Al(NO3)3·9H2O and Mg(NO3)2·6H2O and alkali solution of NH4OH were concurrently added to a beaker and heated under refluxed condition. The pH of the suspension is maintained at 8–10 by adding NH4OH base under magnetic stirring at ambient temperature until the gel formation is achieved. The resultant gel like product is filtered, washed properly with deionized water via re-dispersion/centrifugation and dried overnight. The formed gel was re-dispersed in water by ultra-sonication to produce LDH single layer nanosheets (SLNSs) dispersion. A portion of the LDH SLNS gel was further tried in an oven at 80 ◦C for 24 h to yield a well-crystallized LDH SLNS sol sample. The LDHs synthesized using sol-gel method is thermally very stable, but less crystalline than those synthesized via the co-precipitation method.

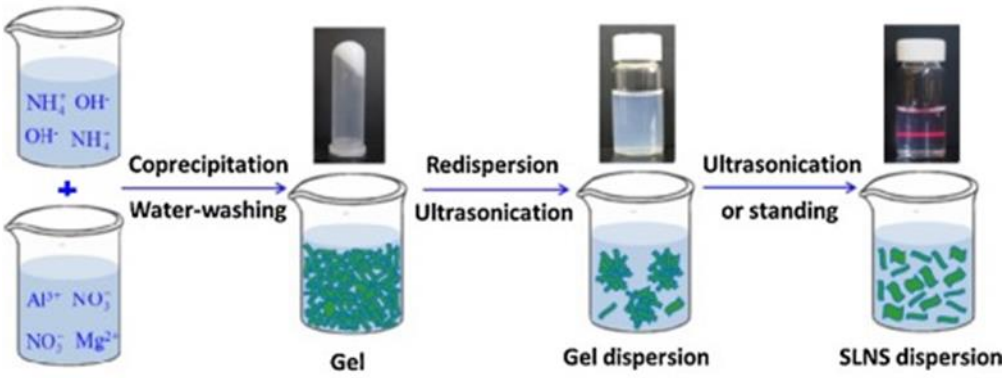

Figure 3.9 Schematic representation of sol-gel method of layered double hydroxide (LDH). Reproduced with permission from Reference [77]. Copyrights 2016, Elsevier.

3.2.3.8 Induced hydrolysis method

In this method, metal oxides are added dropwise to an acidic solution containing M3+ metal salts. The metal oxides are dissolved progressively in the acidic solution and precipitated into LDH. The pH is cushioned at 8–10 by the oxide suspension [59]. The obtained solid precipitate is collected, filtered, washed methodically with deionized water and dried at 80 ◦C for 24 h. This method of induced hydrolysis can also be used for synthesis of LDH with di-divalent, di-tetravalent and tri-trivalent systems.

3.2.3.9 Urea method

In general, urea is added to an aqueous solution of preferred M2+ and M3+ metal salts and heated under reflux condition for several hours. The precipitate product is collected by filtration, washed thoroughly with deionized water and dried overnight. The rate of urea hydrolysis can possibly increase significantly with an increase in the reaction temperature to 100 ◦C [59]. The urea molecules undergo degradation to form ammonium carbonate, which initiates the precipitation into LDH with CO_3^{2-} as interlayer anion. This urea method provides high degree of crystallinity and a fine particle size distribution. Urea-based co-precipitation provided the better crystallinity and particle size due to thermal treatment and hydrolysis of urea which is proceeded in a very slow manner [57,59,60].

In comparison to many other nanoclays or layered materials, LDHs have compositional multiplicities in the cationic layers and in the hydrated interlayer of anions for charge balance which lead to some functional diversities. This implies that LDHs among layered materials have the great advantages and number of possible compositions, metal-anion combinations and morphologies useful for synthesis and processing methods. Apart from that, LDHs can be used in a variety of potential applications due to their anion exchangeability, compositional flexibility, good biocompatibility, low cost, facile synthesis, pH dependent solubility, thermal stability and high chemical versatility [78]. Due to their tunable chemistry and high charge density tailored properties, LDHs have attracted great attentions in various technologically significant fields and applications such as production of renewable energy [4,21,29], adsorbents [7,41,79], water purification [8–10,80,81], antimicrobial activities [10,24], sensors [29,82–84], flame resistance

[48], drug delivery [85,86], cosmetics [87,88] and environmental catalysis [57,89,90]. In our previous work [91], detailed discussion about various applications were made and the current work focuses more on water purification.

3.2.4. Preparation methods of polymer-clay nanocomposites (PCNCs) and surface modification

The manufacturing of PCNCs depends mainly on a proper method selection which ensures acceptable level of dispersion of the nanofillers throughout the polymer matrix. Several processing methods were employed in preparing polymer-based clay nanocomposites such as in situ polymerization, the melt blending, and solution blending techniques [92,93] (see Figure 3.10). In each preparation method, an absolute goal is to achieve a desired uniform dispersion of nanoclays in the pristine polymer matrix. However, there are currently numerous interesting views about the applications and usage of these methods. According to the following studies [18,94,95], melt blending is regarded as a significantly, industrially viable and ecofriendly technique with high economic potential for preparation of polymer–clay nanocomposites. The in situ polymerization method is a commonly used synthesis technique and easy to modify by changing the polymerization conditions [96] and provides uniform dispersion. Both these methods require either a large amount of organic solvent or high viscosity or thermally unstable polymers at high temperatures. In comparison to melt blending, the solution-blending technique often produces pleasing dispersion of clay layers in the polymer matrix [31] due to its low viscosity and high agitation power. Each technique has its own relevant significance and limitations in relation to certain required industrial applications.

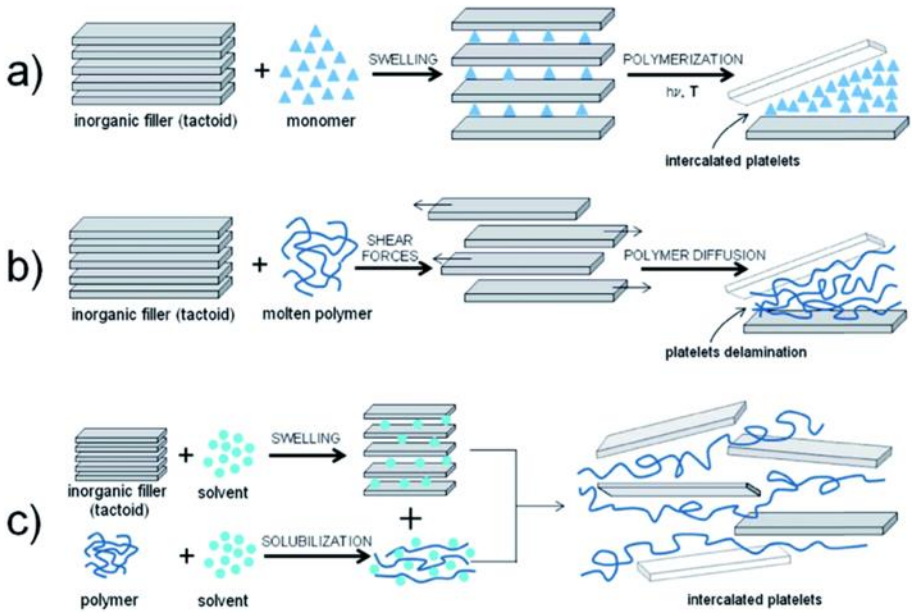

Figure 3.10. Illustration of (a) in situ polymerization, (b) melt intercalation, (c) solution intercalation. Reproduced with permission from Reference [97]. Open Access 2014, Royal Society of Chemistry.

3.2.4.1. In-Situ polymerization technique

Due to the silicate dispersion deduced information, in situ polymerization is more effective in the preparation of composites and can sidestep the harsh thermodynamic requirements related to the polymer intercalation process [18,31,98] (Figure 3.10a). Furthermore, this polymerization technique (i) tolerates resourceful molecular strategies of the polymer matrix; (ii) it provides an effective approach to the synthesis of different polymer/nanoclay composites with prolonged property range and (iii) facilitates the development of the interface between the filler and the polymeric matrices by modification of the matrix composition and structure. Many studies focus on preparing novel polymer/nanoclay composites via the in situ polymerization method and demonstrate the benefits of this method in comparison with other types of synthesis methods [18,31,98,99]. For instance, Ozkose et al. [100] investigated the synthesis of poly(2-ethyl-2-oxazoline)/nanoclay composites for the first time using in-situ polymerization. In their finding, a ring-opening polymerization method was applied, which then initiated the delamination of clay layers in the polymer matrix and led to a composite formation.

3.2.4.2. Melt blending technique

Melt blending technique involves direct mixing of layered clay into the molten polymer matrix and can either be immobile or active. In an immobile melt blending (melt annealing), the process is performed under a vacuum at temperatures of approximately 50 ◦C above transition temperatures in the absence of mixing. In an active melt blending, the polymer melting is performed during a melt mixing in the presence of an inert gas [27,101]. As a result, the polymer clay nanocomposites are produced from the enthalpic driving force and influence of the polymer–organoclay interactions. The melt-mixing method (Figure 3.10b) provides better mixing of the polymer and nanoclay fillers and is well-suited with current industrially and ecofriendly viable processes such as extrusion and injection molding for thermoplastic and elastomeric material manufacturing. The absence of solvents reduces the environmental impact and minimizes potential interactions between the host and polymer solvents, which, in many cases, limits clay dispersion [18,102–104]

3.2.4.3. Solution blending technique

Solution-blending is a solvent based process in which the polymer and the prepolymer are soluble, which causes swelling of the clay layers, see Figure 3.10c. This technique involves thoroughly dispersing the layered silicate within appropriate solvents, which includes polymer/soluble prepolymer. These clay layers are dispersed into the solvent and further mixing with a dissolved polymer would be done to prepare the solution which allows polymer chains to be embedded into the exfoliated clay layers. Upon reaction completion stage, the solvent molecules would have evaporated, trapping the polymer chains intercalated into the gallery of clay interlayers [105,106] and the matrix segments combine with the dispersed clay layers. The major driving force of intercalation process in solution mixing is the increased total disorder of the system referred to as desorption process of solvent molecules. This entire process normally consists of three stages known as (i) the dispersion of clay in a polymer solution, (ii) well-ordered solvent removal and (iii) lastly composite film casting [102,106,107]. The dispersion of clay in neat polymer necessitates active agitation such as stirring, reflux and shear mixing. It is well documented that the morphology and dispersion of clay nanoplatelets in polymers is one of the key factors affecting their gas barrier properties [95,108]. One of the most vital challenges in the preparation of polymer/clay nanocomposites with improved barrier performances [95] is to achieve high level of

exfoliation and orientation. In general, polymer/clay nanocomposites may result into three possible morphologies referred to as (i) phase-separated, intercalated and exfoliated structures (see Figure 3.11) [95]. For attainment of phase-separated nanocomposites, clay tactoids are formed throughout the pure polymer matrix, and no separation of clay nanoplatelets occurs. Polymer chains surround clay nanoplatelets but do not penetrate between the clay layers [109] and absence of platelets separation may result in large, micron-sized agglomerates. In intercalated nanocomposties, some of the polymer molecular chains have penetrated the interlayer galleries of the clay tactoids. Due to the penetration of polymer molecular chains, the spacing between individual clay platelets and the overall order of the clay layers is increased and maintained [110]. In exfoliated nanocomposite structures, the clay nanoplatelets are fully separated and dispersed uniformly within the continuous polymer matrix. Exfoliated nanocomposites produce the highest surface area interaction between clay nanoplatelets and neat polymer [111]. After a successful exfoliation, an enhancement in properties can be manifested in barrier properties, as well as improved mechanical properties, decreased solvent uptake, increased thermal stability and flame retardancy [112,113]. However, the main drawback to achieve homogeneous dispersion of most inorganic clays within organic polymers is closely related to the incompatibility between hydrophilic clay and hydrophobic polymer, which often causes agglomeration of clay mineral in the polymer matrix. Thus, surface modification of clay minerals for a good compatibility with the polymer is the most important step to achieve homogeneous dispersion of clay nanoplatelets in polymer matrix [29,31,76,109].

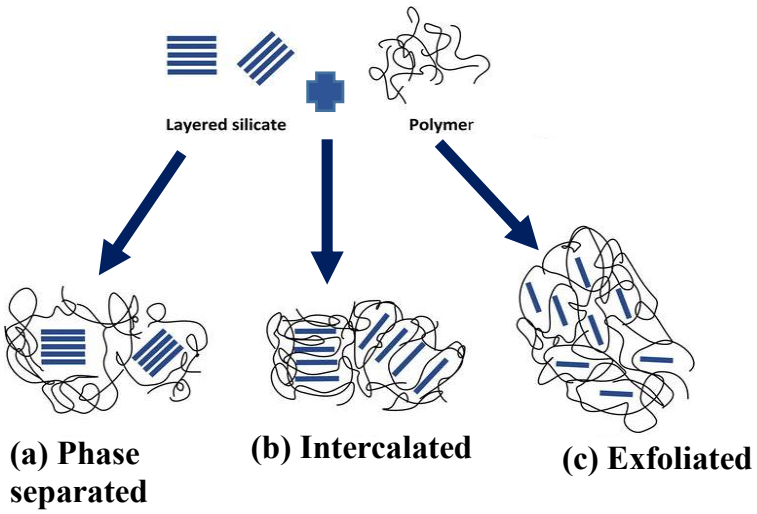

Figure 3.11. The main types of nanocomposites. (a) Intercalated, (b) Flocculated, (c) Exfoliated. Reproduced with permission from Reference [113]. Open Access 2018, IntechOpen.

3.2.4.4. Surface modification of nanoclays and LDHs

Layered silicates including nanoclays and layered double hydroxides (LDHs) can be intercalated with hydrophilic polymers such as thermoplastic, thermosetting and elastomeric polymers. Most commonly used polymers are hydrophobic, while others such as poly(vinyl alcohol) (PVA), poly(ethylene glycol) (PEG), poly(acrylic acid) (PAA), poly(2-oxazoline) (POX), poly(methyl methacrylate) (PMMA), poly (ethylene-co-vinyl acetate) (EVA) are hydrophilic in nature. Despite their various applications, silicate layers also have one primary drawback due to the intrinsic incompatibility of hydrophilic silicate minerals and the hydrophobic polymer matrix. The incorporation of hydrophilic silicate minerals into a hydrophobic polymer causes agglomeration/aggregation, which lead to incompatibility between the components and weak extent of dispersion. Thus, it is indispensable to augment the degree of dispersion and the compatibility between the polymer matrix and the clay by surface modification [114]. The miscibility between layered silicates and the polymer matrices is enhanced as the clay becomes hydrophobic after surface modification using organic materials. For fabrication of layered silicates with engineering polymers such as thermoplastic or thermosetting, the surfaces of the layered silicate have to be modified by ion-exchange processes using cationic surfactants like quaternary alkylammonium salt, alkylphosphonium-based positively charged species or coupling agents [49]. The surface energy of layered silicates is reduced due to the modification, providing the efficiency and reinforcing characteristics in controlling the stability of the polar polymer matrix [105]. As a result, the interlayer spacing increases to high margins, producing better anchoring of the polymer chains for improvement of the overall properties of the system. The most preferential modification is the addition of coupling agent such as silane, which ensures good compatibility or chemical bonding with polymers, an exchange of the interlayer inorganic cations such as Na+ with organic ammonium cations. In addition to ionic modifications, covalent and dual modifications (ionic and covalent are possible [115]. Other approaches, such as grafting polymer chains directly onto the surface of a nanoclay or using non-ionic surfactant have also been used [116]. There are two ways of ionic modification, called directly reacting anionic or cationic surfactants with the nanoclay or using ionic liquids. Imidazolium, pyridinium, trihexyltetradecylphosphonium tetrafluoroborate,

and trihexyltetradecylphosphonium decanoate salts are commonly used for ionic liquid modification of nanoclays which show better properties [117–122]. The modified clay is commonly referred to as organoclay and the schematic illustration for the modification of clay particles is shown in Figure 3.12. Chang et al. [119] prepared and characterized bio-oil phenolic foam (BPF) and surfactant modified bio-oil phenolic foam (MBPF) reinforced with Montmorillonite (MMT) as secondary phase. Their findings showed remarkably enhanced toughness as well as good flame resistance and improved the thermal stability of modified bio-oil phenolic foam (MBPF)-MMT nanocomposite foams compared to unmodified BPF-MMT nanocomposites. Covalently modified clay silicate is often synthesized via a step-reaction polymerization called condensation polymerization. During this process, the reaction is taking place between the hydroxyl groups from the surface of clays with mono- or tri-alkoxy silanes such as methoxy(dimethyl)octylsilane, tri-alkoxy silanes, trimethoxy(octyl)silane, (3-aminopropyl) triethoxysilane and others. The covalent modification renders the clay surface more hydrophobic [120]. Uwa et al. [121] studied the effect of nanoclay as reinforcing agent on the mechanical properties and thermal conductivity of polypropylene (PP) and maleic-anhydride-grafted-polypropylene (MAPP). The results of PP/MAPP/nanoclay composites exhibited a significant improvement in tensile strength and stiffness with low clay contents. Thermal conductivity analysis revealed that composites with high clay loadings have high resistance to heat. Twofold modifications can be done possibly by first covalently modified clay silicate followed by an ionic modification or vice versa. In comparison to single modifications (either ionic or covalent), dually modified clays show even more improved properties in terms of mechanics, thermal stability, dimensional stability, and viscoelastic characteristics.

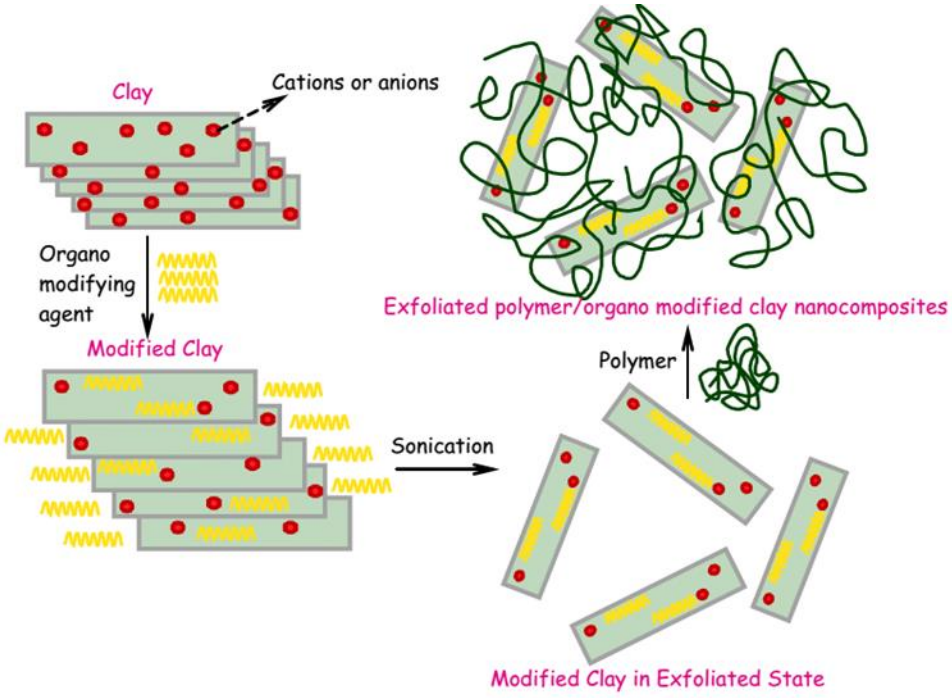

Figure 3.12. Schematic representation for the preparation of exfoliated polymer/organomodified clay nanocomposites. Reproduced with permission from Reference [122]. Copyrights 2017, Elsevier Ltd.

Various polymer-based layered silicates nanocomposite systems have been investigated, and their methods, structure and properties are compared and summarized in Table 3.3. The comparison of polymeric categories such as thermoplastic, elastomeric and thermoset matrices including thermoplastic polyurethane (TPU), polyisoprene (PIP), nacre-thermoset, poly(l-lactic acid) (PLLA), polypropylene (PP), polyamide 11 (PA11), nitrile butadiene rubber (NBR), styrene-butadiene rubber (SBR), Vinyl ester (VE), epoxy (EP), polylactic acid (PLA), Polybutylene terephthalate (PBT), polymethyl methacrylate (PMMA) reinforced with corresponding LDHs and other nanoclays are also included in Table 3.3 summary. Nevertheless, it is evident in the literature that the polymeric-thermoplastic matrices are utilized more preferentially over the thermosets because of their features such as light weight, can be re-melted/molded, and shaped. Recently, there is a growing demand to safeguard and deal with environmental contaminants and pollutants in preparation of biodegradable matrix/LDHs nanocomposites which are referred to as eco-friendly

materials. Layered double hydroxides (LDHs) systems appeared to have better overall properties than most of other nanoclays due to their varied chemical compositions and methods of synthesis. LDHs possess higher layer charge densities and prefer multivalent anions within their interlayer space due to strong electrostatic interactions between the brucite-type sheets and the anions. Therefore, swelling is more difficult in LDHs than for other clay minerals. In short, LDHs containing monovalent anions like nitrate or chloride ions are viewed as good precursors for exchange reactions with charge balance, which lead to some functional diversities.

Table 3.3. Comparison of polymer-unmodified/modified layered double hydroxide and other nanoclays for water purification.

Polymer-category	Layered Silicate	Processing methods	Observed morphology & removal of dyes or other heavy metal pollutants	Refs.
Polyacrylamide (PAM)-thermoset	Sodium-montmorillonite (Na-MMT)	Free-radical cross-linking Polymerization (In-situ polymerization)	A slightly intercalated MMT structure and incomplete exfoliation. PAM/Na-MMT nanocomposites efficiently removed the heavy metal ions such as Ni^{2+} and Co^{2+} wastewater with removal yield between 87.40% and 94.50%.	[125]
N-isopropylacrylamide (NIPAm) nanogel polymer-thermoset	Sodium-montmorillonite (Na-MMT)	Surfactant free dispersion radical crosslinking polymerization	Exfoliated structure. The Na-MMT nanogel composites showed drastic reduction in water surface tension and efficiently remove methylene blue (MB) dye, Co and Ni cations from water within an hour. The prepared Na-MMT nanogels desorbed and reused four times to remove the heavy metal from water with the same efficiency.	[126]
Polyethylene (PE)-thermoplastic	Green-clay	Solution mixing	An exfoliation nanocomposite morphology was achieved. The adsorption increased with increasing methylene blue concentration, the pH values and with increasing temperature due to the increased kinetic energies of the molecules. The removal of methylene	[127]

			blue (MB) from water solution was effectively achieved.	
Cellulose-thermoplastic	Montmorillonite (MMT)	Aqueous solution method	Intercalated nanocomposite morphology was observed. The adsorption was not considerably affected by pH due to the presence of hydrophobic interaction between MB and hydrogels. The hydrogel samples containing intercalated clays showed high removal efficiency for MB aqueous solution with concentrations of 10 and 100 mg L^{-1}. The removal efficiency for MB increased with the clay contents of hydrogel networks, and was reported as high as 97%.	[128]
PP-Thermoplastic	Montmorillonite	Melt blending technique using twin-screw extruder	Structural morphology of intercalated PP/MMT is observed, while PP-g-MA/MMT appeared to have obtained an exfoliation morphology. Neat PP and synthesised PP-*g*-MA/MMT nanocomposites were used for removal of heavy metal adsorbent for adsorption of Pb(II) from aqueous solutions. The results revealed that adsorption efficiency of 96% for the removal of Pb(II) ion contaminant with neat PP and 0.5 wt% MMT were attained and conform the Langmuir isotherm. The PP-*g*-MA/MMT at 0.5 wt% nanocomposites showed can efficiently and effectively	[129]

			be used as super adsorbent for optimized removal percentage of contaminants like Pb(II) ions from wastewater.	
Chitosan (CS)-thermoplastic	Bentonite	Both melt compounding and crosslinking reaction between chitosan and glutaraldehyde	Intercalated structures and morphology was observed. The adsorption of an azo dye called Amido Black 10B (AB 10B) adsorbate onto the crosslinked chitosan (CCS)/Bentonite (BT) clay composites was reported to be optimal at high temperatures and low pH value of 2. CCS/BT composite is an effective biosorbent for the removal of AB10B from aqueous solutions.	[130]
Polyethylene glycol (PEG)-thermoplastic	Mg−Al-layered double hydroxides (LDHs)	Simple chemical precipitation method.	The morphology of the synthesized PEG-modified Fe_3O_4/Mg−Al-layered double hydroxides (LDHs) nanocomposites is heterogeneous and spherical with an average diameter of around 16−30 nm. It is a common knowledge that the morphologies of nanocomposites significantly influenced their adsorption capacity. Adsorbents exhibited a remarkable high adsorption capacity for the removal of methyl orange (MO) from water within a short time interval of 5 min and easy separation of adsorbents	[131]

			after successful adsorption process was achieved with the help of a magnet.	
Polystyrene-thermoplastic	MgAl-LDH	Solution blending technique	The structural morphology of PS/LDH observed to be fibrous membranes. LDH-based sorbent showed a 67% adsorption efficiency of Cd^{2+} ion removal, while LDH-PS fibrous sorbents reached 10-15% adsorption efficiencies of Cd^{2+} ion removal based on the concentration of LDH in each of the sorbents. Since PS fibrous-based sorbents is hydrophobic, then the adsorption efficiency removal of Cd^{2+} ion can be attributed to the involvement of LDH-based sorbents which have better ion exchange capability.	[132]
Polyaniline (PANI)-conductive thermoset	Mg/Al Layered Double Hydroxide	Situ oxidative polymerization	A uniform fibrillar nanostructure is observed by SEM. The maximum adsorption efficiency of the PANI/LDHs is strongly affected by the initial solution pH for Cr(VI) wastewater treatment. Therefore, the adsorption efficiency removal of Cr(VI) decreases while the initial solution pH is above 7.0. This is probably due to the fact that the surface charge of PANI/LDHs was negative when pH > 7.0 and weakened electrostatic repulsion forces and	[133]

	significantly reduced adsorption efficiency/removal percentage of Cr(VI) from wastewater.

3.3. Properties of polymer/ other clays and LDHs nanocomposites.

The intention for the addition of clay minerals to the polymers is to improve the polymer properties and to produce the polymer/clay nanocomposites with desired applications. The key step is to prepare nanocomposites with highly preferred and value-added demand properties, which overcome downsides of polymers while maintaining their intrinsic advantages. Due to the low cost, availability, high aspect ratio as well as desirable nanostructure and interfacial interactions, clays can provide considerable improved properties at very low filler loadings, which help to obtain more useful properties. The nature and properties of constituents as well as preparation methods and conditions affect the final properties of polymer/clay nanocomposites. In this review, various improved properties of polymer/clay nanocomposites as well as the adsorption capacities and removal efficiency of dyes or heavy metal ions in water including morphology are discussed.

3.3.1. Morphology of polymer/other clays and LDHs nanocomposites

The morphology of the polymer/layered clay silicate nanocomposites significantly influenced their adsorption capacities and the removal efficiency of dyes or other heavy metal ions in water. The key aspect in nanocomposite structure is the clay–polymer interaction, which affects the dispersion level of clay in polymer matrix. Depending on the dispersion level of layered silicates, the structure can either be separated, intercalated or exfoliated structure [108,132–135]. Surface modification plays also important role in achieving good interaction between polymer and clay which affects the extent of dispersion and improves significantly the adsorption as well as removal of dyes or heavy metal ions from water. Thus, organically modified clay silicates such as montmorillonite (OMMT), kaolinite and LDH are mostly preferred nano reinforcement for proper selection of the functional groups and their abilities of ion-exchange. It is well-known that acid-modified clay resulted in higher rate of dye adsorption, an increased specific surface area and high porosity than in the case of base-modified clay [136]. Highly flame-retardant polymer/deoxyribonucleic acid (DNA)-modified clay nanocomposites were investigated by transmission electron microscopy (TEM) as shown in Figure 3.13a–f. The dark lines observed in Figure 3.13a,d are closely related to the layered silicate nanoclays and the light segments are associated to epoxy matrix. Naebe et al. [137] explained that intra-gallery reactions due to interfacial interactions made diffusion of more epoxy monomers within DNA-modified clay possible to enhance clay layers' separation and

therefore induced formation of exfoliated structures as seen in Figure 13b. In addition, three individual intercalated ordered structures known as intercalated tactoids could be observed for epoxy nanocomposite at higher contents of clay (Figure 3.13e).

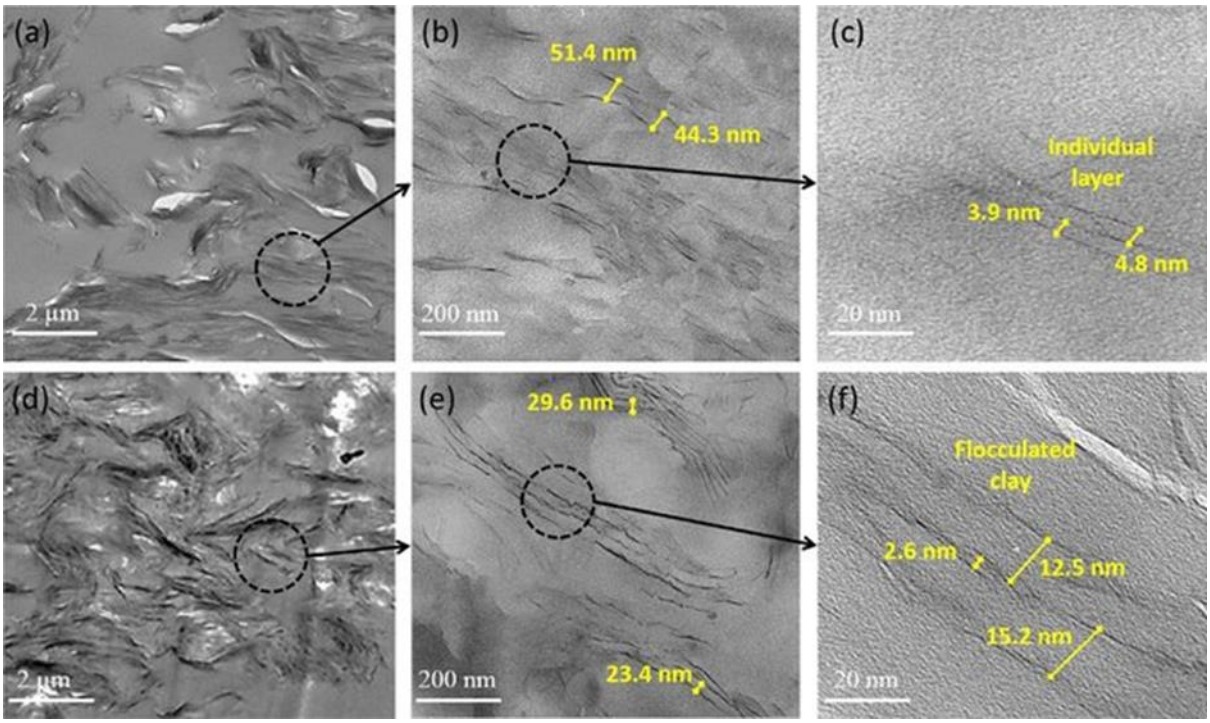

Figure 3.13. TEM micrographs of epoxy-2.5 wt% of DNA-clay (a–c), and epoxy-5 wt% of DNA-clay (d–f) nanocomposites. Reproduced with permission from Reference [137]. Open Access 2016, Springer Nature.

However, few clay layers possess thin and small tactoids which are uniformly and randomly dispersed in the epoxy resin. This indicates that the DNA-clay modification is an effective approach to improve both the exfoliation and dispersion of clay. In addition to achieved dispersion, most of microcracks under an effective load are initiated within the intra-layer of semi-stacked clay instead of epoxy-clay interfacial region. This phenomenon verifies that higher contents of clay (5 wt%) resulted in lower reinforcing impact in the overall mechanical properties. Evidently, low clay content formed an exfoliated structural configuration with individual layers, well-dispersed with more homogeneous distribution (Figure 3.13c), while high content of clay resulted

in flocculated structures. It can be seen in Figure 3.13f that phase-separated clay tactoid structures are formed and agglomeration at high content prevail over complete delamination of clay layers due to low penetration of epoxy monomers into stacked layers of modified clay [138]. Zubitur et al. [139] studied the poly(lactic acid) (PLA)/modified drug 4-biphenyl acetic acid (Bph)-layered double hydroxide (LDH) nanocomposites. The nanocomposites were prepared by solvent casting with 5 wt% of drug-modified LDH, and the hydrolytic degradation was carried out in a Phosphate-buffered saline (PBS) solution at pH 7.2 and 37.8 ◦C. From their XRD results, PLA/LDH-Bph nanocomposites showed no peaks corresponding to LDH-Bph observed and this was attributed to an exfoliation or to the presence of entropic LDH layers. The degree of dispersion of acid/base-modified LDH was found to be good with small tactoids at low magnification, exfoliated layers were observed at higher magnification using TEM images. A number of studies reported the acid modification of clay silicate and layered double hydroxides (LDHs) reinforced with polymer matrices. Table 3.4 represents the summary of selective studies on acid/base-modification of polymer/clay and LDH nanocomposites for water purification.

Table 3.4. Summary of selective studies on acid/base-modification of polymer/clay and LDH nanocomposites for water purification.

Polymer Systems	Preparation methods	Acid/base-modification	Dispersion & structural morphology good for removal of dyes or heavy metal ions.	Refs.
PLA/ NiAl/LDHs	Melt mixing	SDBS	Good dispersion and predominantly exfoliated structures. Maximum adsorption capacity of dyes or heavy metal ions.	[143]
LDH/PEG$_{400}$	Physicochemical modification	PEG$_{400}$	Good dispersion and LDH layers were exfoliated in PEG$_{400}$ and showed higher dye adsorption capacity and effectively removed the azo dye, Acid Orange II (AO-II) in aqueous medium.	[144]
Polyethersulfone (PES)/AA-MMT	Phase inversion method	Acid Activated (AA)	The proper dispersion of nanoparticles in the membrane matrix was observed and PES/AA-MMT showed better dye removal in the basic pH for MO and acidic pH for MB. The nanocomposite membranes exhibited considerably higher dye removal than neat PES. When the nano-clay content was increased, the dye removal percentage also increased in both dyes even in neutral pH due to the remarkable role of MMT particles in dye adsorption.	[145]

Ppy NF/Zn-Fe LDH	Interfacial polymerization of pyrrole	HCl as oxidant	The dispersion was observed to be weak and structural morphology was separated grain or agglomerated particles-like stacked structure. Ppy NF/Zn-Fe LDH) composites enhanced adsorption capacity and high efficiency in the removal of safranin dye from raw water samples including tap water, groundwater, and sewage water.	[146]
Chitosan (CS)/laponite	Acid Activated (AA) aqueous solution	2-acrylamido-2-methyl-propanesulfonic acid (AMPS)	The degree of dispersion is better after being pre-adsorbed by AMPS and exfoliated microstructure morphology with high surface area, large pore volume and average pore size is observed. High surface area and large amount of micropores in adsorbent is suitable for the penetration of water and heavy metal ions into the interior and thus enhances the adsorption rate and removal efficiency. Thus, these nanocomposites showed an excellent adsorption capacity for removal of Cd(II), MB and CR from aqueous solution rapidly and efficiently.	[147]
Zeo/PVA/SA	Melt blending	The mixture of glutaraldehyde (GA) the cross-linking agent consists of 75	Zeo/PVA/SA NC beads have more pores and showed rougher and loose surfaces with porous structure. The dispersion of Zeo NPs had some agglomerations and exhibited an irregular inner	[148]

		wt% (2% GA, 2% HCl and 71% acetone): 25 wt% DI water.	morphology with stacks of tiny interspace structure with a very limited number of dents. The results revealed the removal efficiency of heavy metal ions such as Pb^{2+}, Cd^{2+}, Sr^{2+}, Cu^{2+}, Zn^{2+}, Ni^{2+}, Mn^{2+} and Li^{2+} using Zeo/PVA/SA NC modified beads reached the maximum at the pH value of 6.0, while the highest removal is achieved at pH = 5 for Fe^{3+} and Al^{3+} with 96.5 and 94.9%, respectively.	
Chitosan/modified Bijoypur clay	Solution blending	HCl-purifier; Dodecylamine	The morphology of modified clay/chitosan showed smooth but discrete spherical particles with some dispersion. Chitosan/modified clay composite with high clay loading showed a better performance for cationic dye (MB) uptake, whereas heavy metals (Cr (VI) and Pb (II)) were better adsorbed on the composite, with high chitosan content.	[149]

3.3.2. Adsorption of polymer/nanoclay and LDH systems

Various types of polymer/nanoclay composites are currently being explored for the primary usage in water purification and many other applications due to their unique properties, which are different from their counterparts. Polymer/clay nanocomposites used in water purifications technology and their corresponding applications as well as the removal of various heavy metal ions are shown in Figure 3.14. Adsorption is a removal of soluble material/adsorbed materials called adsorbate (heavy metal ions) present in water and clay nanomaterials (solid adsorbents) are used for the adsorption of contaminants. This process can either be physical (physisorption) or chemical (chemisorption) in nature. Nanoclay minerals have the high specific surface area and high sorption capacity giving high structural and chemical stability towards the adsorption of organic and inorganic contaminants.

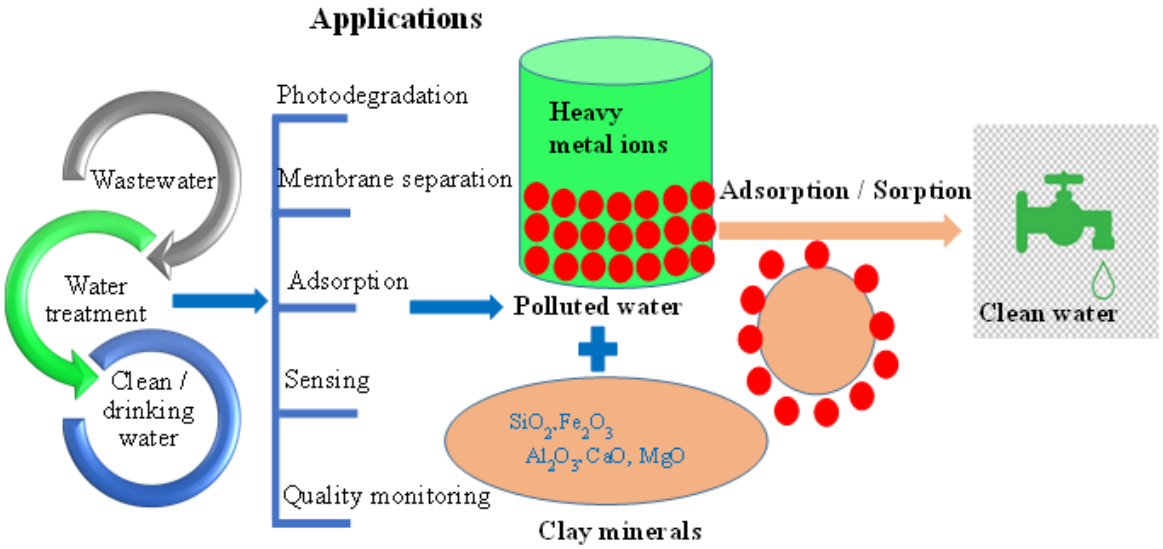

Figure 3.14. Role of nanocomposite in water purification and the removal of various heavy metal ions.

Due to its high internal surface area in the range of 500–1500 m2 /g, the most popular solid adsorbent material is activated carbon which is primarily used in large-industrial scale for water purification systems [41,49]. Thus, adsorption is a surface phenomenon commonly found in nature and plays a key role in water purification technology. Adsorption increases with the increase in the surface area of the adsorbent. This implies that more finely divided or rougher the surface of

the adsorbent is, then the greater is the surface area and the adsorption. However, adsorption affinity of the surface area of the adsorbent is independent of the surface area and dependent on the favorable attractive interactions present at the pH value range below 7. When the pH is higher than 7, the electrostatic repulsion forces of the adsorbate-adsorbent are weakened, hence, the reduced adsorption efficiency or removal percentage of contaminants [41,49,131]. The adsorption of contaminants from water mostly depends on hydrophobic interactions between adsorbate and adsorbent, which make great contributions to the affinity of the organic anion to LDH. Therefore, the hydrophobic interactions interconnect many segments into a cluster in order for each natural organic anion to show a stronger affinity to LDH. The high hydrophilic nature of contaminants reduced significantly the adsorption capacity. The main reason for this is dominant force that decreases the surface tension between the matrix (adsorbent) and the solid adsorbed (adsorbate). The detailed discussion of the effect of pH as one of many factors affecting the adsorption, advantages and disadvantages of various methods of synthesis would also be outlined in the paragraphs or Table 3.5 below.

Table 3.5. Advantages and disadvantages of different methods of LDHs and clays in water purification.

Methods	Advantages	Disadvantages	Refs.
Co-precipitation	Has high contaminant removal ability, applicable to communities and low reaction temperature and short reaction time.	Requires high maintenance and optimization of treatment is difficult.	[58,60,62]
Ion exchange	Able to effectively remove inorganic contaminants, has capacity to regenerate and inexpensive. No loss of sorbent on regeneration, effective.	It has high operating costs over a long period of time and cannot effectively remove pyrogens or bacteria. Causes economic limitations, not effective for dispersing and removing the dyes.	[63]
Sonochemical	Produces a better shear thickening transition at lower shear rate and significantly reduced the water content contamination. Improves reaction rate, involves high energies and pressures in a short time; no additives needed; reduced number of reaction steps.	Reactions need to be at certain temperature and there is not enough power to carry out the reaction. Extension of problems; inefficient energy; low yield.	[62,66-68]
Hydrothermal / Solvothermal	Has ability to synthesize large crystals of high quality and crystalline substances that are unstable near the melting point.	High cost of equipment.	[69,70]
Adsorption	The most effective adsorbent, great, capacity, produce a high-quality treated effluent.	Ineffective against disperse and dyes, the regeneration is expensive and results in loss of the adsorbent, non-destructive process.	[73-77]

Sol-gel method	Can produce a thin coating to ensure excellent adhesion between the substrate and the top layer. It has the capacity of sintering at low temperatures, between 200-600°C, simple, economical and efficient method to produce high quality coverage and high purity products.	The contraction that occurs during processing; long processing time; fine pores; use of organic solutions that can be toxic.	[78,79]
Urea/Induced hydrolysis	Cheap, easy to store.	Loss through leaching and volatisation, acidifying.	[58,60,61]
In situ polymerization	Easy processing method based on the dispersion of the filler in the polymer precursors.	Difficult control of intragallery polymerization and limited applications.	[18,31,100]
Melt mixing method	One step technique, economical and environmentally viable and easy to process and compatible with industrial polymer processes.	Sensitivity to reaction conditions, limited applications to low molecular weight polymers.	[104-106]
Solution mixing technique	Preparation of homogeneous dispersion of fillers.	The industries and sectors use a huge amounts of solvents and this technique is very expensive.	[107,108]

In recent times, different synthesis and preparation methods of LDHs and other nanoclays have been applied as discussed in Sections 2.3 and 2.4, respectively. These different methods influence the adsorption performance of the nanocomposite and noticeably assist to reduce and remove the high concentration levels of contamination in water [147,148]. Individually, each method has some advantages and disadvantages as represented in Table 3.5. Amongst all the methods, adsorption is considered the most efficient, economical technique and easy processing to drive for contaminants removal from wastewater. Furthermore, the adsorption is reversible, and adsorbents can be regenerated. In general, there are three types of adsorption known as physisorption (the interaction between adsorbent-adsorbate), chemisorption (adsorbent-solvent) and electrostatic interactions (adsorbate-solvent) [149]. The underpinning principles/mechanisms involved in the adsorption material surface have been studied and reported in relation to factors affecting systems.

3.3.2.1 Factors governing the performance of clays/LDH based adsorbents

In this review, the application of nanomaterials as adsorbents for removal of contaminants such as heavy metal ions and dyes from wastewater has been reviewed. It is important to understand how adsorbents interact with different adsorbates such as heavy metal ions and dyes in the laboratory small scale to determine their potential for application in water purification and their contribution to large scale [148,149]. However, the main challenges for adsorption process are waste products, non-selectivity, instability and low/poor heat transfer leading to long heating and cooling times. To address these challenges, the development and design of suitable and more effective nanoadsorbents with optimum adsorption efficiency for the removal of contaminants in water should be prioritized. In the field of wastewater treatment, different materials prepared through various methods bring about unique functionalities for adsorption efficiency for the removal of contaminants from industrial effluents, surface water, groundwater and tap/drinking water. As stated, many key factors affect the efficiency and performance of LDH/clay adsorbents including pH value, contact time, adsorbent dosage, initial ion concentration, temperature, coexisting ions, and sorption kinetics [148,149]. In this section, the influence of these factors on adsorption performance and capacity by LDH/clay adsorbents is explained as presented in Table 3.5.

Influence of pH value

The pH of an adsorbate-adsorbent solution is most significant aspect for adsorptive removal of contaminants. This affects the type of the surface charge of the adsorbent during water purification by the adsorption technique. It is also the main factor taking care of the type of the surface of the adsorbent, degree of ionization and aqueous adsorbates [149]. The effect of solution pH was studied at different pH values from 3.0 to 11.0, and the results are shown in Figure 3.15a,b. The pH of solution noticeably changed by the addition of diluted HCl/NaOH. The maximum fluoride adsorptions of 98%, 94% and 91%, respectively for cerium bentonite clay-malic acid chitosan (CeBC-A@CS), lanthanum bentonite clay-malic acid chitosan (LaBC-A@CS) and aluminum bentonite clay-malic acid chitosan (AlBC-A@CS) adsorbents was attained at pH of 3.0. It was also reported that the minimum fluoride adsorption for these three different adsorbents was achieved as 43%, 37% and 35%, respectively at pH of 11. At neutral pH of 7.0, the maximum fluoride adsorption was 84%, 82% and 80% for, respectively. The maximum fluoride adsorption capacity can be attributed to the change in the surface charge of the adsorbent. The pH value at point of zero charge (pHzpc) for the adsorbents is 7.1 [150] as represented in Figure 3.15b. When the pH of solution was less than pHzpc, the fluoride ions moved towards the positively charged surface of the chitosan composites formed by the protonation of OH^- and carboxylic acid groups leading to the fluoride adsorption onto the surface [151]. At a pH value above the pHzpc, the fluoride adsorption was exceptionally low. This is probably because the composite surfaces were negatively charged due to deprotonation of the hydroxyl groups, ensuring mutual repulsion forces between the fluoride ions and the composite surfaces [152]. It can be observed that cerium bentonite clay-malic acid chitosan (CeBC-A@CS) adsorbent showed a higher fluoride adsorption capacity than lanthanum bentonite clay-malic acid chitosan (LaBC-A@CS) and aluminum bentonite clay-malic acid chitosan (AlBC-A@CS) adsorbents.

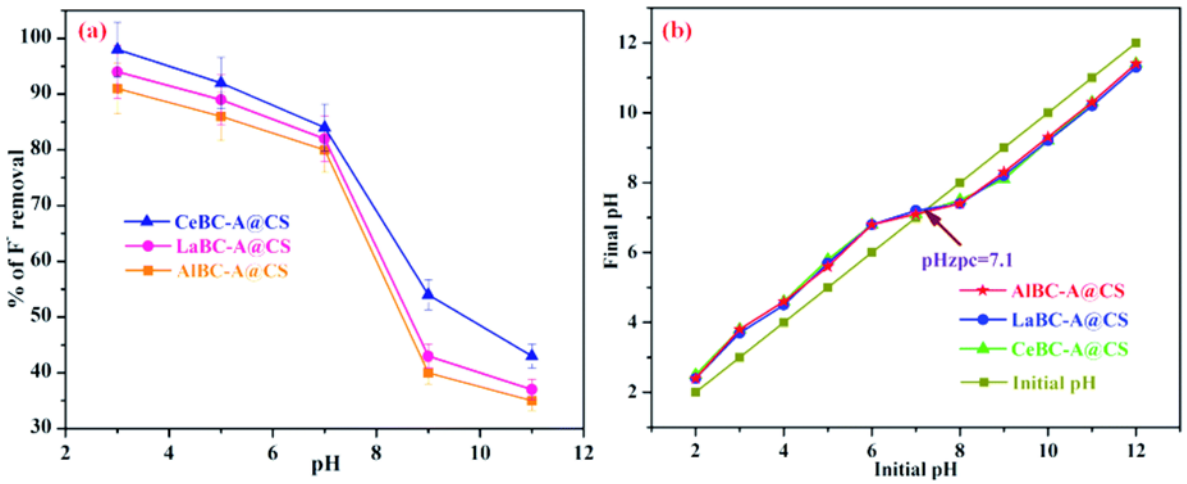

Figure 3.15. (a) Effect of pH and (b) pHzpc values of cerium bentonite clay-malic acid chitosan (CeBC-A@CS), lanthanum bentonite clay-malic acid chitosan (LaBC-A@CS) and aluminium bentonite clay-malic acid chitosan (AlBC-A@CS) adsorbents. Reproduced with permission from Reference [151]. Open Access 2020, RSC Advances.

Wei et al. [153] investigated the novel hydrotalcite-like material layered double hydroxide (FeMnMg-LDH) adsorbent synthesized by co-precipitation and its adsorption capacity for the removal of lead ions in water. In order to prevent the precipitation of Pb2+ at the high pH, the experiment pH was set below pH 6. The pH of 6 was maintained to prevent the precipitation of Pb2+, and effects of pH on the adsorption are discussed. It was reported that the Pb2+ removal percentage by FeMnMg-LDH adsorbent mostly increased with the increasing pH value. The Pb^{2+} removal percentage higher than 97% at the pH range 3–6, was achieved. This is an indication of the outstanding efficiency and performance of FeMnMg-LDH adsorbent in Pb2+ adsorption except when pH is equal to 2. The suspension of the absorbent might take place at extremely low pH resulting into the collapse of the structure of FeMnMg-LDH and therefore reduce Pb2+ adsorption efficiency and capability. Comparing the bentonite clay and LDH-based adsorbent, it can be concluded that FeMnMg-LDH adsorbent has a higher adsorption capacity of more 97% than others except the cerium bentonite-malic acid chitosan, which appears to have more or less similar adsorption capacity percentage.

Influence of contact time

The contact time significantly affects the adsorption process and the economic efficiency of the process including the adsorption kinetics. Therefore, contact time is profoundly important and dependent factor for performance determination in adsorption process [154]. Figure 3.16a represents the fluoride adsorption capacity of the three adsorbents (cerium bentonite clay-malic acid chitosan (CeBC-A@CS), lanthanum bentonite clay-malic acid chitosan (LaBC-A@CS) and aluminum bentonite clay-malic acid chitosan (AlBC-A@CS)) at different contact times in the range of 10 to 90 min with neutral pH and initial concentration. The fluoride adsorption capacity of the adsorbents was gradually increased with an increase in contact time. Cerium bentonite clay-malic acid chitosan (CeBC-A@CS) adsorbent obtained the higher fluoride adsorption capacity of 84% than other adsorbents with 62%, 67%, 80%, 82%). Moreover, an equilibrium at 60 min and 45 min was achieved with different adsorbents which suggests the surfaces of the adsorbents CS and BC were completely covered with fluoride ions.

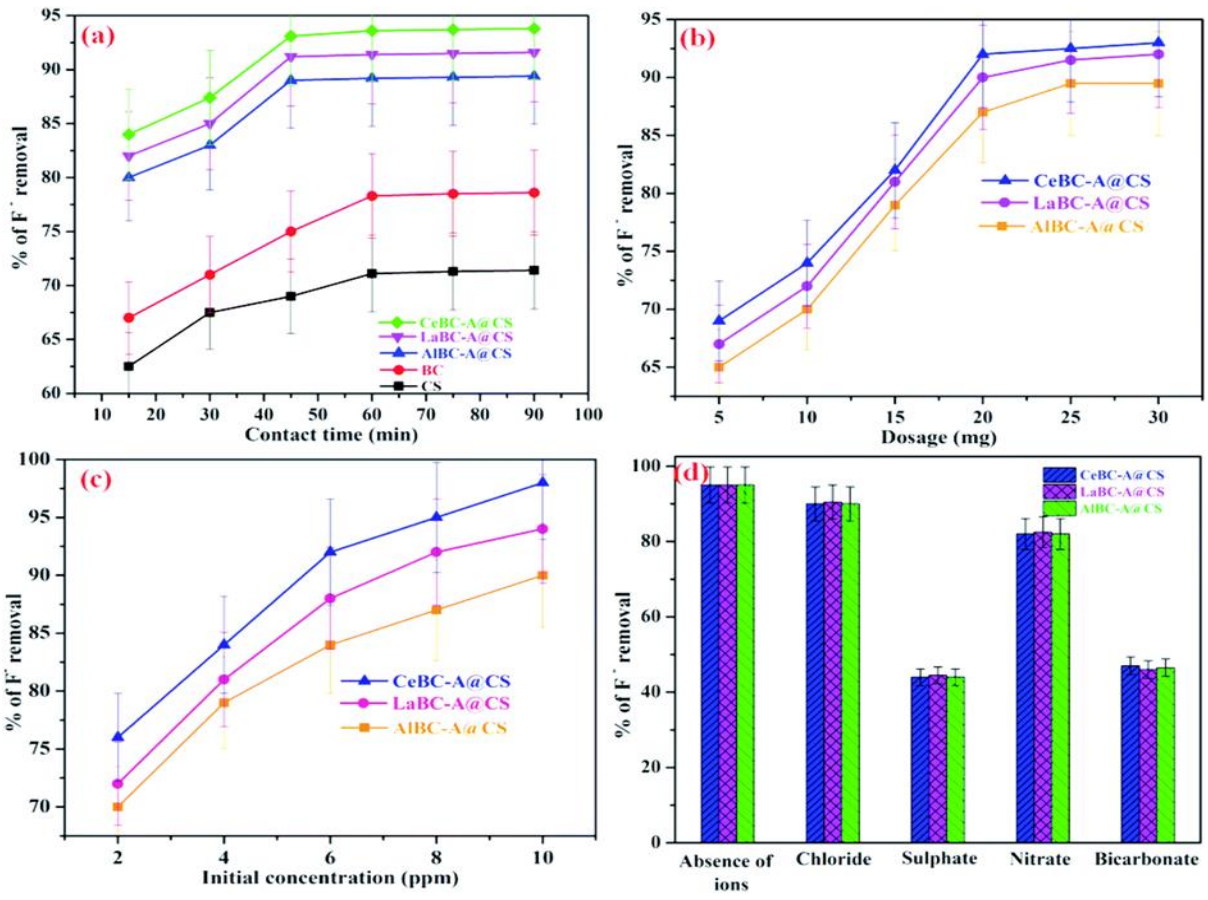

Figure 3.16. (a) Effect of contact time (b) effect of dosage (c) effect of initial fluoride concentration and (d) effect of co-ions on the fluoride adsorption of the adsorbents AlBC-A@CS, LaBC-A@CS and CeBC-A@CS at 303 K in neutral pH. Reproduced with permission from Reference [151]. Open Access 2020, RSC Advances.

Jaiswal and Chattopadhyaya [155] studied the effect of contact time on adsorption of Pb(II) on the Co/Bi-LDH synthesized by using co-precipitation method. Their impressive finding was that 90.0% of the adsorptive removal of contaminant, called heavy metal, was accomplished within 120 min of contact time. It was also observed that beyond 120 min, contact time has no effect in heavy metal removal percentage. At the beginning, very high adsorption rates were observed simply because of the larger number of vacancy sites available for the sorption and adsorption equilibria that were then steadily reached [139]. Effect of contact time for bentonite clay and LDH adsorbents using the same co-precipitation method were compared, and it can be concluded that LDH adsorbent seems to have an upper hand in terms of the adsorption capacity percentage for removal of contaminants. The reason for this is that LDH adsorbent has higher surface charge density and more ion exchange binding sites for good adsorption. This could also be attributed to the adsorption on the LDH layers via hydroxide precipitation or metal complexation.

Influence of adsorbent dosage

As matter of principle, the degree of adsorption of a solute increase with the increase in the content of an adsorbent. This can be attributed to the increase in adsorbent dosage, which indicates the increased active exchangeable adsorption surface vacancy sites. Nevertheless, the total solute adsorption per unit weight of an adsorbent can decline subsequent to the upsurge in adsorbent dosage because of meddling initiated by the interaction of active sites of an adsorbent [156]. In Figure 3.16b, the results showed the most favorable dose achieved as 25 mg for the adsorption of fluoride ions via three bentonite clay-based adsorbents. The resultant adsorption capacities of 87%, 90% and 92% were reported for aluminum bentonite clay-malic acid chitosan (AlBC-A@CS), lanthanum bentonite clay-malic acid chitosan (LaBC-A@CS) and cerium bentonite clay-malic acid chitosan (CeBC-A@CS) adsorbents, respectively. Beyond 25 mg, the results showed no significant increase in the fluoride removal limit due to the lower availability of active adsorption sites [157]. Li and co-authors [158] studied Mg–Al layered double hydroxides/MnO2(Mg–Al

LDHs/MnO2) adsorbents for removal of Pb(II) from aqueous solutions synthesized by one-pot hydrothermal method. It was reported that the adsorbent dosage of Mg–Al LDHs/MnO2 considerably influenced the adsorptive removal of contaminants like lead ions. It was also observed that the percentage adsorptive removal of Pb(II) contaminant increased fivefold from 18.48% to 99.56% with the adsorbent dosage increasing by a factor of 9 from 0.01 to 0.09 g. In addition, the higher adsorbent dose results in a reduced adsorption capacity of Mg–Al LDHs/MnO2 at Pb(II) concentration of 50 mg/L. This observation can probably be associated with the low adsorbent dosage leading to the dispersion of Mg–Al LDHs/MnO2 particles in aqueous solutions. The maximum adsorption efficiency and performance of LDH-based adsorbent and bentonite clay-based adsorbent was achieved at 99.56% and 92%, respectively. The LDH-based adsorbent achieved higher percentage removal efficiency of Pb(II) contaminant than bentonite clay-based adsorbent. This is attributed to the increase in the concentration of adsorption sites in aqueous solution, which enables the contaminants adsorption on a larger number of actives sites.

Influence of initial ion concentration

The influence of the initial ion concentration of the contaminant on the adsorption is one of the most important factors to be studied. It can be seen from Figure 3.16c that the adsorption capacity of fluoride ions increased with increase in initial concentration. The initial concentrations improved from 2.0 mg per liter to 10 mg per liter where the adsorption capacity/proficiency of the aluminum bentonite clay-malic acid chitosan (AlBC-A@CS), lanthanum bentonite clay-malic acid chitosan (LaBC-A@CS) and cerium bentonite clay-malic acid chitosan (CeBC-A@CS) adsorbents moved from 70.1% to 98% [151]. Thus, the adsorption limit was observed to be straight forward undertaking related to the adsorption of fluoride ions. Mostafa et al. [159] investigated the effect of different Fe(II) concentrations on adsorption capacity of Co/Mo-LDH with carbonate $(CO3)2^{-}$ as an interlayer anion prepared through co-precipitation method. Their results revealed that the Co/Mo-LDH seemingly removed a significant amount of Fe(II) contaminant from the aqueous solutions. The maximum adsorption efficiency improved to a 99.74%, and the saturation occurred when no more metal ions could be adsorbed on the surface of Co/Mo-LDH. A high efficiency for ferrous adsorption was obtained through a relatively short period of time up to 60

min at initial concentrations of 1.0, 2.0, 3.0 and 5.0 mg/L. The LDH-based adsorbent has 99.74% higher maximum adsorption capacity than bentonite clay-based adsorbent with 98%.

Influence of co-existing ions

The adsorptive removal efficiency of contaminant is typically influenced by the presence of co-existing ions in solution leading to competitive adsorption on the adsorbent surface [160]. The influence of various negatively charged anions such as chloride (Cl−), sulfate (SO4 2−), nitrate (NO3 −) and bicarbonate (HCO3 −) ions on the adsorption of fluoride by the three adsorbents (aluminum bentonite clay-malic acid chitosan (AlBC-A@CS), lanthanum bentonite clay-malic acid chitosan (LaBC-A@CS) and cerium bentonite clay-malic acid chitosan (CeBC-A@CS)) was examined in Figure 16d. The findings suggest that the Cl− and NO3 − ions did not change the fluoride adsorption efficiency, while the SO4 2− and HCO3 − ions had an adverse effect. This can be associated with high coulombic repulsion forces in existence, which reduced the mobility of fluoride ions during interaction with the active sites of the adsorbent. The larger degree of interference of the SO4 2− and HCO3 − ions is due to the arrival of OH− ions which induced the arrangement of sodium sulfate and sodium bicarbonate increasing the solution pH and thus made possible for these ions to compete with fluoride ions on the surface of the adsorbent [160]. Zhu et al. [161] studied the effect of calcined Mg/Al layered double hydroxides (Mg-Al LDH) as efficient adsorbents for polyhydroxy fullerenes (PHF) prepared by co-precipitation method. Naturally, PHF may co-exist with other inorganic anions, which may affect its adsorption on layered double oxide (LDO). The effect of selected various coexisting anions such as Cl−, CO3 2−, SO4 2−, and HPO4 2− at approximately pH of 10 was analyzed. Their results proved that Cl−, CO3 2−, and SO4 2− slightly improved the adsorption of the PHF on LDO. The adsorption capacity of PHF on LDO lessened considerably in the entire concentration range of PHF with the presence of HPO4 2− ions. The increase in PHF concentration implies that the negative effect of HPO4 2− declined noticeably due to the improved competitive effect of PHF. The effect of co-existing anions on the adsorption of LDH adsorbent may influence the surface property of the adsorbents resulting into two effects known as inhibiting effect and synergistic effect. These happen by occupying some of the adsorption vacant sites (an inhibiting effect) and providing additional adsorption sites (a synergistic effect) [161]. This means that the properties of the adsorbates are influenced by

promoting the aggregation or dispersion of adsorbates. Ultimately, the co-existing ions may have various effects such as promoting, inhibiting, or no effect at all on the adsorption of adsorbates of the adsorbents.

Influence of Temperature

The effect of temperature is typically one of the factors governing the adsorption efficiency and performance of adsorbents in water purification systems. An increase in temperature with an increase in the adsorption percentage enables the adsorption capacity of clay/LDH-based adsorbents at various temperatures [162]. This is due to the increase in the mobility of contaminants in aqueous solution, which leads to the improvement in the availability of adsorption vacant surface-active sites. Temperature parameter is well-known to have a strong effect on different chemical processes. It affects the adsorption rate by varying the molecular chain interactions and the solubility of the adsorbate. The effect of temperature on the adsorption of Pb(II) on clay/LDH was investigated by Ayawei et al. [162]. It was observed that on increasing the temperature, the percentage removal of metal ions increased (Figure 3.17). This presented sufficient evidence to conclusively refer to this adsorption process as an endothermic kind of the process.

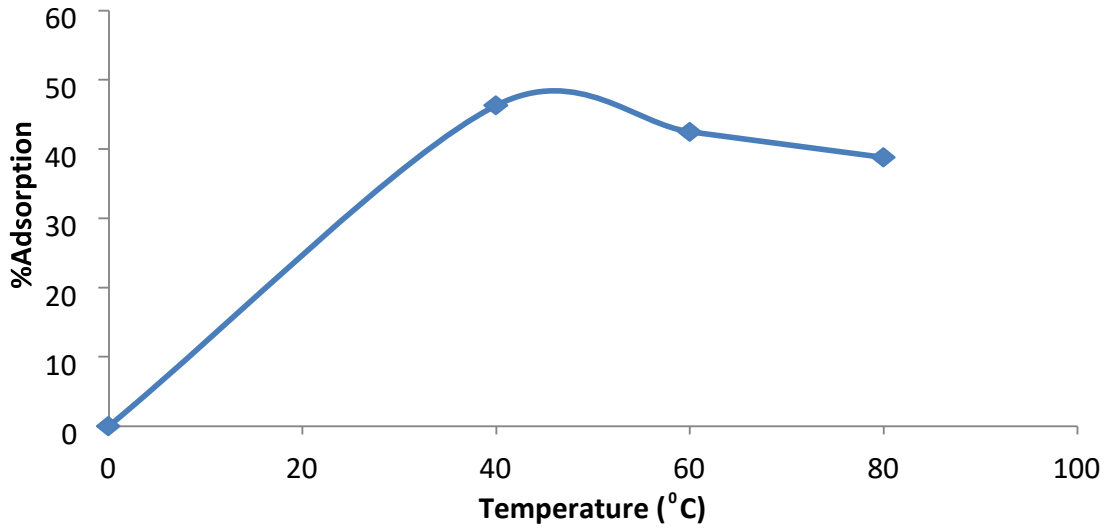

Figure 3.17. Adsorption capacity and percentage as a function temperature. Reproduced with permission from Reference [162]. Open Access 2015, International Journal of Chemistry.

Influence of Sorption kinetics and isotherms

The information on adsorption/desorption process and isotherms is one of the key factors required for proper analysis, structure and understanding of the adsorbent–adsorbate system [160]. In recent times, various models have been explored to explicitly explain the adsorption behavior including isotherm models. The latter provide valuable information about adsorption property of a system and the distribution of exchangeable sites on the surface of the adsorbent. In general sorption, diffusion, desorption, sorption isotherms will be discussed in this section [163]. Some of the factors that play a major role in the adsorption/sorption process are explained below. The nanocomposites usually exhibit a very high amount of barrier properties with even a small amount of layered silicate [29]. Some small molecules such as oxygen, carbon dioxide, water and nitrogen permeate through a polymer membrane due to a gas chemical potential gradient through the membrane. The chemical potential difference ($\Delta\mu$) acts as the driving force for the molecules to permeate from the high chemical potential side to the side of low chemical potential. The mode occurrence of permeant transport in polymers is described using the solution–diffusion model. According to this model, the permeation in polymers consists of three steps as illustrated in Figure 3.18a (i) sorption of the permeant from the high concentration side onto the membrane/film surface, (ii) diffusion of the permeant along the concentration gradient through the membrane and (iii) desorption through evaporation from the low concentration surface of the membrane. When the permeating molecule interacts with the polymer, then the deviations from a gradient with a straight line can be observed and is known as non-Fickian diffusion explained by the diffusion–relaxation model [164,165]. In this review, we discuss the tortuosity of the diffusive path for nanoplatelets for the gas barrier properties of nanocomposites in Figure 3.18b. Layered silicate nanoclays such as montmorillonite and kaolinite are the most innovative and promising nanofillers due to their ability to exfoliate to form single nanoplatelets when dispersed in a polymer matrix. The basic theory of the model is that the presence of impermeable clay platelets forces the permeant (gas) molecules to follow a longer diffusion path by traversing around the platelets. Therefore, this is also known as the tortuous path model as illustrated in Figure 3.18b. The nanoplatelets hinder the diffusion process of small gases through them and form a tortuous path which act as a barrier structure for gases. Tortuous paths explicitly explain the principle of the barrier behavior and its noticeable improvement in nanocomposites, which can be attributed to the impermeability of the layered clay

silicate into the polymer matrix. Therefore, the intercalation molecules are placed in a wiggle shape around the nanoparticles in a random way [166,167] as seen in Figure 3.18b.

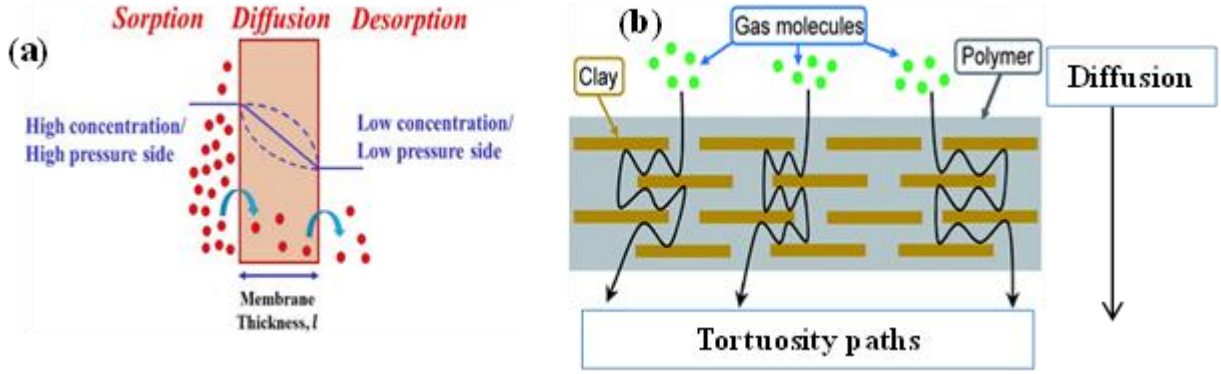

Figure 3.18. (a) Schematic illustration of the solution diffusion model. Reproduced with permission from Reference [168]. Open Access 2020, MDPI Polymers (b) Schematic illustration of the tortuous path model. Reproduced with permission from Reference [95]. Open Access 2017, RSC Advances.

Follain et al. [169] investigated the water vapor transport properties by pervaporation and sorption measurements and evaluated nanoclay extent of dispersion in polymer matrix. They prepared nanocomposites based on poly(ethylene-co-vinyl acetate) (EVA)/organo-modified Cloisite clays at varying contents by melt blending. Their results showed a noticeable decrease in water permeation flux obtained when nanoplatelets are incorporated into the neat EVA matrix (Figure 3.19a). This barrier effect is typically attributed to the remarkable increase of the diffusion pathways due to organo-modified Cloisite clay-induced tortuosity effects. Furthermore, the water permeation flux seems to be proportional to the diffusion coefficient, which was found to be reduced due to a plasticization effect of water. The water-induced plasticization effect of sorbed water molecules was highlighted through sorption kinetics, and water barrier behavior was observed.

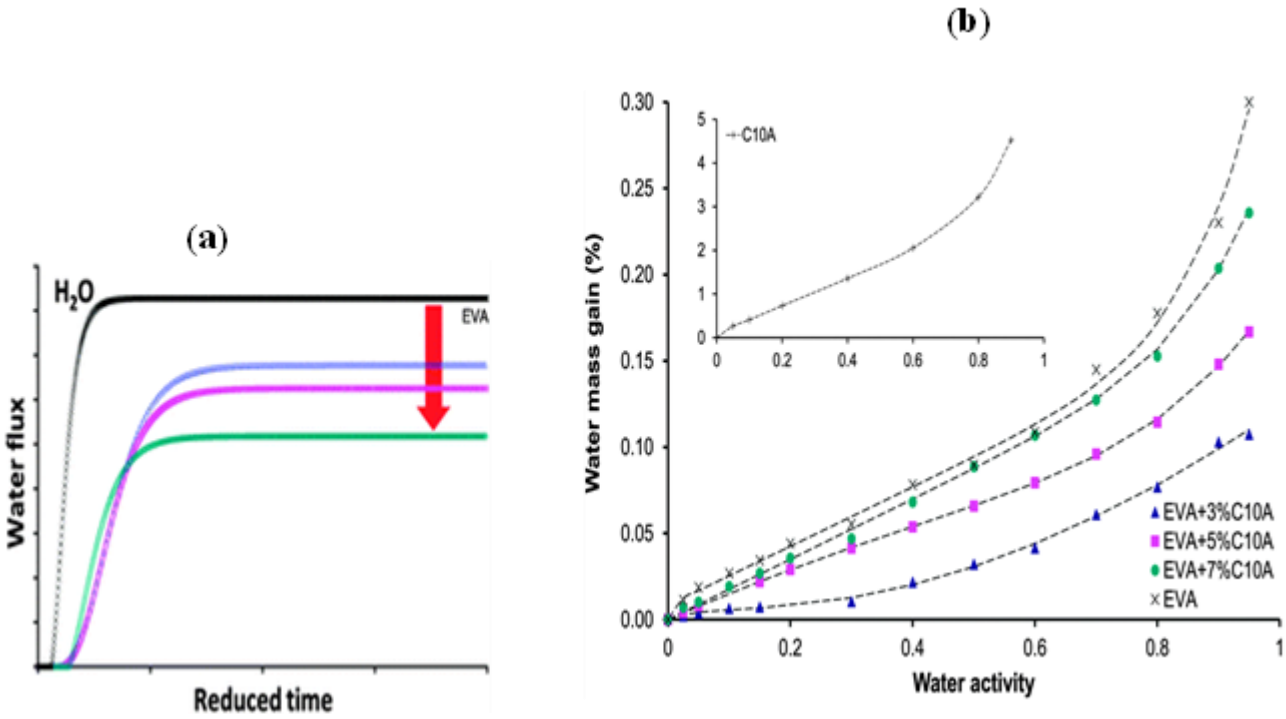

Figure 3.19. (a) Water permeation flux as a function reduced time. (b) Water vapor sorption isotherms of the neat EVA matrix and its nanocomposites with an inset of C10A nanoclay isotherm. The dotted lines correspond to the fitting of experimental data with Park's model. Reproduced with permission from Reference [169]. Open Access 2015, The Royal Society of Chemistry.

The water vapor sorption isotherm curves are also known as water mass gain in the equilibrium state versus water activity deduced from water sorption kinetics, reported in Figure 3.19b. The water sorption capacity of nanoclays is evidently higher than that of the EVA matrix. The incorporation of Cloisite (C10A) into the EVA matrix induced the shift of isotherm curves to lower values at a given activity (Figure 3.19b), reproducing a reduction in water mass gain. As a result, C10A sorbed higher water mass gain than the matrix, which contributed to increasing sorption capacity of nanocomposites, and this finding is in good agreement with the reduction of water permeability. The decrease in mass gain can be related to tortuosity effects induced by nanoclays in a matrix and which counterbalance the strong water sorption capacity of nanofillers [170]. An increase in nanoclay content, reproduced an increase in water mass gain for nanocomposite

samples, which is measured for the whole water activity range due to a more hydrophilic character of nanoclays than the matrix one. This can be attributed to the increase of the polar site number of surfactant-modified nanoclays. The sorption process of the resulting nanocomposites is thus driven by the nanoclay sorption capacity, and the incorporation of nanoclay content into the nonpolar matrix. The nanocomposite with the highest nanoclay loading is categorized by the highest water mass gain. Water molecules are implicitly located in the matrix/nanoclay interfacial regions, and the conclusion is water absorption behavior of nanocomposites obeyed Fick's law. The increased tortuosity within the EVA matrix/nanoclays is therefore in opposite effect to the increased water solubility due to the hydrophilic character of nanoclays. Rajan et al. [171] studied the role of dicarboxylic acid (malic acid (A)) in chitosan (CS)/modified-metal ion decorated bentonite clay (BC) and the defluoridation efficiency in fluoride contaminated groundwater. The samples were prepared through the solution mixing and their findings revealed the chemical changes of the adsorbent as shown in Figure 3.20. The bands observed in the range of 3413–3440 cm−1 in the spectra of chitosan confirm the presence of O–H bond stretching and N–H bond stretching frequency [172]. The bands at 3046 cm−1 and 2900 cm−1 related to aliphatic stretching vibrations of –CH, while the bands at 2927 and 2860 cm−1 can be attributed to the C–H stretching vibration of the –CH2 groups in chitosan. The aliphatic stretching vibrations of –CH have very low intensity in chitosan [171].

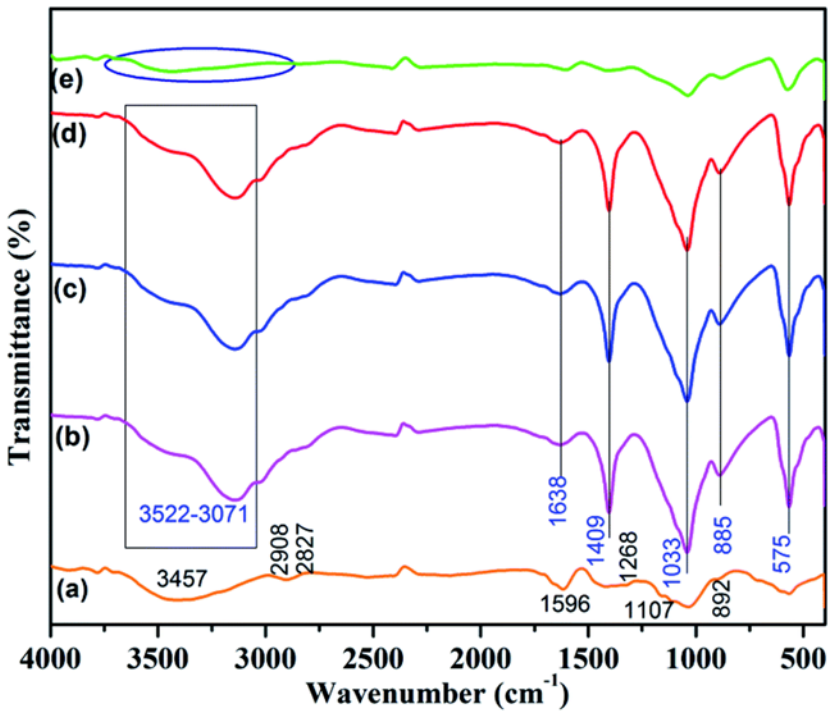

Figure 3.20. FTIR spectrum of (a) chitosan (CS), (b) aluminum bentonite clay-malic acid chitosan (AlBCA@CS), (c) LaBC-A@CS, (d) cerium bentonite clay-malic acid chitosan (CeBC-A@CS) and (e) fluoride adsorbed CeBC-A@CS. Reproduced with permission from Reference [151]. Open Access 2020, RSC Advances.

The peak observed at 1596 cm−1 is related to N–H bond scission from the primary amine because of free amino groups in the crosslinked chitosan segments [173]. The peak which appeared at 1596 cm−1 indicates the aromatic ring stretching vibration. The C=O adsorption peak of secondary hydroxyl groups becomes more pronounced and shifts to 1107 cm−1 [174]. It can be seen in Figure 20e that the peak intensity of the hydroxyl group was remarkably reduced because of the fluoride adsorption. Furthermore, the nitrogen adsorption–desorption analysis was done by Rajan and co-authors [170] as evident in Figure 3.21. The surface area, pore width and pore volume of the synthesized CeBC-A@CS adsorbent was characterized by Brunauer–Emmett–Teller (BET) analysis and reported as 103 m2 ·g −1 , 12.71 nm and 0.0321 cm3 ·g −1 . The synthesized CeBC-A@CS adsorbent possessed high surface area, higher pore width and larger microspore volume, which confirmed that the synthesized adsorbent has maximum adsorption capacity.

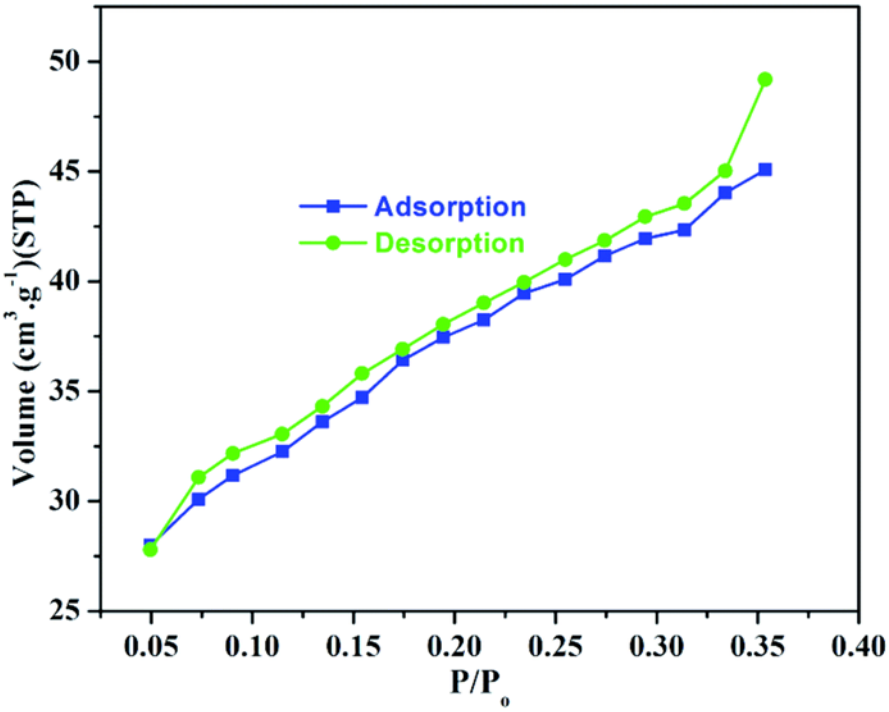

Figure 3.21. Nitrogen adsorption–desorption isotherm spectrum of cerium bentonite clay-malic acid chitosan (CeBCA@CS) adsorbent. Reproduced with permission from Reference [151]. Open Access 2020, RSC Advances.

3.4. Concluding Remarks and Future Prospects

In summary, polymer/layered clay nanocomposites are the most progressive and alternative procedures for water purification systems. Synthesis of nanomaterials such as nanoclays and/or LDHs play a pivotal role in improving the physicochemical properties of adsorbents for pollutant removal in water. Furthermore, layered double hydroxides (LDHs) materials have attracted considerable attention and are preferred candidates as sorbents in water treatment because of their remarkable ability to eliminate a variety of water contaminants instantaneously. Their unique properties as anion exchangers and their compositional versatility among other factors is an advantage over other types of clays in the field of water treatment. Various modification techniques were discussed for the preparation of functionalized clay and LDH nanomaterials and showed influence on the dispersion of nanoclay fillers in the polymer matrices. The desired properties for the polymer/clay and LDH nanocomposites are primarily dependent on the type of modifying agents used for functionalization of layered silicates. Solution blending technique and in situ

polymerization method seemed to provide good dispersion of clay layers in polymer matrix compared to melt blending technique. This is mainly because of the low viscosity and high agitation power associated with solution blending. However, melt blending is considered as an industrially viable as well as ecofriendly technique and shows high economic potential. The addition of stabilizers and/or compatibilizers during the processing stage is believed to lead to an improved number the properties of polymer/clay and LDH nanocomposites. Development of an appropriate understanding of the structure, property and formulation relationship in both clay-based nanocomposites and LDH based hybrids needs to be further researched for better output in water purification. LDH-containing hybrids are the new emerging areas of research in water purification processes. Due to their nontoxicity, higher surface area than individual constituents and notable adsorption capacity, these LDH hybrids have attracted a considerable interest in water treatment applications. The polymer/modified-clay nanocomposites with exfoliated morphology disclosed strong reduction in water surface tension and efficiently remove methylene blue (MB) dye and other contaminants from water. The adsorption increased with increasing dye concentration, pH values and increasing temperature due to the increased kinetic energies of the molecules. The morphologies of polymer/LDH nanocomposites exhibited a remarkable high adsorption capacity for the efficient removal of dyes and heavy metal ions from water within a short time interval.

Author Contributions: M.M., J.S.S. and M.J.M. conceptualized, co-designed and steered the review as well as co-writing Sections 1, 2, 2.1–2.3 and 3. S.I.M. and K.L. co-wrote Sections 2.4 and 4, while M.M., J.S.S. and M.J.M. compiled the article together. J.S.S. and M.J.M. were responsible for funding acquisition of the manuscript. All authors have read and agreed to the published version of the manuscript.

Funding: This research was funded by the National Research Foundation (NRF) of South Africa, grant number (s) 114270 and 127278.

Acknowledgments: The National Research Foundation (NRF) of South Africa is highly acknowledged for financial support of this research work.

Conflicts of Interest: No conflict of interest declared by the authors.

Abbreviations

LDHs	Layered double hydroxides	Cl	Chloride ion
2D	Two-dimensional	NO3−	Nitrate ion
WHO	World Health Organization	CO32−	Carbonate ion
WASH	Water, sanitation and hygiene	N2	Nitrogen
SDGs	Sustainable development goals	M2+	Divalent cation
MF	Microfiltration	M3+	Trivalent cation
UF	Ultrafiltration	LBL	Layer-by-layer
NF	Nanofiltration	NH4OH	Ammonium hydroxide
RO	Reverse osmosis	SLNSs	Single layer nanosheets
SMNs	Surface modification of nanomaterials	PVA	Poly(vinyl alcohol)
PCNCs	Polymer clay nanocomposites	PEG	Poly(ethylene glycol)
PNCs	Polymer nanocomposites	HT	Hydrotalcite
MDPI	Multidisciplinary Digital Publishing Institute	PAA	Poly(acrylic acid)
NCs	Nanoclays	POX	Poly(2-oxazoline)
MMT	Montmorillonite	PP	Polypropylene
CEC	Cation exchange capacity	PIP	Polyisoprene
PMMA	Poly(methyl methacrylate)	PLLA	Poly(l-lactic acid)
Mg(OH)2	Magnesium hydroxide	PA11	Polyamide
EVA	Poly(ethylene-co-vinyl acetate)	PAM	Polyacrylamide
Al(NO3)3.9H2O	Aluminum nitrate nonahydrate	PE	Polyethylene
Mg(NO3)2.6H2O	Magnesium nitrate hexahydrate	PLA	Poly(lactic acid)
BPF	Bio-oil phenolic foam	PS	Polystyrene
MBPF	Modified bio-oil phenolic foam	BT	Bentonite
MAPP	Maleic-anhydride-grafted polypropylene	MB	Methylene Blue

TPU	Thermoplastic polyurethane	CCS	Crosslinked chitosan
NBR	Nitrile butadiene rubber	MO	Methyl orange
PBT	Polybutylene terephthalate	PANI	Polyaniline
NIPAM	N-isopropylacrylamide	DNA	Deoxyribonucleic acid
SEM	Scanning electron microscopy	AA	Acid activated
OMMT	Organically modified montmorillonite	PES	Polyethersulfone
TEM	Transmission electron microscopy	AO-II	Acid Orange II
PBS	Phosphate-buffered saline	Ppy	Polypyrrole
SDBS	Sodium dodecylbenzene sulfonate	CS	Chitosan
AMPS	2-acrylsmido-2-methyl-propanesulfonic acid	SA	Sodium alginate
GA	Glutaraldehyde	NaOH	Sodium hydroxide
HCl	Hydrochloric acid	BC	Bentonite clay
CeBC-A@CS	Cerium bentonite clay-malic acid chitosan		
LaBC-A@CS	Lanthanum bentonite clay-malic acid chitosan		
AlBC-A@CS	Aluminum bentonite clay-malic acid chitosan		
pHzpc	pH zero charge	MnO2	Manganese dioxide
FeMnMg-LDH	Iron Manganese Magnesium-layered double hydroxide		
DI	Deionized	Pb(II)	Lead ion
RSC	The Royal Society of Chemistry	HCO_3^-	Bicarbonate ion
Co/Mo-LDH	Cobalt/Molybdenum-layered double hydroxide		

PHF	Polyhydroxy fullerenes	SO_4^{2-}	Sulphate ion
SBR	Styrene-butadiene rubber	Cl^-	Chloride ion
VE	Vinyl ester	EP	Epoxy
LDO	Layered double oxide	NO_3^-	Nitrate ion
Mg-Al-LDH	Magnesium-Aluminum-layered double hydroxide		
XRD	X-ray Diffractometry	AB	Amido Black
HPO_4^{2-}	Hydrogen phosphate ion	CH_2	Methylene
N-H	Imidogen	C=O	Carbon monoxide
C10A	Cloisite 10A	C-H	Methylene group
$\Delta\mu$	Chemical potential difference		
BET	Brunauer-Emmett-Teller		
NRF	National Research Foundation		

References

1. Briggs, A. M., Cross, M. J., Hoy, D. G., Sanchez-Riera, L., Blyth, F. M., Woolf, A. D., March, L. Musculoskeletal health conditions represent a global threat to healthy aging: a report for the 2015 World Health Organization world report on ageing and health. The Gerontologist 2016, 56(2), S243-S255.
2. Ortigara, A. R. C., Kay, M., Uhlenbrook, S. A review of the SDG 6 synthesis report 2018 from an education, training, and research perspective. Water 2018, 10(10), 1353.
3. Ait-Kadi, M. Water for development and development for water: realizing the sustainable development goals (SDGs) vision. Aquat. Procedia 2016, 6, 106-110.
4. Le, N. L., Nunes, S. P. Materials and membrane technologies for water and energy sustainability. Sustain. Mater. Techno. 2016, *7*, 1-28.
5. Anjum, M., Miandad, R., Waqas, M., Gehany, F., Barakat, M. A. Remediation of wastewater using various nano-materials. Arab. J. Chem. 2019, 12(8), 4897-4919.
6. Krstić, V., Urošević, T., Pešovski, B. A review on adsorbents for treatment of water and wastewaters containing copper ions. Chem. Eng. Sci. 2018, 192, 273-287.
7. Warsinger, D.M., Chakraborty, S., Tow, E.W., Plumlee, M.H., Bellona, C., Loutatidou, S., Karimi, L., Mikelonis, A.M., Achilli, A., Ghassemi, A., Padhye, L.P. A review of polymeric membranes and processes for potable water reuse. Prog. Polym. 2018, 81, 209-237.
8. Pandey, N., Shukla, S. K., Singh, N. B. Water purification by polymer nanocomposites: an overview. Nanocomposites 2017, 3(2), 47-66.
9. Tlili, I., Alkanhal, T. A. Nanotechnology for water purification: electrospun nanofibrous membrane in water and wastewater treatment. J. Water Reuse Desal. 2019, 9(3), 232-248.
10. Yaqoob, A. A., Parveen, T., Umar, K., Mohamad Ibrahim, M. N. Role of nanomaterials in the treatment of wastewater: A review. Water 2020, 12(2), 495.
11. Guerra, F. D., Attia, M. F., Whitehead, D. C., Alexis, F. Nanotechnology for environmental remediation: materials and applications. Molecules 2018, 23(7), 1760.
12. Selatile, M. K., Ray, S. S., Ojijo, V., Sadiku, R. Recent developments in polymeric electrospun nanofibrous membranes for seawater desalination. RSC adv. 2018, 8(66), 37915-37938.
13. Liao, Y., Loh, C. H., Tian, M., Wang, R., Fane, A. G. Progress in electrospun polymeric nanofibrous membranes for water treatment: Fabrication, modification and applications. Prog. Polym. 2018, 77, 69-94.

14. Umar, K., Parveen, T., Khan, M. A., Ibrahim, M. N. M., Ahmad, A., Rafatullah, M. Degradation of organic pollutants using metal-doped TiO2 photocatalysts under visible light: a comparative study. Desal. Water Treat. 2019, 161, 275-282.
15. Tang, K., Gong, C., Wang, D. Reduction potential, shadow prices, and pollution costs of agricultural pollutants in China. Sci. Total Environ. 2016, 541, 42-50.
16. Richter, K. E., Ayers, J. M. An approach to predicting sediment microbial fuel cell performance in shallow and deep water. Res. J. Appl. Sci. 2018, 8(12), 2628.
17. Sizmur, T., Fresno, T., Akgül, G., Frost, H., Moreno-Jiménez, E. Biochar modification to enhance sorption of inorganics from water. Bioresour. Technol. 2017, 246, 34-47.
18. Wang, J., Wang, Z., Vieira, C. L., Wolfson, J. M., Pingtian, G., Huang, S. Review on the treatment of organic pollutants in water by ultrasonic technology. Ultrason. Sonochem. 2019, 55, 273-278.
19. Liu, C., Hong, T., Li, H., Wang, L. From club convergence of per capita industrial pollutant emissions to industrial transfer effects: An empirical study across 285 cities in China. Energy Policy 2018, 121, 300-313.
20. Bayoumi, T. A., Saleh, H. M. Characterization of biological waste stabilized by cement during immersion in aqueous media to develop disposal strategies for phytomediated radioactive waste. Progress in Nuclear Energy 2018, 107, 83-89.
21. Ma, H., Guo, Y., Qin, Y., Li, Y. Y. Nutrient recovery technologies integrated with energy recovery by waste biomass anaerobic digestion. Bioresour. Technol. 2018, 269, 520-531.
22. Hlongwane, G. N., Sekoai, P. T., Meyyappan, M., Moothi, K. Simultaneous removal of pollutants from water using nanoparticles: A shift from single pollutant control to multiple pollutant control. Sci. Total Environ. 2019, 656, 808-833.
23. Rajasulochana, P., Preethy, V. Comparison on efficiency of various techniques in treatment of waste and sewage water–A comprehensive review. Res.-Efficient Technol. 2016, 2(4), 175-184.
24. Jeevanandam, J., Barhoum, A., Chan, Y. S., Dufresne, A., Danquah, M. K. Review on nanoparticles and nanostructured materials: history, sources, toxicity and regulations. Beilstein J. Nanotechnol. 2018, 9(1), 1050-1074.
25. Palmero, P. Structural ceramic nanocomposites: a review of properties and powders' synthesis methods. Nanomaterials 2015, 5(2), 656-696.

26. Chen, J., Liu, B., Gao, X., Xu, D. A review of the interfacial characteristics of polymer nanocomposites containing carbon nanotubes. RSC Adv. 2018, 8(49), 28048-28085.
27. Kumar, S., Nehra, M., Dilbaghi, N., Tankeshwar, K., Kim, K. H. Recent advances and remaining challenges for polymeric nanocomposites in healthcare applications. Prog. Polym. Sci. 2018, 80, 1-38.
28. Lofrano, G., Carotenuto, M., Libralato, G., Domingos, R.F., Markus, A., Dini, L., Gautam, R.K., Baldantoni, D., Rossi, M., Sharma, S.K. Chattopadhyaya, M.C. Polymer functionalized nanocomposites for metals removal from water and wastewater: an overview. Water Res. 2016, 92, 22-37.
29. Müller, K., Bugnicourt, E., Latorre, M., Jorda, M., Echegoyen Sanz, Y., Lagaron, J.M., Miesbauer, O., Bianchin, A., Hankin, S., Bölz, U. and Pérez, G. Review on the processing and properties of polymer nanocomposites and nanocoatings and their applications in the packaging, automotive and solar energy fields. Nanomaterials 2017, 7(4), 74.
30. Ashraf, M. A., Peng, W., Zare, Y., Rhee, K. Y. Effects of size and aggregation/agglomeration of nanoparticles on the interfacial/interphase properties and tensile strength of polymer nanocomposites. Nanoscale Res. Lett. 2018, 13(1), 214.
31. Guo, F., Aryana, S., Han, Y., Jiao, Y. A review of the synthesis and applications of polymer–nanoclay composites. Appl. Sci. 2018, 8(9), 1696.
32. Crucho, C. I., Barros, M. T. Polymeric nanoparticles: A study on the preparation variables and characterization methods. Mater. Sci. Eng. C 2017, 80, 771-784.
33. Tessema, A., Zhao, D., Moll, J., Xu, S., Yang, R., Li, C., Kumar, S.K., Kidane, A. Effect of filler loading, geometry, dispersion and temperature on thermal conductivity of polymer nanocomposites. Polym. Test 2017, 57, 101-106.
34. Ghadimi, M., Zangenehtabar, S., Homaeigohar, S. An Overview of the water remediation potential of nanomaterials and their ecotoxicological impacts. Water 2020, *12*(4), 1150.
35. Nasir, A., Masood, F., Yasin, T., Hameed, A. Progress in polymeric nanocomposite membranes for wastewater treatment: Preparation, properties and applications. J. Ind. Eng. Chem. 2019, 79, 29-40.
36. Schaming, D., Remita, H. Nanotechnology: from the ancient time to nowadays. Found. Chem. 2015, 17(3), 187-205.

37. Usmani, M. A., Khan, I., Ahmad, N., Bhat, A. H., Sharma, D. K., Rather, J. A., Hassan, S.I. Modification of Nanoclay Systems: An Approach to Explore Various Applications. In Nanoclay Reinforced Polymer Composites. Springer, Singapore 2016; pp. 57-83.
38. Uddin, M. K. A review on the adsorption of heavy metals by clay minerals, with special focus on the past decade. Chem. Eng. J. 2017, 308, 438-462.
39. Nadziakiewicza, M., Kehoe, S., Micek, P. Physico-chemical properties of clay minerals and their use as a health promoting feed additive. Animals 2019, 9(10), 714.
40. M. Jawaid, A.K. Qaiss, R. Bouhfid. Nanoclay Reinforced Polymer Composites: Nanocomposites and Bionanocomposites. Springer: Singapore, 2016; pp. 391.
41. Awasthi, A., Jadhao, P., Kumari, K. Clay nano-adsorbent: structures, applications and mechanism for water treatment. SN Applied Sciences 2019, 1(9), 1076.
42. Jlassi, K., Krupa, I., Chehimi, M. M. Overview: clay preparation, properties, modification. In Clay-polymer nanocomposites. Elsevier, 2017; pp. 1-28.
43. Ghadiri, M., Chrzanowski, W., Rohanizadeh, R. Biomedical applications of cationic clay minerals. RSC Adv. 2015, 5(37), 29467-29481.
44. Lázaro, B.B. Halloysite and kaolinite: Two clay minerals with geological and technological importance. J. Acad. Exact Phys. Chem. Nat. Sci. Zaragoza 2015, 70, 7–38.
45. Yu, F., Deng, H., Bai, H., Zhang, Q., Wang, K., Chen, F., Fu, Q. Confine clay in an alternating multilayered structure through injection molding: a simple and efficient route to improve barrier performance of polymeric materials. ACS Appl. Mater. Inter. 2015, 7(19), 10178-10189.
46. Ferrari, P. C., Araujo, F. F., Pianaro, S. A. Halloysite nanotubes-polymeric nanocomposites: characteristics, modifications and controlled drug delivery approaches. Cerâmica 2017, 63(368), 423-431.
47. Yusoh, K., Kumaran, S. V., Ismail, F. S. Surface modification of nanoclay for the synthesis of polycaprolactone (PCL)–clay nanocomposite. In MATEC Web of Conferences. EDP Sciences 2018, Vol. 150, p. 02005
48. Irshidat, M. R., Al-Saleh, M. H. Thermal performance and fire resistance of nanoclay modified cementitious materials. Constr. Build. Mater. 2018, 159, 213-219.
49. Murugesan, S., Scheibel, T. Copolymer/Clay Nanocomposites for Biomedical Applications. Adv. Funct. Mater. 2020, 30(17), 1908101.

50. Wang, W., Wang, A. Nanoscale Clay Minerals for Functional Ecomaterials: Fabrication, Applications, and Future Trends. Handbook of Ecomaterials. Springer, Cham, 2019; pp 1-82.
51. Satish, S., Tharmavaram, M., Rawtani, D. Halloysite nanotubes as a nature's boon for biomedical applications. Nanobiomedicine 2019, 6, 1–16.
52. Gaaz, T. S., Sulong, A. B., Kadhum, A. A. H., Al-Amiery, A. A., Nassir, M. H., Jaaz, A. H. The impact of halloysite on the thermo-mechanical properties of polymer composites. Molecules 2017, 22(5), 838.
53. Lazzara, G., Cavallaro, G., Panchal, A., Fakhrullin, R., Stavitskaya, A., Vinokurov, V., Lvov, Y. An assembly of organic-inorganic composites using halloysite clay nanotubes. Curr. Opin. Colloid In. 2018, 35, 42-50.
54. Ursino, C., Castro-Muñoz, R., Drioli, E., Gzara, L., Albeirutty, M. H., Figoli, A. Progress of nanocomposite membranes for water treatment. Membranes 2018, 8(2), 18.
55. Sajid, M., Basheer, C. Layered double hydroxides: emerging sorbent materials for analytical extractions. Trac-Trend Anal. Chem. 2016, 75, 174-182.
56. Mir, Z. M., Bastos, A., Höche, D., Zheludkevich, M. L. Recent Advances on the Application of Layered Double Hydroxides in Concrete—A Review. Materials 2020, 13(6), 1426.
57. Mohapatra, L., Parida, K. A review on the recent progress, challenges and perspective of layered double hydroxides as promising photocatalysts. J. Mater. Chem. 2016, 4(28), 10744-10766.
58. Jaśkaniec, S., Hobbs, C., Seral-Ascaso, A., Coelho, J., Browne, M.P., Tyndall, D., Sasaki, T., Nicolosi, V., Low-temperature synthesis and investigation into the formation mechanism of high quality Ni-Fe layered double hydroxides hexagonal platelets. Sci. Rep. 2018., 8(1), 1-8.
59. Mishra, G., Dash, B., Pandey, S. Layered double hydroxides: A brief review from fundamentals to application as evolving biomaterials. Appl. Clay Sci. 2018, 153, 172-186.
60. Barahuie, F., Hussein, M.Z., Gani, S.A., Fakurazi, S., Zainal, Z. Synthesis of protocatechuic acid–zinc/aluminium–layered double hydroxide nanocomposite as ananticancer nanodelivery system. J. Solid State Chem. 2015, 221, 21–31.
61. Yu, J., Wang, Q., O'Hare, D., Sun, L. Preparation of two dimensional layered double hydroxide nanosheets and their applications. Chem. Soc. Rev. 2017, 46, 5950.

62. He, X., Qiu, X., Hu, C., Liu, Y. Treatment of heavy metal ions in wastewater using layered double hydroxides: A review. Journal of Dispersion Science and Technology 2018, 39(6), 792−801.
63. Sokol, D., Klemkaite-Ramanauske, K., Khinsky, A., Baltakys, K., Beganskiene, A., Baltusnikas, A., Pinkas, J., Kareiva, A. "Reconstruction effects on surface properties of Co/Mg/Al layered double hydroxide," Materials Science. 2017, 23,144−149.
64. Abo El-Reesh, G.Y., Farghali, A.A., Taha, M., Mahmoud, R.K. Novel synthesis of Ni/Fe layered double hydroxides using urea and glycerol and their enhanced adsorption behavior for Cr(VI) removal. *Sci Rep.* 2020, 10, 587.
65. Pahalagedara, M.N., Samaraweera, M., Dharmarathna, S., Kuo, C. H., Pahalagedara, L.R., Gascón, J.A., and Suib, S.L. Removal of azo dyes: Intercalation into sonochemically synthesized NiAl layered double hydroxide. J. Phys. Chem. C. 2014, 118(31),17801–17809.
66. Skorb, E.V., Möhwald, H., Andreeva, D.V. Effect of cavitation bubble collapse on the modification of solids: Crystallization aspects. Langmuir 2016, 32, 43, 11072–11085.
67. Altay, R., Sadaghiani, A.K., Sevgen, M.I., Sisman, A., A. Koşsar. Numerical and experimental studies on the effect of surface roughness and ultrasonic frequency on bubble dynamics in acoustic cavitation. *Energies* 2020, *13*(5), 1126.
68. Daud, M., Kamal, M.S., Shehzad, F., Al-Harthi, M.A. Graphene/layered double hydroxides nanocomposites: a review of recent progress in synthesis and applications. Carbon 2016, 104, 241–252.
69. Zhao, X., Cao, J.-P., Zhao, J., Hu, G.-H., Dang, Z.-M. A hybrid Mg–Al layered double hydroxide/graphene nanostructure obtained via hydrothermal synthesis. Chem. Phys. Lett. 2014, 605–606, 77–80.
70. Liu, W., Xu, S., Liang, R., Wei, M., Evans, D.G., Duan, X. *In situ* synthesis of nitrogen-doped carbon dots in the interlayer region of a layered double hydroxide with tunable quantum yield. **J. Mater. Chem. C**. 2017, **5**, 3536−3541.
71. Cermelj, K., Ruengkajorn, K., Buffet, J.-C. O'Hare, D. Layered double hydroxide nanosheets via solvothermal delamination. J. Ener. Chem. 2019, 35(1), 88−94.
72. Wang, L., Shi, C., Wang, L., Pan, L., Zhang, X., Zou, J.-J. Rational design, synthesis, adsorption principles and applications of metal oxide adsorbents: a review. **Nanoscale** 2020,**12(8)**, 4790−4815.

73. Forano, C., Bruna, F., Mousty, C., Prevot, V. Interactions between biological cells and layered double hydroxides: Towards functional materials. Chem. Rec. 2018, 18, 1–18.
74. Larocca, N.M., Filho, R.B., Pessan, L.A. Influence of layer-by-layer deposition techniques and incorporation of layered double hydroxides (LDH) on the morphology and gas barrier properties of polyelectrolytes multilayer thin films.
75. Shao, M., Zhang, R., Li, Z., Wei, M., Evans, D.G., Duan, X. Layered double hydroxides toward electrochemical energy storage and conversion: design, synthesis and applications. **Chem. Commun.**, 2015,**51,** 15880−15893.
76. Danks, A.E., Hall, S.R. Schnepp, Z. The evolution of 'sol–gel' chemistry as a technique for materials synthesis**. Mater. Horiz.,** 2016,**3**, 91−112.
77. Zhang, Y., Li, H., Du, N., Zhang, R., Hou, W. Large-scale aqueous synthesis of layered double hydroxide single-layer nanosheets. Colloids and Surfaces A: Physicochem. Eng. Aspects 2016,501, 49–54.
78. Sarma, G. K., Rashid, M. H. Synthesis of Mg/Al layered double hydroxides for adsorptive removal of fluoride from water: A mechanistic and kinetic study. J. Chem. Eng 2018, 63(8), 2957-2965.
79. Sajid, M., Nazal, M. K., Baig, N., Osman, A. M. Removal of heavy metals and organic pollutants from water using dendritic polymers based adsorbents: a critical review. Sep. Purif. Technol. 2018, 191, 400-423.
80. Maziarz, P., Matusik, J., Leiviskä, T. Mg/Al LDH Enhances Sulfate removal and Clarification of AMD Wastewater in Precipitation Processes. Materials 2019, 12(14), 2334.
81. Daud, M., Hai, A., Banat, F., Wazir, M. B., Habib, M., Bharath, G., Al-Harthi, M. A. A review on the recent advances, challenges and future aspect of layered double hydroxides (LDH)–Containing hybrids as promising adsorbents for dyes removal. J. Mol. Liq. 2019, 288, 110989.
82. Li, M., Tian, R., Yan, D., Liang, R., Wei, M., Evans, D. G., Duan, X. A luminescent ultrathin film with reversible sensing toward pressure. ChemComm 2016, 52(25), 4663-4666.
83. Asif, M., Aziz, A., Azeem, M., Wang, Z., Ashraf, G., Xiao, F., Chen, X., Liu, H. A review on electrochemical biosensing platform based on layered double hydroxides for small molecule biomarkers determination. Adv. Colloid Interface Sci. 2018, 262, 21-38.
84. Baig, N., Sajid, M. Applications of layered double hydroxides based electrochemical sensors for determination of environmental pollutants: A review. Trends Environ. Anal. 2017, 16, 1-15.

85. Guan, S., Liang, R., Li, C., Yan, D., Wei, M., Evans, D. G., Duan, X. A layered drug nanovehicle toward targeted cancer imaging and therapy. J. Mater. Chem. B. 2016, 4(7), 1331-1336.
86. Yan, L., Gonca, S., Zhu, G., Zhang, W., Chen, X. Layered double hydroxide nanostructures and nanocomposites for biomedical applications. J. Mater. Chem. B. 2019, 7(37), 5583-5601.
87. Bastianini, M., Faffa, C., Sisani, M., Petracci, A. Caffeic Acid-layered Double Hydroxide Hybrid: A New Raw Material for Cosmetic Applications. Cosmetics 2018, 5(3), 51.
88. Amberg, N., Fogarassy, C. Green consumer behavior in the cosmetics market. Resources 2019, 8(3), 137.
89. Caminade, A. M., Ouali, A., Laurent, R., Turrin, C. O., Majoral, J. P. Coordination chemistry with phosphorus dendrimers. Applications as catalysts, for materials, and in biology. Coordination Chemistry Reviews 2016, 308, 478-497.
90. Jing, M., Hou, H., Banks, C. E., Yang, Y., Zhang, Y., Ji, X. Alternating voltage introduced NiCo double hydroxide layered nanoflakes for an asymmetric supercapacitor. ACS Appl. Mater. Inter. 2015, 7(41), 22741-22744.
91. Mochane, M.J., Magagula, S.I., Sefadi, J.S., Sadiku, E.R., Mokhena, T.C. Morphology, Thermal Stability, and Flammability Properties of Polymer-Layered Double Hydroxide (LDH) Nanocomposites: A Review. Crystals 2020, 10, 612.
92. Salavagione, H. J., Diez-Pascual, A. M., Lázaro, E., Vera, S., Gomez-Fatou, M. A. Chemical sensors based on polymer composites with carbon nanotubes and graphene: the role of the polymer. J. Mater. Chem. A 2014, 2(35), 14289-14328.
93. Bhattacharya, M. Polymer nanocomposites—a comparison between carbon nanotubes, graphene, and clay as nanofillers. Materials 2016, 9(4), 262.
94. Madhumitha, G., Fowsiya, J., Mohana Roopan, S., Thakur, V. K. Recent advances in starch–clay nanocomposites. Int. J. Polym. Anal. Charact. 2018, 23(4), 331-345.
95. Cui, Y., Kumar, S., Kona, B. R., van Houcke, D. Gas barrier properties of polymer/clay nanocomposites. RSC Adv. 2015, 5(78), 63669-63690.
96. Hammad, S., Noby, H., Elkady, M. F., El-Shazly, A. H. In-situ of polyaniline/polypyrrole copolymer using different techniques. Mater. Sci. Eng. 2017, 290, 012001.
97. Unalan, I. U., Cerri, G., Marcuzzo, E., Cozzolino, C. A., Farris, S. Nanocomposite films and coatings using inorganic nanobuilding blocks (NBB): current applications and future opportunities in the food packaging sector. RSC adv. 2014, 4(56), 29393-29428.

98. Abedi, S., Abdouss, M. A review of clay-supported Ziegler–Natta catalysts for production of polyolefin/clay nanocomposites through in situ polymerization. Appl. Catal. A-Gen. 2014, 475, 386-409.
99. Reddy, K. R., El-Zein, A., Airey, D. W., Alonso-Marroquin, F., Schubel, P., Manalo, A. Self-healing polymers: Synthesis methods and applications. Nano-Structures & Nano-Objects 2020, 23, 100500.
100. Ozkose, U. U., Altinkok, C., Yilmaz, O., Alpturk, O., Tasdelen, M. A. In-situ preparation of poly (2-ethyl-2-oxazoline)/clay nanocomposites via living cationic ring-opening polymerization. Eur. Polym. J. 2017, 88, 586-593.
101. Cruz, S. M., Viana, J. C. Structure–Properties Relationships in Thermoplastic Polyurethane Elastomer Nanocomposites: Interactions between Polymer Phases and Nanofillers. Macromol. Mater. Eng. 2015, 300(11), 1153-1162.
102. Jafarbeglou, M., Abdouss, M., Shoushtari, A. M., Jafarbeglou, M. Clay nanocomposites as engineered drug delivery systems. RSC adv. 2016, 6(55), 50002-50016.
103. Zabihi, O., Ahmadi, M., Nikafshar, S., Preyeswary, K. C., Naebe, M. A technical review on epoxy-clay nanocomposites: Structure, properties, and their applications in fiber reinforced composites. Compos. B. Eng. 2018, 135, 1-24.
104. Ercan, N., Durmus, A., Kaşgöz, A. Comparing of melt blending and solution mixing methods on the physical properties of thermoplastic polyurethane/organoclay nanocomposite films. J. Thermoplast. Compos. Mater. 2017, 30(7), 950-970.
105. Mohd Zaini, N. A., Ismail, H., Rusli, A. Short review on sepiolite-filled polymer nanocomposites. Polym. Plast. Technol. Eng. 2017, 56(15), 1665-1679.
106. Saeed, K., Khan, I. Characterization of clay filled poly (butylene terephthalate) nanocomposites prepared by solution blending. Polímeros 2015, 25(6), 591-595.
107. Luecha, W., Magaraphan, R. A novel and facile nanoclay aerogel masterbatch toward exfoliated polymer-clay nanocomposites through a melt-mixing process. Adv. Mater. Sci Eng. 2018, 2018, 1-14.
108. Kong, J., Li, Z., Cao, Z., Han, C., Dong, L. The excellent gas barrier properties and unique mechanical properties of poly (propylene carbonate)/organo-montmorillonite nanocomposites. Polym. Bull. 2017, 74(12), 5065-5082.

109. Fu, S., Sun, Z., Huang, P., Li, Y., Hu, N. Some basic aspects of polymer nanocomposites: A critical review. Nano Materials Science 2019, 1(1), 2-30.
110. Pesetskii, S. S., Bogdanovich, S. P., & Aderikha, V. N. Polymer/clay nanocomposites produced by dispersing layered silicates in thermoplastic melts. In Polymer Nanocomposites for Advanced Engineering and Military Applications, IGI Global, 2019, pp. 66−94.
111. Bai, C., Ke, Y., Hu, X., Xing, L., Zhao, Y., Lu, S., Lin, Y. Preparation and properties of amphiphilic hydrophobically associative polymer/montmorillonite nanocomposites. R. Soc. Open Sci. 2020, 7, 200199.
112. Szadkowski, B., Marzec, A., Rybiński, P., Żukowski, W., Zaborski, M. Characterization of Ethylene–propylene Composites Filled with Perlite and Vermiculite Minerals: Mechanical, Barrier, and Flammability Properties. Materials 2020, 13,585.
113. Al-Shahrani, A., Taie, I., Fihri, A., Alabedi, G. Polymer-Clay Nanocomposites for Corrosion Protection. Current Topics in the Utilization of Clay in Industrial and Medical Applications, IntechOpen 2018, pp. 61−79.
114. Alvi, M. U., Zulfiqar, S., Sarwar, M. I., Kidwai, A. A. Preparation and properties of nanocomposites derived from aromatic polyamide and surface functionalized nanoclay. Chem. Eng. Commun. 2016, 203(2), 242−250.
115. Chen, H. H., Thirumavalavan, M., Lin, F. Y., Lee, J. F. A facile approach for achieving an effective dual sorption ability of Si/SH/S grafted sodium montmorillonite. **RSC Adv.** 2015, **5(71),** 57792−57803.
116. Haider, S., Kausar, A., Muhammad, B. Overview on polystyrene/nanoclay composite: physical properties and application. Polym. Plast. Technol. Eng. 2017, 56(9), 917−931.
117. Grishina, E. P., Ramenskaya, L. M., Kudryakova, N. O., Vagin, K. V., Kraev, A. S., Agafonov, A. V. Composite nanomaterials based on 1-butyl-3-methylimidazolium dicianamide and clays. J. Mater. Res. Technol. 2019, 8(5), 4387−4398.
118. Bischoff, E., Simon, D. A., Liberman, S. A., Mauler, R. S. Adsorption of ionic liquid onto halloysite nanotubes: Thermal and mechanical properties of heterophasic PE-PP copolymer nanocomposites. In AIP Conference Proceedings. AIP Publishing LLC 2016; 1713:1−5.
119. Xu, P., Yu, Y., Chang, M., Chang, J. Preparation and Characterization of Bio-oil Phenolic Foam Reinforced with Montmorillonite. Polymers 2019, 11, 1471.

120. Chanra, J., Budianto, E., Soegijono, B. Surface modification of montmorillonite by the use of organic cations via conventional ion exchange method. In IOP Conference Series: Materials Science and Engineering 2019, 509, 012057.

121. Uwa, C. A., Jamiru, T., Sadiku, E. R., Huan, Z., Mpofu, K. Polypropylene/nanoclay Composite: A solution to refrigerated vehicles. Procedia Manuf. 2019, 35, 174–180.

122. Valapa, R. B., Loganathan, S., Pugazhenthi, G., Thomas, S., Varghese, T. O. An overview of polymer–clay nanocomposites. In Clay-Polymer Nanocomposites. Elsevier 2017, pp. 29-81.

123. Moreno-Sader, K., García-Padilla, A., Realpe, A., Acevedo-Morantes, M., Soares, J.B.P. Removal of Heavy Metal Water Pollutants (Co2+ and Ni2+) Using Polyacrylamide/Sodium Montmorillonite (PAM/Na-MMT) Nanocomposites. ACS Omega 2019, 4, 10834−10844.

124. Atta, A.M., Al-Lohedan, H.A., ALOthman, Z.A., Abdel-Khalek, A.A., Tawfeek, A.M. Characterization of reactive amphiphilic montmorillonite nanogels and its application for removal of toxic cationic dye and heavy metals water pollutants. Journal of Industrial and Engineering Chemistry 2015, 31, 374–384.

125. Şen, F., Demirbaş, Ö., Çalımli, M.H., Aygün, A., Alma, M.H., Nas, M.S. The dye removal from aqueous solution using polymer composite films. Applied Water Science 2018, 8,206.

126. Peng, N., Hu, D., Zeng, J., Li, Y., Liang, L., Chang, C. Superabsorbent cellulose−clay nanocomposite hydrogels for highly efficient removal of dye in water. ACS Sustainable Chem. Eng. 2016, 4, 7217−7224.

127. Moja, T.N., Bunekar, N., Mojaki, S., Mishra, S.B., Tsai, T.-Y., Hwang, S.S., Mishra, A.K. Polypropylene–Polypropylene-Grafted-Maleic Anhydride–Montmorillonite Clay Nanocomposites for Pb(II) Removal. Journal of Inorganic and Organometallic Polymers and Materials 2018, 28, 2799–2811.

128. Liu, Q., Yang, B., Zhang, L., Huang, R. Adsorption of an anionic azo dye by cross-linked chitosan/bentonite composite. International Journal of Biological Macromolecules 2015, 72, 1129–1135.

129. Natarajan, S., Anitha, V., Gajula, G.P., Thiagarajan, V. Synthesis and characterization of magnetic superadsorbent Fe_3O_4-PEG-Mg-Al-LDH nanocomposites for ultrahigh removal of organic dyes. ACS Omega 2020, 5, 3181−3193.

130. Alnaqbi, M.A., Samson, J.A., Greish, Y.E. Electrospun polystyrene/LDH fibrous membranes for the removal of Cd^{2+} ions. Journal of Nanomaterials 2020, 12, 5045637.

131. Quispe-Dominguez, R., Naseem, S., Leuteritz, A., Kuehnert, I. Synthesis and characterization of MgAl-DBS LDH/PLA composite by sonication-assisted masterbatch (SAM) melt mixing method. RSC Adv. 2019, 9, 658.

132. Devi, K. U., Ponnamma, D., Causin, V., Maria, H. J., Thomas, S. Enhanced morphology and mechanical characteristics of clay/styrene butadiene rubber nanocomposites. Appl. Clay Sci. 2015, 114, 568–576.

133. Sari, M. G., Ramezanzadeh, B., Shahbazi, M., Pakdel, A. S. Influence of nanoclay particles modification by polyester-amide hyperbranched polymer on the corrosion protective performance of the epoxy nanocomposite. Corros. Sci. 2015, 92, 162−172.

134. Tsai, T. Y., Bunekar, N., Liang, S. W. Effect of Multiorganomodified LiAl-or MgAl-Layered Double Hydroxide on the PMMA Nanocomposites. Adv. Polym. Technol. 2018, 37(1), 31-37.

135. Nagendra, B., Mohan, K., Gowd, E. B. Polypropylene/layered double hydroxide (LDH) nanocomposites: influence of LDH particle size on the crystallization behavior of polypropylene. ACS Appl. Mater. Inter. 2015, 7(23), 12399–12410.

136. Adeyemo, A.A., Adeoye, I.O., Bello, O.S. Adsorption of dyes using different types of clay: a review. Appl. Water Sci. 2017, 7, 543–568.

137. Zabihi, O., Ahmadi, M., Khayyam, H., Naebe, M. Fish DNA-modified clays: Towards highly flame retardant polymer nanocomposite with improved interfacial and mechanical performance. Sci. Rep. 2016, 6, 38194.

138. Bashar, M., Mertiny, P., Sundararaj, U. Effect of nanocomposite structures on fracture behavior of epoxy-clay nanocomposites prepared by different dispersion methods. J. Nanomater. 2014, 70, 1−12.

139. Oyarzaba, A., Mugica, A. Müller, A.J., Zubitur, M. Hydrolytic degradation of nanocomposites based on poly(L-lactic acid) and layered double hydroxides modified with a model drug. J. Appl. Polym. Sci. 2016, 133(28), 43648.

140. Leng, J., Kang, N., Wang, D. Y., Falkenhagen, J., Thünemann, A. F., Schönhals, A. Structure–property relationships of nanocomposites based on Polylactide and layered double hydroxides–comparison of MgAl and NiAl LDH as Nanofiller. Macromol. Chem. Phys. 2017, 218(20), 1700232.

141. Mandal, S., Kalaivanan, S., Mandal, A.B. Polyethylene glycol-modified layered double hydroxides: Synthesis, characterization, and study on adsorption characteristics for removal of acid orange II from aqueous solution. ACS Omega 2019, 4, 3745−3754.

142. Mahmoudian, M., Balkanloo, P.G., Nozad, E. A facile method for dye and heavy metal elimination by pH sensitive acid activated montmorillonite/polyethersulfone nanocomposite membrane. Chinese J. Polym. Sci. 2018, 36, 49−57.

143. Mohamed, F., Abukhadra, M.R., Shaban, M. Removal of safranin dye from water using polypyrrole nanofiber/Zn-Fe layered double hydroxide nanocomposite (Ppy NF/Zn-Fe LDH) of enhanced adsorption and photocatalytic properties. Science of the Total Environment 2018, 640–641, 352–363.

144. Xu, G., Zhu, Y., Wang, X., Wang, S., Cheng, T., Ping, R., Cao, J., Kaihe, L. Novel chitosan and Laponite based nanocomposite for fast removal of Cd(II), methylene blue and Congo red from aqueous solution. e-Polymers 2019, 19, 244–256.

145. Isawi, H. Using Zeolite/Polyvinyl alcohol/sodium alginate nanocomposite beads for removal of some heavy metals from wastewater. Arabian Journal of Chemistry 2020, 13, 5691–5716.

146. Biswas, S., Rashid, T.U., Debnath, T., Haque, P., Rahman, M.M. Application of chitosan-clay biocomposite beads for removal of heavy metal and dye from industrial effluent. J. Compos. Sci. 2020, 4(16), 1−14.

147. Sharma, S., Bhattacharya, A. Drinking water contamination and treatment techniques. Appl. Water Sci. 2017, 7, 1043–1067.

148. Sarma, G.K., Sen Gupta, S. & Bhattacharyya, K.G. Nanomaterials as versatile adsorbents for heavy metal ions in water: a review. Environ. Sci. Pollut. Res. 2019, 26**,** 6245–6278.

149. Crini, G., Lichtfouse, E., Wilson, L., Morin-Crini, N. Adsorption-oriented processes using conventional and non-conventional adsorbents for wastewater treatment. Green Adsorbents for Pollutant Removal, 18, Springer Nature, pp.23-71, 2018, Environmental Chemistry for a Sustainable World, 978-3-319-92111-2.

150. Nagaraj, A., Munusamy, M. A., Ahmed, M., Kumar, S.S., Rajan, M. Hydrothermal synthesis of a mineral-substituted hydroxyapatite nanocomposite material for fluoride removal from drinking water. New J. Chem., 2018, 42, 12711–12721.

151. Nagaraj, A., Pillay, K., Kumar, S. K., Rajan, M. Dicarboxylic acid cross-linked metal ion decorated bentonite clay and chitosan for fluoride removal studies. RSC Adv. 2020, 10, 16791.

152. Schneckenburger, T., Riefstahl, J., Fischer, K. Adsorption of aliphatic polyhydroxy carboxylic acids on gibbsite: pH dependency and importance of adsorbate structure. Environ Sci Eur. 2018, 30(1), 1.

153. Zhou, H., Jiang, Z., Wei, S. A new hydrotalcite-like absorbent FeMnMg-LDH and its adsorption capacity for Pb2+ ions in water. Applied Clay Science 2018,153, 29–37.

154. Srivastava, V., Sharma, Y., Sillanpää, M. Green synthesis of magnesium oxide nanoflower and its application for the removal of divalent metallic species from synthetic wastewater. Ceram. Int. 2015, 41, 6702−6709.

155. Jaiswal, A., Chattopadhyaya, M.C. Synthesis and characterization of novel Co/Bi-layered double hydroxides and their adsorption performance for lead in aqueous solution. Arabian Journal of Chemistry 2017, 10, S2457–S2463.

156. Xie, J., Lin, Y., Li, C.,Wu, D., Kong, H. Removal and recovery of phosphate from water by activated aluminum oxide and lanthanum oxide. Powder Technol. 2015, 269, 351−357.

157. Rout, T. K., Verma, R., Dennis, R. V., Banerjee, S. Study the removal of fluoride from aqueous medium by using nanocomposites. Journal of Encapsulation and Adsorption Sciences. 2015, 5(1), 38–52.

158. Bo, L., Li, Q., Wang, Y., Gao, L., Hu, X., Yang, J. One-pot hydrothermal synthesis of thrust spherical Mg–Al layered double hydroxides/MnO2 and adsorption for Pb(II) from aqueous solutions. J. Environ. Chem. Eng. 2015, 3, 1468–1475.

159. Mostafa, M.S., Bakr, A.A., Eshaq, G., Kamel, M.M. Novel Co/Mo layered double hydroxide: synthesis and uptake of Fe(II) from aqueous solutions (Part 1), Desalination and Water Treatment. 2014, 56(1), 239−247.

160. Zhang, L., Zeng, Y., Cheng, Z. Removal of heavy metal ions using chitosan and modified chitosan: a review. J. Mol. Liq. 2016, 214, 175−191.

161. Zhu, Y., Zhu, R., Chen, Q., Laipan, M., Zhu, J., Xi, Y., He, H. Calcined Mg/Al layered double hydroxides as efficient adsorbents for polyhydroxy fullerenes. Applied Clay Science 2018, 151, 66–72.

162. Ayawei, N., Ekubo, A.T., Wankasi, D., Dikio, E.D. Synthesis and Application of Layered Double Hydroxide for the removal of Copper in Wastewater. International Journal of Chemistry. 2015, 7(1), 122−132.

163. Zhou, Q., Zhu, R., Parker, S. C., Zhu, J., He, H., Molinari, M. Modelling the effects of surfactant loading level on the sorption of organic contaminants on organoclays. RSC Adv. 2015, 5, 47022.
164. El Afif, A. Flow and non-Fickian mass transport in immiscible blends of two rheologically different polymers. Rheol. Acta 2015, 54, 929–940.
165. Hairch, Y., El Afif, A. Mesoscopic modeling of mass transport in viscoelastic phase-separated polymeric membranes embedding complex deformable interfaces. J. Membr. Sci. 2020, 596, 117589.
166. Akin, O., Tihminlioglu, F. Effects of organo-modified clay addition and temperature on the water vapor barrier properties of polyhydroxy butyrate homo and copolymer nanocomposite films for packaging applications. J. Polym. Environ. 2018, 26, 1121–1132.
167. Barik, S., Badamali, S. K., Behera, L., Jena, P. K. Mg–Al LDH reinforced PMMA nanocomposites: a potential material for packaging industry. Compos. Interfaces 2018, 25(4), 369−380.
168. Singha, S., Hedenqvist, M. S. A Review on Barrier Properties of Poly (Lactic Acid)/Clay Nanocomposites. Polymers 2020, 12, 1095.
169. Wilson, R., Follain, N., Tenn, N., Kumar, A., Thomas, S., Marais, S. Tunable water barrier properties of EVA by clay insertion?. Phys. Chem. Chem. Phys. 2015, 17(29), 19527−*19537.*
170. Trifol, J., Plackett, D., Szabo, P., Daugaard, A. E., Giacinti Baschetti, M. Effect of Crystallinity on Water Vapor Sorption, Diffusion, and Permeation of PLA-Based Nanocomposites. ACS Omega 2020, 5(25), 15362–15369.
171. Smit, W.J., Tang, F., Nagata, Y., Sánchez, M.A., Hasegawa, T., Backus, E.H., Bonn, M., Bakker, H.J. Observation and identification of a new OH stretch vibrational band at the surface of ice. J. Phys. Chem. Lett. 2017, 8, 3656−3660.
172. Lichawska, M. E., Bodek, K. H., Jezierska, J., Kufelnicki, A. Coordinative interaction of microcrystalline chitosan with oxovanadium (IV) ions in aqueous solution. Chem. Cent. J. 2014, 50(8), 1–9.
173. Ivanova, O. P., Krinichnaya, E. P., Morozov, P. V., Zav'yalov, S. A., Zhuravleva, T. S. The Effect of Filler Content on the IR Spectra of Poly (p-xylylene)–Sulfide Nanocomposites. Nanotechnol. Russ. 2019, 14, 7–15.
174. Homaeigohar, S. The nanosized dye adsorbents for water treatment. Nanomaterials 2020, 10, 295.

Chapter 4: Materials and methods

4.1 Materials

4.1.1 Polylactic acid (PLA)

Polylactic acid (PLA) was purchased from 2M Biotech, India; and its density is 1.24 g/cm^3. PLA is a biobased polymer fabricated from natural resources, and it provides a hope for a great potential in terms of reducing carbon footprint in comparison to oil-based plastics. PLA is a high viscosity, low flow, transparent resin (Figure 4.1) with a melting temperature of 155 °C, melt flow index of 6 g/10 mins, and glass transition of 60 °C. The stereo chemical purity of the PLA which was done by the Total Corbion PLA method was found to be 96% (L-isomer). Figure 4.1 illustrate a typical PLA pellets.

Figure 4.1 A typical example of the PLA pellets

4.1.2 Montmorillonite Clay (MMT)

The nano clay in the form of Montmorrilonite (MMT) was supplied in powder by Sigma Aldrich. This Montmorillonite clay surface was modified with 15-35 wt% octadecylamine, and 0.5-5 wt% aminopropyltriethoxysilane. The nanoclay has density of 2 - 3 g/cm3, molecular weight 360.31.

4.1.3 Halloysite Clay

The Nanoclay halloysite was supplied in a nanopowder form by Sigma Aldrich. The nanoclay has a pore size of 1.26-1.34 mL/g volume, surface area of 64 m^2/g, capacity of 8.0 meq/g cation exchange capacity, and a density of 2.53.

4.1.4 Kaolin

The Nanoclay kaolin in the form of powder was supplied by Athi River Mining LTD. The nanoclay has melting point of 740-1785 °C and density 2.65 g/cm3.

4.1.5 Zinc Borate

The inorganic compound zinc borate in a form of white powder was supplied by Sigma Aldrich. This Zinc borate contains ≥45% ZnO basis, ≥36% B_2O_3 basis, moisture content ≤ 1, weight loss on heating at 270°C is ≤6, Weight loss on heating at 850°C is ≤16, particle size D50 is ≤5, and dehydration temperature of 330°C -340°C.

4.1.6 Congo red

Congo red, organic anionic dye, in a form of powder was procured from Sigma Aldrich. It contained dye content ≥35% with nitrogen content of 4.2-12% and molecular weight of 696.66 g/mol.

4.2 Preparation method

4.2.1 Preparation of the PLA/Clays based Nanocomposites

Before preparation, PLA and clays were dried at 70 °C in a vacuum oven for a period of 48 hours. To prepare the nanocomposites, PLA and clay(s) were physically mixed in a beaker and then the mixture was extruded using a co-rotating twin-screw extruder with an *L/D* ratio of 40 (L=720 mm).

The extruder was operated at various temperature profile set at 175, 180, 185, 190, 195 °C (i.e., for different zones from hopper to die). Figure 4.2 illustrates the type of extruder utilized in this study.

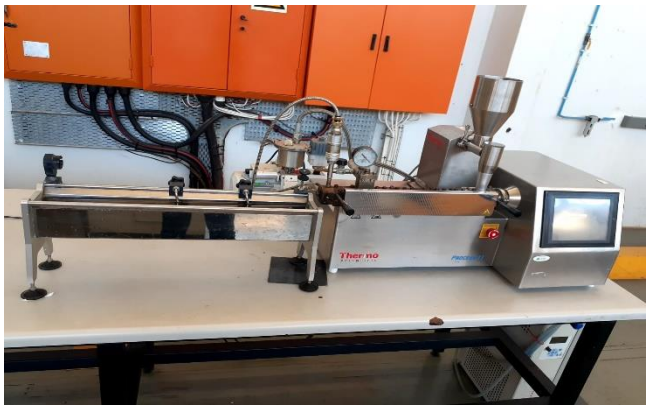

Figure 4.2 A co-rotating twin-screw extruder used for fabrication of PLA/Clay based nanocomposites

The samples were cooled in an ice-bath immediately after each processing and then dried in an oven for 24 hours. In order to characterize various properties for different techniques, the samples were compressed molded at 190 °C, and at the pressure of 20 MPa under atmosphere. Table 4.1 shows the sample ratios of all the investigated samples.

Table 4.1: Illustration of all the investigated samples used in this study

Polymer/Clay Nanocomposites	**Content (%)**
Neat PLA	100
PLA/kaolin	97/3
PLA/MMT	97/3
PLA/halloysite	97/3
PLA/zinc borate	97/3
PLA/MMT/halloysite	97/1.5/1.5
PLA/MMT/kaolin	97/1.5/1.5
PLA/kaolin/zinc borate	97/1.5/1.5

PLA/halloysite/zinc borate	97/1.5/1.5
PLA/MMT/zinc borate	97/1.5/1.5

4.3 Sample analysis and characterization

4.3.1 Transmission electron microscopy (TEM)

Transmission electron microscopy (TEM) has traditionally been used for diffraction, imaging, and chemical analysis of solid materials [4, 5]. TEM is a powerful and comprehensive analysis tool for analysing the electrical and chemical structure at the nanoscale with diameters less than 100 nm (or even atomic scale in some contexts) [4,6,7]. It has been used a lot to figure out what shape nanoparticles take [4,6], and been used in material, engineering, and biological science. In order for electrons to travel through a TEM specimen, its thickness should be less than 100 nm. Many specimen characteristics such as composition, and density could influence electron beam transmission [6]. A Philips CM 200 transmission electron microscope (TEM) equipped with an AMT XR-60 CCD digital camera system was employed to produce images clay-based nanocomposites. An accelerating voltage of 80 kV was used for the TEM analyses.

4.3.2 X-Ray Diffraction (XRD)

X-ray diffraction (XRD) is a multipurpose, non-destructive analytical method for determining material properties such as structure, phase composition, texture, and many others in liquid, powder, and solid samples. Additionally, phase identification is accomplished by comparing an unknown sample's X-ray diffraction pattern to patterns in a reference database [8]. Spieß *et al*. [8, 9] have defined X-rays as high-energy electromagnetic waves with a wavelength of 103 to 101 nm. Seal tubes, synchrotron radiation sources, and spinning anodes are commonly used to generate X-rays [10]. Moreover, XRD methods are based on crystals' capacity to diffract X-rays in a predictable pattern, thus allowing for a detailed investigation of crystalline phase structure. Several micro- and macrostructural characteristics of a material are additively represented in recorded diffraction patterns. Lattice parameters, space group, chemical composition, macro stresses, and

qualitative phase analysis can all be researched using the peak position. Analyses of crystal structure (temperature, occupancy, factor, or atomic locations) as well as texture and quantitative phase can likewise be obtained using peak intensity. Finally, peak shape reveals sample broadening contributions (microstrains and crystallite size) [11]. Below is the X-ray diffraction analysis utilized in this study (Figure 4.3). The neat PLA and clay-based samples were scanned in the reflection mode using an incident X-ray of CuKα with a wavelength of 1.54 and at a step width of 0.05 min^{-1} from 2 θ = 5-100°.

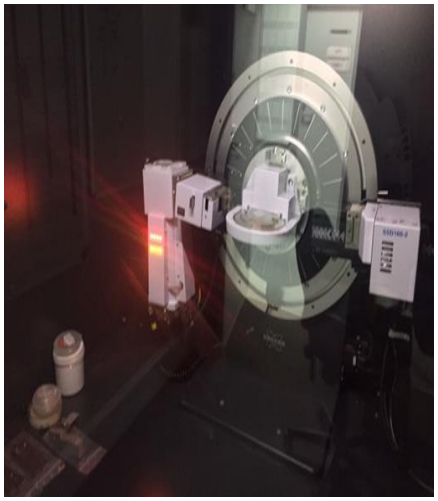

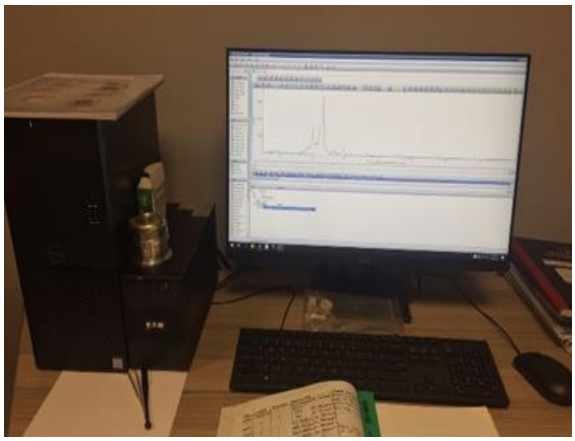

Figure 4.3 X-ray diffraction analysis utilized in this study

4.3.3 Rheology

Rheology is the study of how materials (particularly liquids, and soft matter) flow or deform when a force is applied [12, 13]. Because solids and fluids that flow at different speeds can be deformed to some extent, it is used to describe and assess the deformation, and flow behaviour of these materials [14]. The viscoelastic flow behaviour of a system can be estimated using rheological characterization of materials [14]. Since this study is using clay as a polymer filler to form polymer/clay-based nanocomposites, the melt rheological properties of filled polymers are highly sensitive to the structure, shape, particle size, concentration, and surface features of the fillers. As a result, rheological characterisation of polymer nanocomposites provides a novel method for determining the state of filler dispersion in nanocomposites and investigate the effect of flow conditions on nanofiller dispersion [14]. Figure 4.4 illustrates the techniques utilized for rheological properties. The dynamic rheological properties were conducted at 190 ℃ under atmospheric conditions by utilizing a Physica MCR501 (Anton Paar, Austria) rheometer in a 25-mm-diameter parallel plate configuration.

Figure 4.4 The equipment that was utilized to determine the dynamic rheological measurements

4.3.4 Thermogravimetric Analysis (TGA)

TGAs monitor, and record sample mass, time, and temperature [15]. The primary idea behind thermogravimetric analysis (TGA) is that the mass change of a sample can be investigated under controlled conditions. As a result, TGA is primarily utilized to study vaporization, adsorption breakdown, absorption, oxidation, sublimation, desorption, and reduction. TGA can also be used to assess the amount of volatile or gaseous products lost during chemical reactions in nanomaterials, polymers and polymer nanocomposites, films, fibers, coatings, and paints [16]. TGA's temperature programme may consist of heating, cooling, isothermal holding, or a combination of these [17]. The analyzer comprises of a temperature programmer and controller thermo-balance connected to a sample pan within a furnace with a precise micro balance. In a closed furnace, the balance weighs the sample [18]. Notwithstanding the benefits of TGA, there are a few drawbacks relating to sample size, heat, and mass transfer rates. Heating rates inside the sample are not fast enough to ensure isothermal conditions in bigger samples (> 50 mg), and inadequate mass transfer results in radial and axial concentration gradients [19, 20–22]. Resultantly, kinetic parameters generated by traditional thermogravimetric analysers (TGA) [15] are subject to these restrictions. A Perkin Elmer TGA7 thermogravimetric analyser was used for the TGA analyses in this study. Under nitrogen, samples weighing between 5 and 10 mg were

heated at a rate of 10 °C min^{-1} from 25−700 °C (flow rate of 20 mL min^{-1}) and the corresponding loss was recorded.

4.3.5 UV-Vis Spectroscopy

UVs is a characterisation technique for studying the optic properties of Polymer Matrix Nanocomposites (PMCs). It clarifies the interaction between the matrix and the nanofiller as well as the significance of nanofillers in improving nanocomposites' properties. UVVs, when combined with other characterisation methods is an indispensable tool for determining the appropriate optical properties of nanofillers in a polymer matrix [23]. It is based on the measurement of electromagnetic radiation (EMR) interactions with materials at specific wavelengths [24].

4.3.6 Underwriters Laboratories test standard (UL-94)

A common fire test used for industrial polymeric materials and products is the UL-94 vertical burning. A small-size specimen is exposed to a Bunsen flame for 10 seconds before the flame is extinguished. The Bunsen flame is thereafter applied for an extra 10 seconds after the specimen had put out of the flame [25]. The UL-rating is determined by three factors, namely (i) how long it takes the test specimen to self-extinguish; (ii) whether it drips; and (iii) whether the dripping lights the cotton placed underneath the test specimen. A sample specimen needs to have a V-0 UL rating in order to be considered flame-retardant. This indicates that the sample: (i) self-extinguishes in less than 10 seconds; (ii) does not show any flame drips; and (iii) does not cause the cotton that was placed underneath the sample specimen to catch fire. According to ASTM D 3801 testing protocol, the Bunsen burner method is used to perform the vertical burning test (UL-94), with dimensions of 120 mm x 13 mm x 3 mm (Figure 4.5). During the measurements, the samples were vertically exposed to a Bunsen burner flame for a certain period of time. The classification of the samples is discussed in chapter 5.

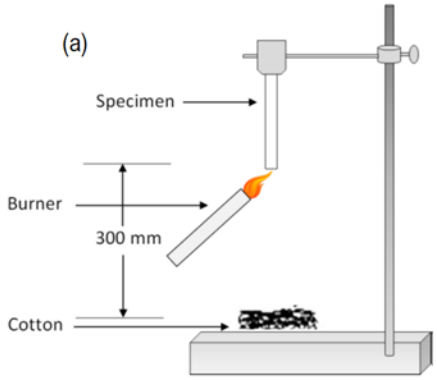

Figure 4.5 (a) A diagram illustrating a vertical burning setup [26]

4.3.7 Dye adsorption studies

Adsorption is one of the commonly used method for the removal of different pollutants from wastewater because of its simplicity and cost effectiveness, when compared to other classic process. The adsorption experiments were carried out using congo red (CR) as model dye. About 25 mL of CR dye solution (10 mg/L) was poured into a 100 mL conical flask equipped with stirrer bar. The flasks were placed on the stirrer plate and stirred at 250 rpm for 30 minutes and then ~50 mg of PLA composite was added into the dye solution and further stirred at room temperature for 12 hours. The adsorption efficiency (R) of the composites was determined using the following:

$$R(\%) = \frac{C_f - C_i}{C_i} \times 100 \qquad (4.1)$$

where C_i is the CR dye absorbance before adsorption and C_f is the MO dye absorbance after 12 hours.

4.4 References

1. Zhou, W., Apkarian, R.P., Wang, Z-L. **(2006)**. Scanning Microscopy for Nanotechnology || *Fundamentals of Scanning Electron Microscopy* (SEM), 1, 1-40.

2. Szynkowska, M.I. **(2005)**. MICROSCOPY TECHNIQUES | Scanning Electron Microscopy. *Encyclopedia of Analytical Science*, 195, 134–143.

3. Mohammed, A., Abdullah A. **(2019)**. Scanning electron microscopy (SEM): a review. In: *Proceedings of 2018 international conference on hydraulics and pneumatics*–Hervex.

4. Wang, Z.L. **(2003)**. New Developments in Transmission Electron microscopy for Nanotechnology. *Adv Mater***,** 15(18), 1497-1514.

5. Wagner, G., Buseck, P.R, Cowley, J.M., Eyring, L. (**1993**) High-Resolution Transmission Electron Microscopy and Associated Techniques. Oxford University Press, Inc. 28(5), 628–628.

6. Tang, C.Y., Yang, Z. **(2017)**. Transmission Electron Microscopy (TEM). In Book: *Membrane Characterization*, 8, 145-159.

7. Wang, Z.L., Kang, Z.C. **(1998)**. Functional and Smart Materials: Structural Evolution and structure Analysis. *Physics Today*, 51(11), 70–71.

8. Igwebike-Ossi, C. D. **(2017)**. *'X-Ray Techniques'. Failure Analysis and Prevention*, IntechOpen, London.

9. Spieß, L., Behnken, H., Genzel, C., Schwarzer, R., Teichert, G. (**2009)**. *Moderne röntgenbeugung*, Vol. 2, 276.

10. Epp, J. **(2016)**. Materials Characterization Using Nondestructive Evaluation (NDE) Methods || *X-ray diffraction (XRD) techniques for materials characterization*, 81–124.

11. Dinnebier, R.E., Billinge, S.J.L. **(2008).** *Powder Diffraction, Theory and Practice*. The Royal Society of Chemistry.

12. Lichinga, K.N., Luanda, A., Sahini, M.G. **(2022)**. A novel alkali-surfactant for optimization of filtercake removal in oil–gas well. *Journal of Petroleum Exploration and Production Technology*. 12, 2121-2134.

13. Morris, B.A. **(2017)**. Rheology of polymer melts. The science and technology of flexible packaging. *Plastics design library*. William Andrew Publishing, 5, 121–147. ISBN 9780323242738.

14. Abraham, J. **(2017)**. *Rheological characteristics of nanomaterials and nanocomposites. In book: Micro and Nano Fibrillar Composites (MFCs and NFCs) from Polymer Blends*. Elsevier Woodhead Publishing, 14, 327–350.

15. Saadatkhah, N., Garcia, A-C., Ackermann, S., Leclerc, P., Latifi, M., Samih, S., Patience, G.S., Chaouki, J. **(2020)**. Experimental Methods in Chemical Engineering: Thermogravimetric Analysis—TGA. *The Canadian Journal of Chemical Engineering*. 98(1), 34-43.

16. Loganathan, S., Valapa, R.B., Mishra, R.K, G. Pugazhenthi, G., Thomas, S. **(2017).** Thermal and Rheological Measurement Techniques for Nanomaterials Characterization . Elsevier, Vol. 3, 271-276.

17. Vyazovkin, S., Burnham, A.K., Criado, J.M., Pérez-Maqueda, L.A., Popescu, C., Sbirrazzuoli, N. **(2011)**. ICTAC Kinetics Committee Recommendations for Performing Kinetic Computations on Thermal Analysis Data. *Thermochimica Acta*, 520, 1-19.

18. Prime, R.B., Menczel, J.D., Bair, H.E., Vyazovkin, S., Gallagher, P.K., Riga, A. **(2009)**. Thermogravimetric analysis (TGA). Thermal analysis of polymers: Fundamentals and applications, 241-317.

19. Cardona, M., Boffito, D.C., Patience, G.S. **(2015)**. Thermogravimetric heat and mass transfer: Modeling of bitumen pyrolysis. *Fuel*, 143, 253–261.

20. Ebrahimpour, O., Chaouki, J., Dubois, J.C. **(2013)**. Diffusional effects for the oxidation of SiC powders in thermogravimetric analysis experiments. *Journal of Materials Science*, 48(12), 4396–4407.

21. Vekemans, O., Laviolette, J-P., Chaouki, J. **(2015)**. Thermal behavior of an engineered fuel and its constituents for a large range of heating rates with emphasis on heat transfer limitations. *Thermochimica Acta*, 60, 54–62.

22. Samih, S., Chaouki, J. **(2017)**. Catalytic ash free coal gasification in a fluidized bed thermogravimetric analyser. *Powder Technology*. 316, 551-559.

23. Venkatachalam, S. **(2016).** Ultraviolet and visible spectroscopy studies of nanofillers and their polymer nanocomposites. *Spectroscopy of Polymer Nanocomposites*, 130–157.

24. Akash, M.S.H., Rehman, K. **(2020).** Ultraviolet-Visible (UV-VIS) Spectroscopy. In: *Essentials of Pharmaceutical Analysis*. Springer, Singapore, 19-29.

25. Joseph, P., Tretsiakova-McNally, S. **(2015).** Melt-flow behaviours of thermoplastic materials under fire conditions: Recent experimental studies and some theoretical approaches. *Materials*, 8(12), 8793-8803.

26. Maqsood, M. and Seide, G. **(2020)**. Biodegradable flame retardants for biodegradable polymer. *Biomolecules*, 10(7), 1038(1-21).

Chapter 5: Results and discussion

5.1 Transmission Electron Microscopy (TEM)

The dispersion of the fillers within a polymer matrix is a very important factor in terms of determining the overall properties of the polymer composites. **Figure 5.1 (a-e)** depicts the TEM images of the three types of clays (*viz.* halloysite, montmorillonite (MMT), and kaolin), and zinc borate incorporated into the PLA matrix. Depending on the three types of clay incorporated into the PLA, three types of morphologies are observed. According to **Figure 5.2**, the dispersion of the clay may be distinguished by immiscibility **(Figure 5.2(a)),** intercalation **(Figure 5.2(b)),** and exfoliation form **(Figure 5.2(c)).** It is clear from **Figure 5.1 (a)** that there is an immiscibility between the PLA matrix and halloysite clay. Similar morphology was also observed in the PLA/kaolin system **(Figure 5.1(c)).** The immiscibility of the clays simply means that there is no affinity between the nanoclay and PLA matrix, and there is a poor dispersion within the PLA matrix accompanied by agglomeration. Wang *et al.* [**1**] reported a partial agglomeration of the halloysite (HNTs) within the polypropylene matrix, while the HNTs-Si modified clays dispersed homogenously within the PP matrix. A better dispersion of the clays was attributed to the presence of the poly-siloxane (poly-DDPM), with the poly-DDPM being partially attached on the surface of the HNTs, and thereby inhibiting the agglomeration of the clay. The incorporation of the MMT into PLA however resulted into an intercalation and exfoliation of the nanoclay within the polymer matrix. The reason that there is a possible intercalation and exfoliation in the MMT/PLA system is associated with the modification of the MMT with organic substances. Similarly, Zehetmeyer *et al.* [**2**] reported the morphology of the PP/MMT nanocomposites, with 1, 2, and 5 wt% of the MMT. The TEM images of their study revealed three types of morphologies: (i) few exfoliated lamellae, (ii) intercalated, and (iii) large agglomerates within the polymer matrix.

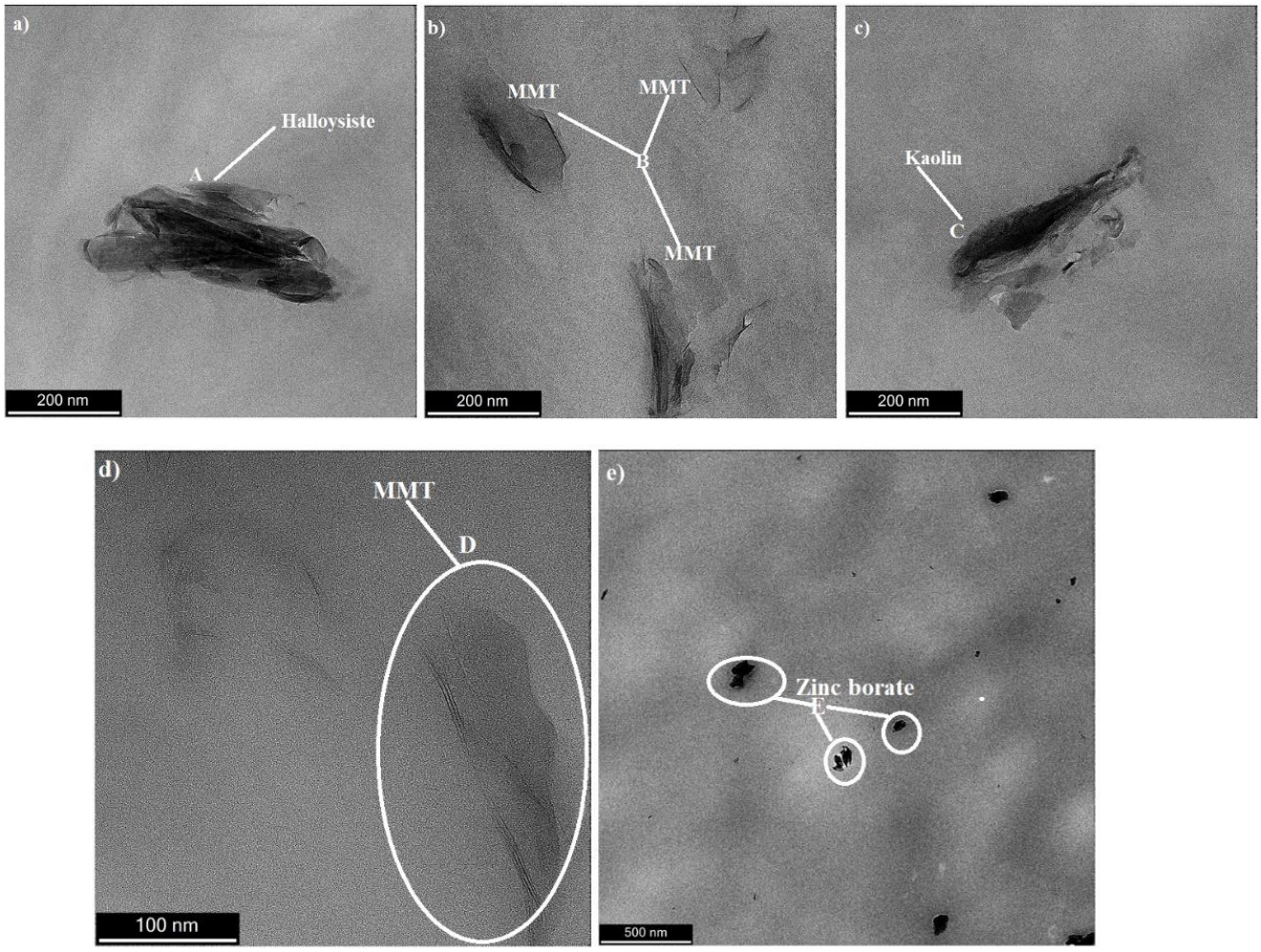

Figure 5.1 TEM images of: a) PLA/halloysite (97/3), b) PLA/MMT (97/3), c) PLA/kaolin (97/3), d) PLA/MMT (97/3), and e) PLA/Zinc borate (97/3).

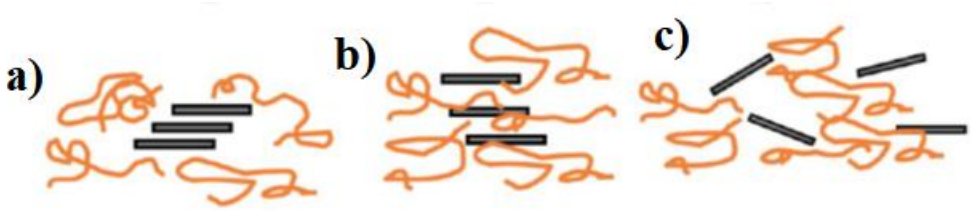

Figure 5.2 Various dispersions of the clay in the polymer(s) matrices

The TEM images of the PLA/Zinc borate (ZnB) revealed a few agglomerates of the ZnB within the PLA matrix **(Figure 5.1(d))**. The agglomerates may be attributed to the fact that ZnB is not modified; and as a result, it is unable to interact with the polymer matrix fully. Furthermore, it is

clear that the shear forces during processing had little impact in terms of improving a better dispersion of ZnB within the PLA matrix. **Figure 5.3** illustrates the TEM images of PLA/kaolin/halloysite, PLA/ZnB/halloysite, and PLA/MMT/halloysite composites. The synergy of the kaolin/halloysite seems to show a little separation between the clay components as shown in **Figure 5.1 (symbol D)** with a lot of agglomerations by the two clays **(symbol E)**. According to **Figure 5.3(b),** there is a clear separation between the clay in the form of halloysite, and zinc borate with **symbol A** noting the ZnB nanoparticle, while **symbol B** indicates the halloysite clay. In **symbol A**, there seems to be ZnB nanoparticles on top of the clay with minimum ZnB interacting with the clay. One can say that there is less synergy being formed with ZnB; however, there is more anti-synergy that is formed between the two nanoparticles. The less interaction between the two nanoparticles might be attributed to the difference in chemical structure with no common functional groups to initiate a strong interaction. **Figure 5.3 (c)** however illustrates a better dispersion of halloysite and MMT within the PLA matrix, which resulted in both intercalation and exfoliation. This may be ascribed to the ability of MMT in terms of dispersing the halloysite platelets.

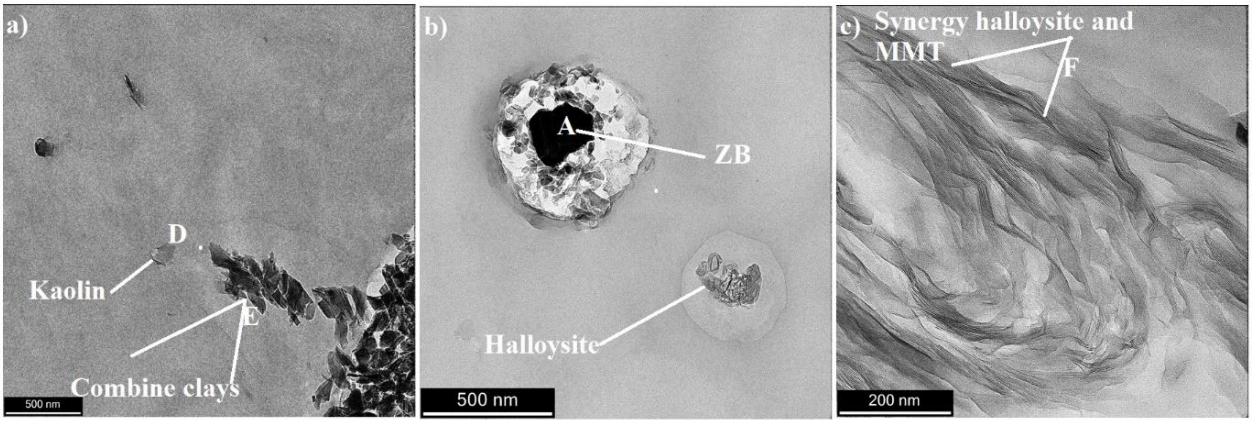

Figure 5.3 TEM images of: a) PLA/kaolin/halloysite, b) PLA/ZnB/halloysite, and c) PLA/MMT/halloysite.

Figure 5.4 (a) and (b) illustrate the TEM images of MMT, and its synergy with kaolin as well as ZnB reinforced incorporated in PLA matrix. Once again, it is very clear that the organically modified clay acts as a catalyst in terms of improving the dispersion of both kaolin and ZnB, thus resulting in both exfoliated, and intercalated structures. This behaviour whereby the organic modified clay improves the dispersion of other clays, and ZnB in PLA is associated with the

interaction of the nanoparticles as well as the PLA chains with organic modifier in MMT, and ease of penetration between the clay platelets, and thereby result in a better dispersion.

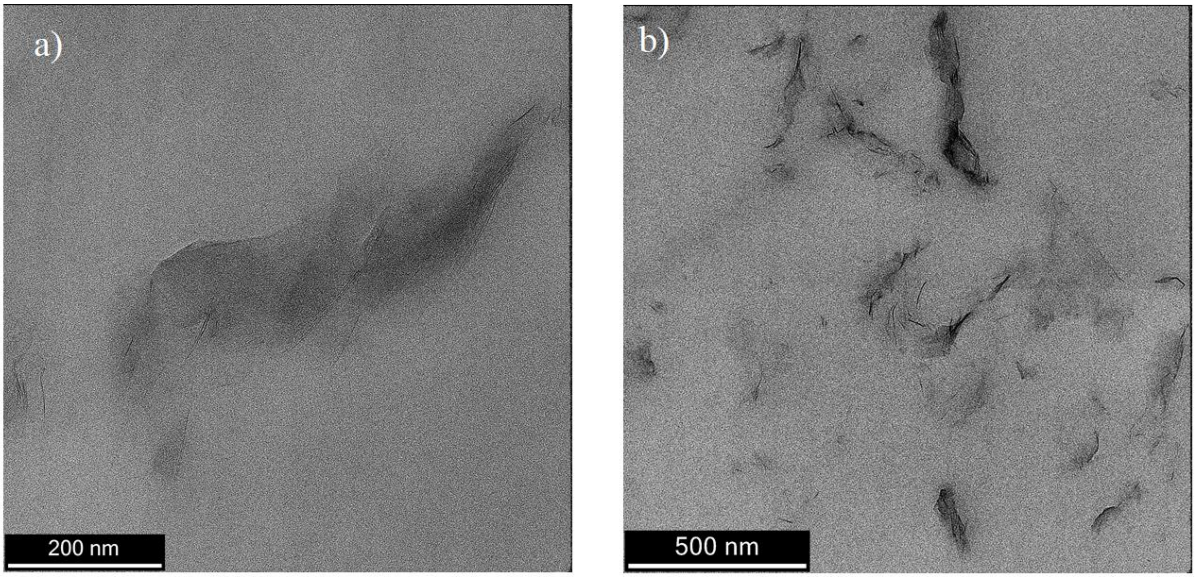

Figure 5.4 TEM images of: a) PLA/MMT/kaolin, b) PLA/MMT/ZnB.

Similarly, as in the previous discussion, kaolin with zinc borate shows an agglomeration of both nanoparticles with the PLA matrix **(Figure 5.5 (a))**. The reason for such an observation may be related to the absence of a modifier within the system due to less penetration of PLA chains within the two nanoparticles. There is a better dispersion however as discussed previously in this section; and in the presence of MMT due to the presence of organic modifiers within the MMT **(Figure 5.5 (b))**.

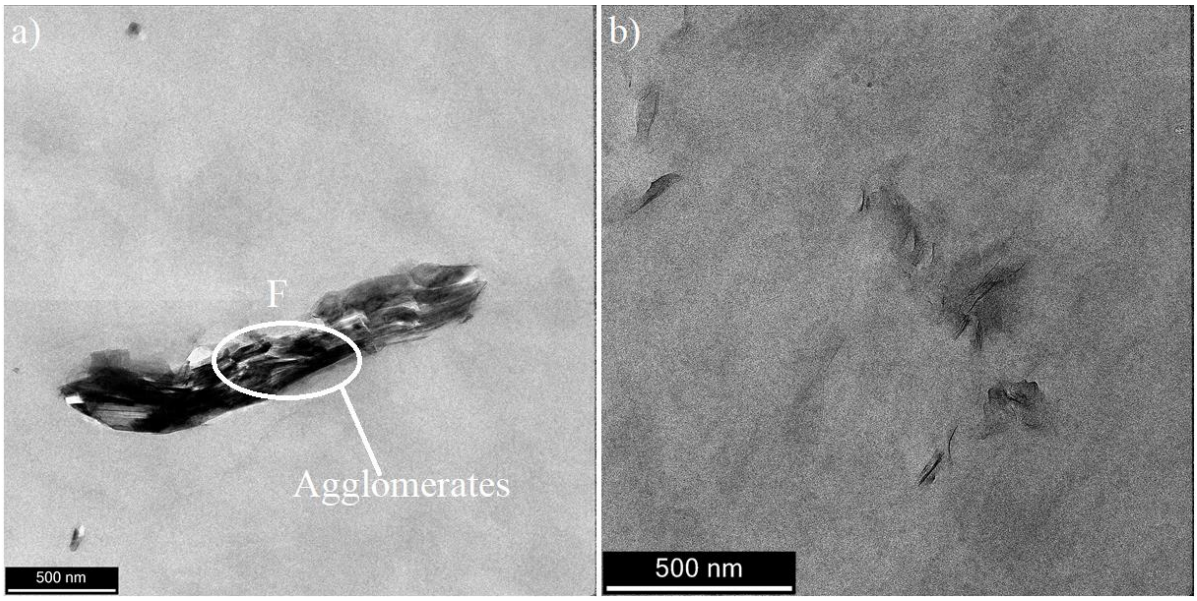

Figure 5.5 TEM images of: a) PLA/kaolin/ZnB, b) PLA/MMT/kaolin

5.2. X-ray crystallography (XRD)

Figure 5.6 depicts the following XRD patterns: (a) Halloysite, (b) Montmorillonite (MMT), (c) Kaolin, and (d) Zinc borate (ZnB). The XRD pattern of the clay in the form of halloysite revealed different diffraction peaks because of the crystalline structure of the halloysite. The reflections at 2θ values of 11.5°, 20.18°, 24.8°, 30.07°, and 65.0° are the characteristics peaks of halloysite, corresponding to the (001), (100), (002), (110), and (300) crystalline planes respectively. Similar results were obtained by Ba *et al* [**3**], and Wu *et al* [**4**]. The fact that there is a peak at 11.5°, which correspond to the (001) is an evidence of the halloysite-7 angstrom. According to **Figure 5.6(b),** MMT shows its characteristic peak at 19.94° which corresponds to 101 [**5**].

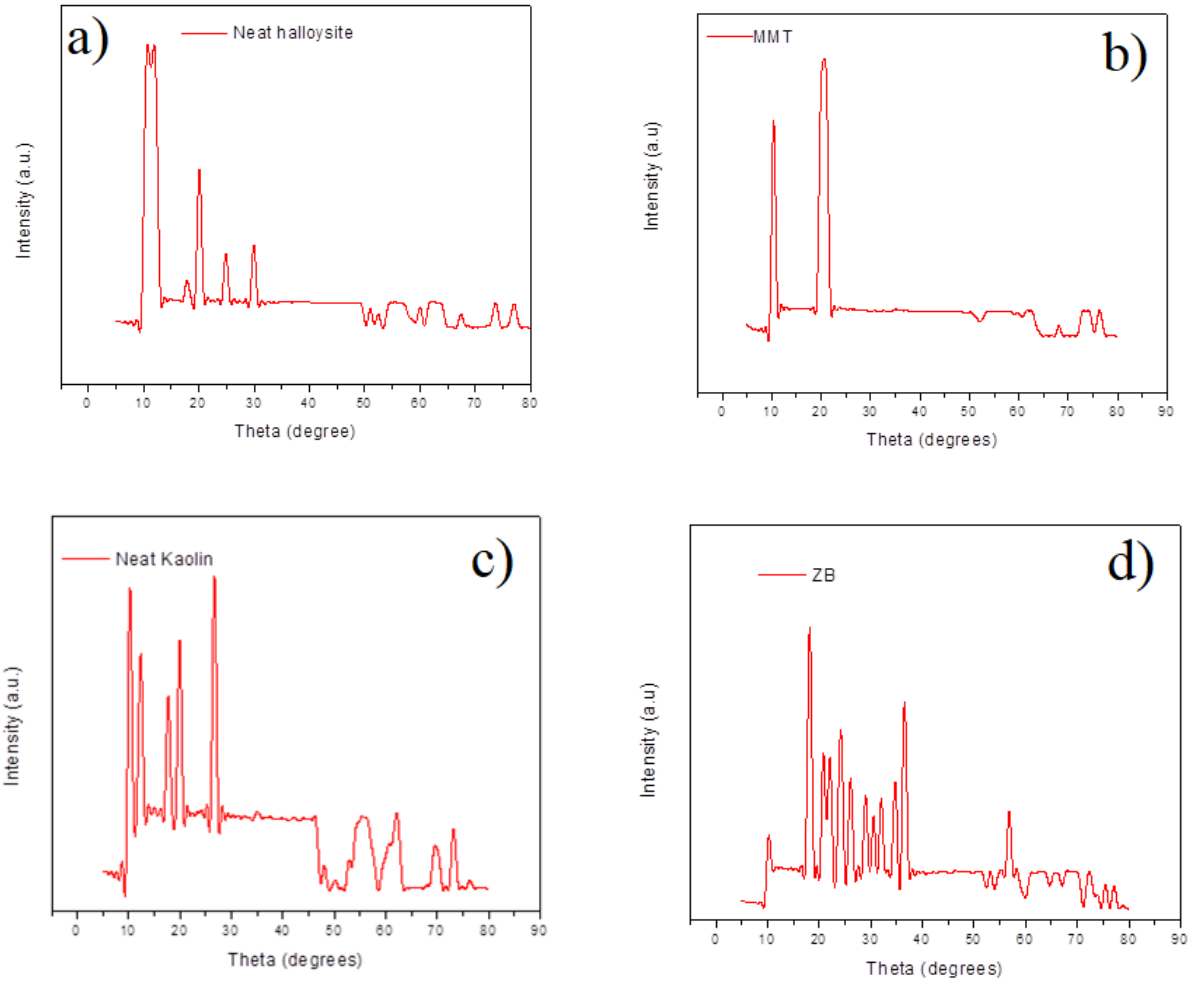

Figure 5.6 XRD patterns of (a) Halloysite, (b) Montmorillonite (MMT), (c) Kaolin, and (d) Zinc borate (ZnB)

The XRD absorption peaks for kaolin are revealed at 2θ (°) i.e. 10.19, 12.25, 18.06, 19.76, 26.68, 34.94, and 37.76 (see **Figure 5.6(c)**) [**6**]. The main characteristic XRD peaks for zinc borate are summarized in **Table 5.1** below with their Miller indexes.

Table 5.1: Characteristic XRD peaks of ZnB and their Miller indexes

Peaks (%)	Plane
18.06	020
20.70	101

21.8	120
24.2	12-1
25.1	210
28.9	012
31.12	22-1
35.7	230

Figure 5.7(a) depicts the XRD pattern for neat PLA, while **Figure 5.7(b)** illustrates the XRD patterns of PLA and its composites. It is important to note that the clays and ZnB were analysed in order to investigate their effect on the crystallinity of biopolymer in the form of PLA. All the samples indicated a broad peak approximately around $2\theta = 15.5\ °$, which denotes the characteristic peak of the PLA [**7**]. According to **Figure 5.7(b),** there is a slight shift in the main peak of the PLA to higher angles in the presence of clays and ZnB. This may be associated with the change in the lattice parameters of PLA, because of the diffusion of the clays, and ZnB into the PLA lattice. Similar behaviour, i.e., shifting; is also observed **in Figures 5.8 and 5.9** with the similar reasoning being the same. In all of the figures, there seems to be a reduction in the peak intensity of PLA in the presence of MMT when compared with neat PLA and other composites. This may be an indication of the suppression of the crystallinity of PLA. The introduction of the MMT in the PLA systems acts as a steric hindrance, and as a result crystallization is restricted causing a reduction in the intact crystalline region [**8**]. Another possible reason could be associated with a good interaction between the MMT-based composites as it was observed by TEM. The strong interaction between MMT and PLA based composites which is associated with strong hydrogen may result in PLA molecules trapping into the MMT nanoparticles which is associated with large specific areas [**9**]. This behaviour in turn might affect the regular planar zigzag structure negatively towards crystallization, and forms more amorphous structure at the interface. Secondly, the reduction in intensity might also be associated with the penetration of the PLA chains into the MMT gallery. The behaviour states that there is an expansion of the clay layers; and therefore, the formation of either exfoliated or intercalated morphology as observed by TEM.

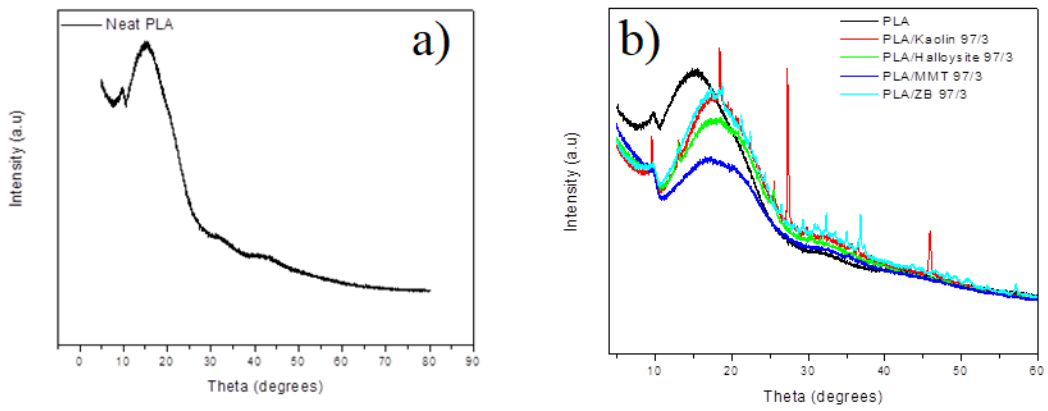

Figure 5.7 Illustration of the XRD pattern for (a) neat PLA, and (b) PLA; and its clay(s) as well as ZnB nanocomposites

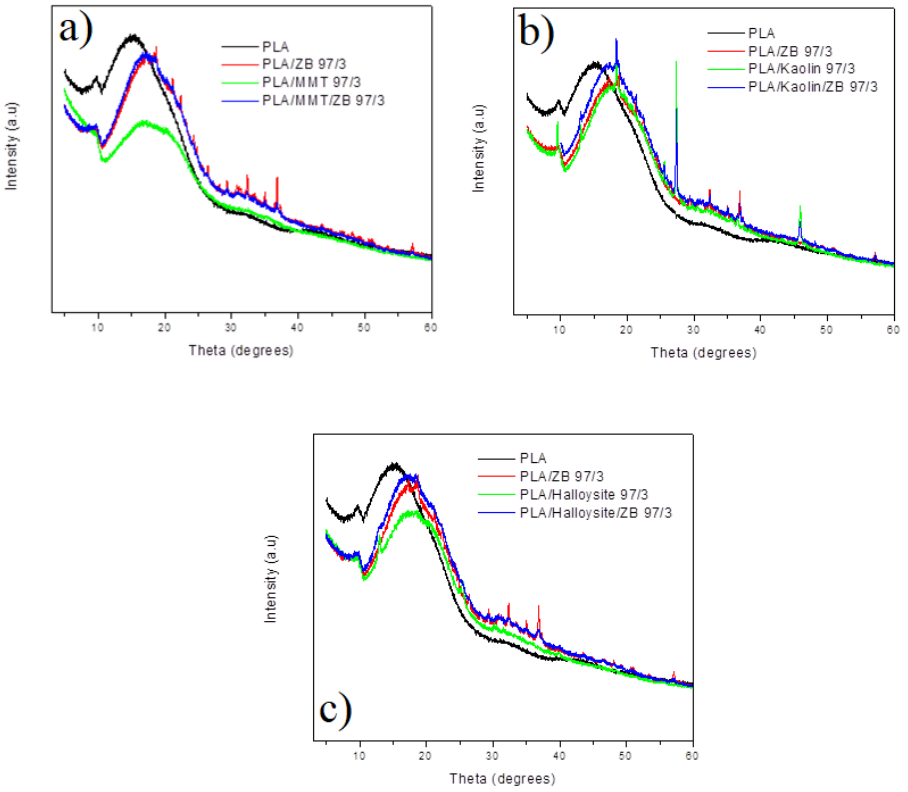

Figure 5.8 Illustration of the XRD patterns for (a) Neat PLA, PLA/ZnB, PLA/MMT, PLA/MMT/ZnB; b) Neat PLA, PLA/ZnB, PLA/kaolin, PLA/kaolin/ZnB; and c) Neat PLA, PLA/ZnB, PLA/Halloysite as well as PLA/Halloysite/ZnB.

Importantly, there seems to be a strong reduction in the PLA main peak intensity of the PLA/MMT/kaolin, which might suggest that the synergy of the two fillers is very strong in the interface with PLA matrix.

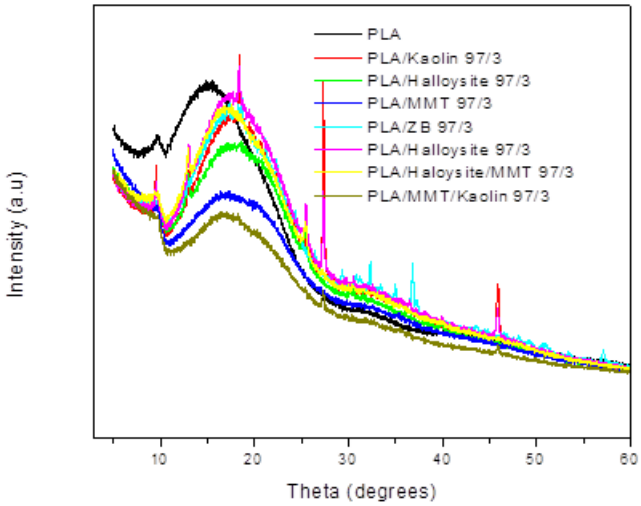

Figure 5.9 XRD pattern of all the investigated samples

5.3 Thermal stability of the investigated composites

Figure 5.10 depicts the TGA curves of the neat zinc borate (ZnB), kaolin, and montmorillonite (MMT). Interestingly, kaolin seems to be thermally stable up to 700 ° C, while MMT shows two step degradation. The degradation of steps for MMT might be associated with the physiosorbed water (below 200 ° C) accompanied by organic component in the MMT, which were utilized for modification of the clay. The second step is associated with the dihydroxylation of the coordinated as well as structural water that occurs around 450 °C and above. It is well known that clay materials have three types of water molecules in their structures **[10]**. Furthermore, MMT shows lower thermal stability when compared with both kaolin and ZnB. This may be associated with the release of the organic components in the MMT clay, which acted as catalysts by enhancing the degradation of the MMT.

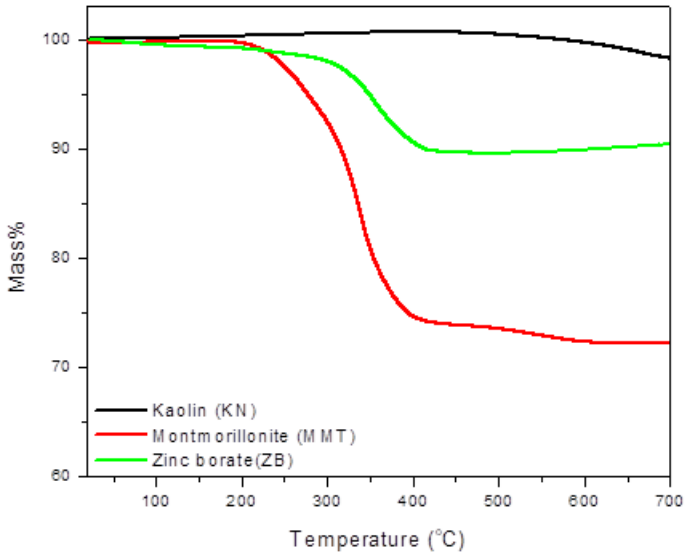

Figure 5.10 TGA curves of kaolin, MMT, and ZnB.

Figures 5.11 (a) and (b) indicate the TGA curves of the PLA, and its composites with clays as well as ZnB. According to **Figure 5.11(a) and (b)**, there is a reduction in the thermal stability of the PLA with the incorporation of the clays (viz kaolin and MMT). For an example, **Table 5.2** ($T_{50\%}$) reveals that there is an approximately a 2% reduction in the thermal stability of PLA with the incorporation of kaolin, while there is a 1% decrease with the addition of MMT. The catalytic behaviour of clays might be associated with the decomposition of the alkylammonium cations modifier, which might have catalyzed the polymer matrix. This process takes place through the replacement of the ammonium linkage on the clay structure with a hydrogen proton because of the β-carbon fracture, which acted as a Brønsted acidic site, and which apparently accelerated the PLA degradation. The halloysite based composites however showed an enhanced thermal stability when compared with the PLA, PLA/kaolin, and PLA/MMT based composites. For an example, at $T_{50\%}$, there is a significant 12% enhancement in thermal stability of the PLA matrix with the addition of 3% halloysite. Furthermore, it is observed that there is 14% enhancement when compared with PLA/kaolin composite, with 13% improvement when compared with PLA/MMT composite at the same clay content of 3%. This behaviour is very interesting due to a low aspect ratio, and specific surface area of the halloysite; as one would expect lower thermal stability contrary to the enhancement observed herein. Another factor that is surprising in terms of higher thermal stability

of the HNTs when compared with the silicate layered clays is that the intercalated layered silicate nanofiller(s) have a better thermal stability than the tubular structure, which contradicts the obtained results whereby the tubular structure showed better thermal stability than the layered silicate clays such as kaolin and MMT. It is deducible in this study that it is possible that several combined factors may play key role in terms of enhanced thermal stability of the halloysite based composites. The tubular structure of the halloysite might have acted as a thermal barrier thereby protecting the substrate in this case PLA from contacting heat and mass transport barrier, which in turn slows down the movement of the volatile's products during the degradation process.

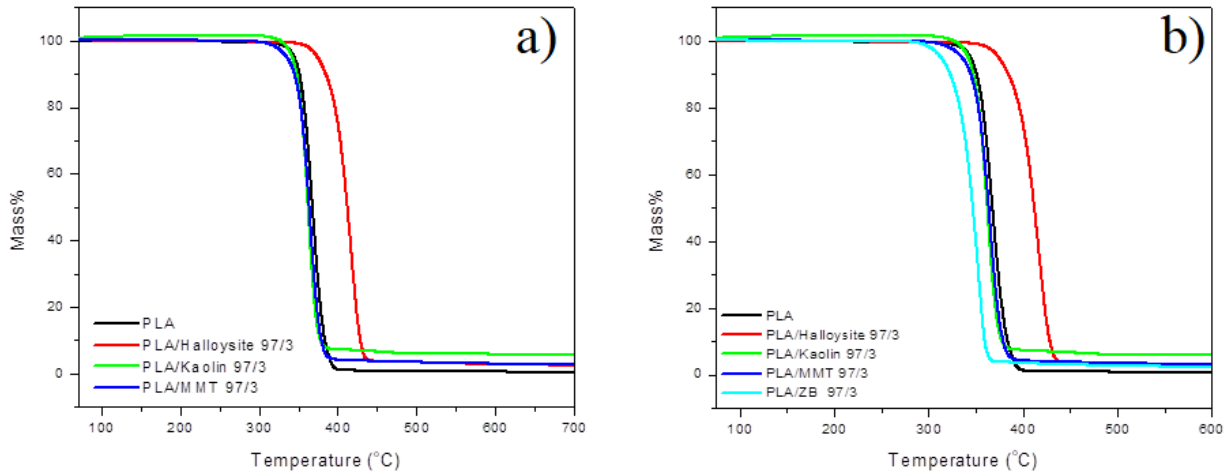

Figure 5.11 PLA and its composites with clays as well as ZnB

The addition of the zinc borate within the PLA matrix showed low thermal stability when compared with all the investigated clays, and PLA in this study. For an example, there was a 7% reduction in the thermal stability of the PLA/ZnB when compared with neat PLA. Furthermore, there was more reductions when compared with Halloysite, as one can observe a 19% reduction. This behaviour of a decrease in thermal stability with the addition of flame-retardant materials is known to be associated with the liberation of water by flame retardant materials; and as a result, a reduction in thermal stability [**11**].

Table 5.2 Degradation temperatures at 50 and 80% mass for all the investigated samples

SAMPLE NAMES	$T_{50\%}$	$T_{80\%}$
PLA	369,84	379,40
PLA/HALLOYSITE	412,85	423,19
PLA/KAOLIN	362,64	370,04
PLA/MMT	364,38	368,08
PLA/ZINC BORATE	345,49	353,79
PLA/MMT/ZINC BORATE	410,12	419,78
PLA/KAOLIN/ZINC BORATE	447,96	455,38
PLA/HALLOYSITE/ZINC BORATE	434,10	443,75
PLA/HALLOYSITE/KAOLIN	473,20	484,52
PLA/MMT/HALLOYSITE	469,50	482,57
PLA/MMT/KAOLIN	478,86	486,27

The synergistic effect of the clays, and ZnB was also reported as depicted by **Figure 5.12** below. One can realize that the synergistic effects of the nanoclays showed better thermal stability than all the single clays reinforced PLA matrix **(Figure 5.12)**. This behaviour is the same for ZnB synergistic composites as all the synergistic composites showed higher thermal stability **(Figure 5.13)**. Generally, the hybrid of fillers can form an effective heat barrier, which is far better than single fillers, and as a result, it can prevent the escape of the volatiles, and the entrance of the heat better than single nanoparticles; and therefore, enhancing the thermal stability more. A careful inspection of **Table 5.2**, **Figure 5.12,** and **5.13** show that the synergy between PLA/MMT/kaolin showed better thermal stability than all samples (*viz.* single clays, and synergy of nanofillers). This behaviour might be associated with a better interaction between kaolin and MMT since both are layered silicate organoclays. Due to their ability to interact better, there is a huge possibility for a formation of an effective heat barrier, which interacted better with the volatiles, and therefore inhibited their decomposition from the molten PLA matrix. Generally, it looks like the dispersion of the clay was very key in terms of improving the thermal stability of the composites. The reason

for such an observation is because the MMT synergies with other clays showed better thermal stability, with the results being well supported by TEM.

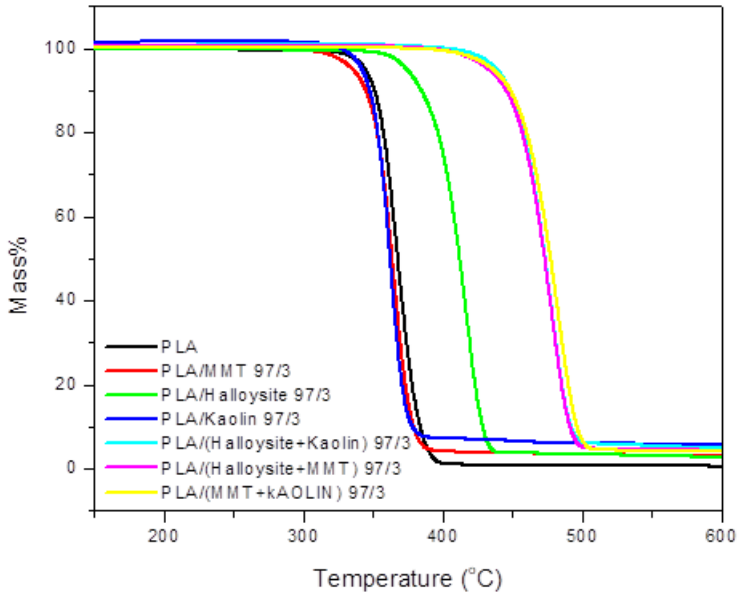

Figure 5.12 TGA curves of the PLA, PLA/ZnB, PLA/clay, and their synergistic composites

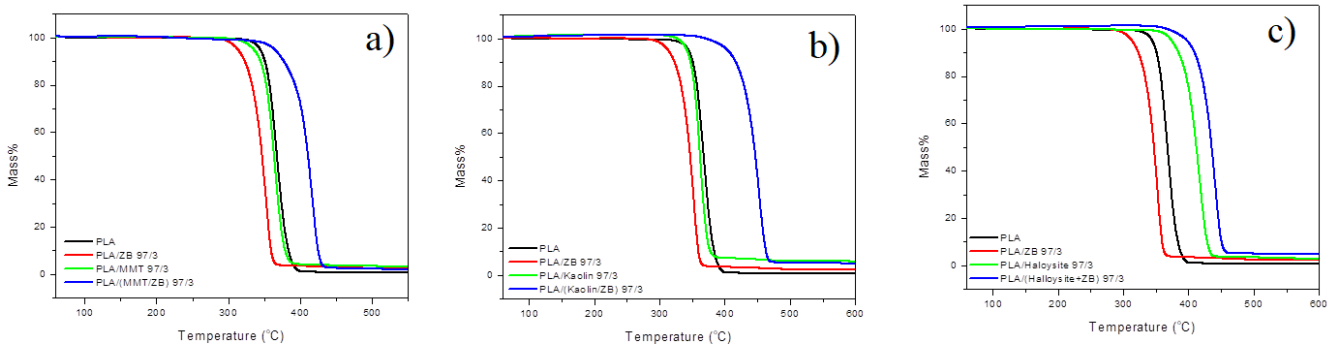

Figure 5.13 TGA curves of the PLA, PLA/clay, and PLA/clay/ZnB composites

5.4 UL-94 Flammability rating

For the purpose of determining how clays affected the flammability properties of polymers, the vertical burning test UL-94 was employed. A specimen is positioned vertically for this test such that the lower end is above a cotton layer (to catch any flaming drip). Flame is administered for 10 seconds to the specimen's bottom, and if it self-extinguishes, another application for 10 seconds is made. According to its performance regarding the individual burning time for each specimen, the aggregate burning time for all specimens, and the presence or absence of burning drips; the material is tested using two sets of five specimens, and it is divided into three categories, namely (V-0, V-1, and V-2) **[12]**. **Table 5.3** classifies the rating in the UL-94 burning test.

Table 5.3 Classification of UL-94 burning test rating

	V-0	**V-1**	**V-2**
Burning time after flame application (s)	≤ 10	≤ 30	≤ 30
Total burning time (s) for flame applications	≤ 50	≤ 250	≤ 250
Burning and afterglow times of specimens after second flame application (s)	≤ 30	≤ 60	≤ 60
Dripping of burning specimens (ignition of cotton batting)	No	No	Yes
Specimens completely burned	No	No	No

PLA was found to have no rating in the UL-94 test, and as a result, it has no flame retardancy classification **[12,13]** (**Table 5.3**). In summary, during the burning test, it seemed as if after applying the flame vertically, the neat PLA did not undergo the self-extinguish, but dripped strongly into the cotton and enhanced ignition, and as a result, failing the test. The addition of the 3% of kaolin clay into the PLA matrix made the PLA to pass a UL -94 V-0 level. Similar outcome was reported by Timochenco *et al.* **[12]** in their results of UL-94 performance of polystryne (PS)

and PS/clay, and it was observed that during the burning of PS/organoclay nanocomposites, a char structure was formed, and no dripping was observed, whereas during the burning of virgin PS specimen, dripping of melted polystyrene in flame was constant. Kouini *et al.* **[13]** also reported similar results, whereby the presence of clay led to an increased in fire retardancy behaviour. In their study, UL-94 was performed for polypropylene/polyamide66 (PP/PA66) system with 2, 4, 5, and 6 wt% of nanoclay. It was observed that the only formulation with 2 wt% of nanoclay (S2) presented an augmentation of the burning rate in relation to unmodified formulation (S0), that is, the burning rate increased (2.4%) with the presence of nanoclay. On contrary, a percentage range from 18.55% to 22.57% decrease was observed when 4, 5, and 6 wt% nanoclay was added, and longer flammability time was noticed with 5 wt% of nanoclay. The addition of 3% MMT made the PLA to achieve a V-2 rating, which showed that there was a limit enhancement in the flame retardancy of the PLA/MMT composite. This behaviour of PLA/MMT is very interesting since one would expect that the layered silicate nature of the montmorillonite (MMT) was expected to enhance the formation of carbonaceous char and the expectations are such that the strong interaction between the decomposing polymer and MMT clay is supposed to have enhanced the surface area, as a result an improvement in flame resistance. This limitation may be explained by the fact that MMT is treated with combustible compounds like octadecylamine and aminopropyltriethoxysilane, which act as catalysts for burning of the PLA matrix. A study by Chow *et al*. **[14]** supported the above behaviour, whereby the unmodified MMT within PLA showed better flame retardancy, and thereby in support of our statement that modified MMT reduces the flame retardancy of the polymers. It is therefore deducible that the modification of the nanoclay plays a role in terms of reducing the flammability resistance of the polymer matrices. Furthermore, the addition of halloysite into the PLA made the PLA to pass a V-0 rating, which emphasized that there was an improvement in the flame retardancy of the PLA/halloysite composite. In the study done by Li *et al.* **[15]**, halloysite nanotubes (HNT) were sequentially grafted with maleic anhydride (MAH), and 9,10-dihydro-9-oxa-10-phosphaphenanthrene-10-oxide (DOPO) to prepare nanohybrid HNT@MAH@DOPO, and incorporate with PLA. The results showed that in parallel, PLA/5HNT@MAH@DOPO possessed limiting oxygen index (LOI) of 38.0%, and passed UL-94 vertical burning rating V-0, a notable enhancement compared to neat PLA (LOI=24.7% and UL-94 V-2). The PLA/ZnB composite revealed a very interesting behaviour in this study, i.e., there was an initial dripping, and then somehow, there was no burning

of the cotton. The above implies that the dripping of the PLA/ZnB is associated with an increase in the melt flow rate which is supported by the rheology results. The results also indicate that even though the sample underwent dripping, the sample did not ignite the cotton due to a better adhesion between MMT, kaolin and halloysite, the PLA/MMT/Halloysite and PLA/MMT/kaolin showed a UL-94 V-0 pass for PLA matrix. Similar results were reported by Zhan *et al.* **[16]** in their investigation of UL-94 and LOI for organophilic montmorillonite (OMT), zinc borate (ZnB), fumed silica (FS), tetraethoxysilane (TEOS), and polytetrafluoroethylene (PTFE) within PLA. The incorporation of the OMT, and ZnB enhanced the LOI values of the IFR PLA composites, while the addition of the TEOS and PTFE reduced the properties. A better interaction between the above systems enhanced the fluidity of the composites, as a result, there is an enhancement in the flame dripping. The synergy between the clay showed an enhanced flame retardancy in the presence of MMT, kaolin and Halloysite. The synergy of halloysite and kaolin showed no sign of dripping and no burning of the cotton, due to a better synergy between the two clays. This may be attributed to the tubular structure of the halloysite and entrapping of the oxygen in the lumen of the halloysite [**17**]. Similarly, with the PLA/Halloysite/Zinc Borate, there was no dripping and burning since the oxygen was entrapped in the lumen of the halloysite, and thereby enhancing the flame retardancy.

Table 5.4 UL-94 rating of Clay/Polymer Nanocomposites

Sample Name	UL-94 Flaming rate	Flame Dripping	Igniting cotton
Neat PLA	NR	Yes	Yes
PLA/kaolin	V0	No	No
PLA/MMT	V2	Yes	Yes
PLA/halloysite	V0	No	No
PLA/zinc borate	V1	Yes	No
PLA/MMT/halloysite	V0	No	No
PLA/MMT/kaolin	V0	No	No
PLA/kaolin/halloysite	V0	Yes	Yes
PLA/kaolin/zinc borate	V1	Yes	No

PLA/halloysite/zinc borate	V0	No	No
PLA/MMT/zinc borate	V1	Yes	Yes

5.5 Rheological properties

Figure 5.14 depicts the complex viscosity vs angular frequency for PLA and PLA-based ZnB composites. The incorporation of the zinc borate reduces the complex viscosity of the PLA matrix. There are several factors that may be associated with the above observation such as the dispersion, particle size, and rigidity of the fillers within the PLA matrix. The main reason for a decrease in complex viscosity in the presence of ZnB incorporated in PLA may be ascribed to a poor dispersion of the filler within the PLA matrix. A poor dispersion of the filler does not hinder the movement of PLA chains, and as a result, it lowers the viscosity within the system. Elsewhere in the literature **[18]**, the authors reported an enhancement in the viscosity of post-consumer polypropylene (PCPP)/organoclay nanocomposite when compared with neat PCPP. The improvement in the viscosity was associated with the strong interactions between the filler, and the polymer matrix. Similar to our results however, there was no enhancement in the composite system consisting of PCPP/Na-clay nanocomposites. The behaviour was associated with poor interaction between the hydrophilic Na-clay and nonpolar PCPP matrix.

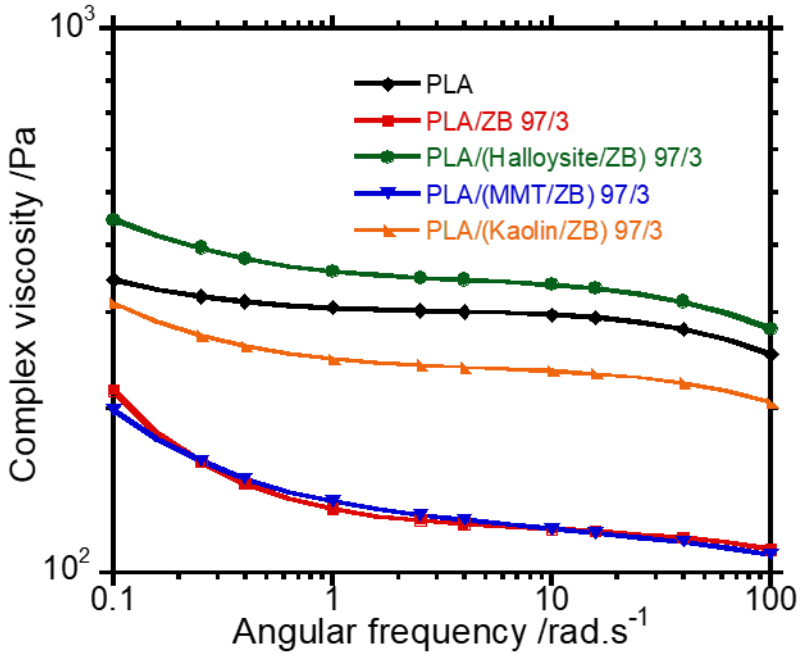

Figure 5.14 The plot of complex viscosity vs angular frequency for PLA, PLA/ZnB, PLA/(Halloysite/ZnB), PLA/(MMT/ZnB) and PLA/(kaolin/ZnB)

The addition of MMT into the PLA/ZnB composites also reduces the complex viscosity when compared with neat PLA and other synergistic composites of ZnB with clays. A lack of better interaction between MMT and ZnB might have played a key role in reducing the complex viscosity due to less hinderance on the PLA chains. In this study however, the presence of the halloysite in the PLA/ZnB system improved the complex viscosity of the system more than all the clays systems and PLA. Generally, halloysite is a stiff material due to its dimensional stable tubular nanostructure, which might have contributed to an increase in the complex viscosity. It seems as if the stiff halloysite might have played a key role in the reduction of the flow part of the PLA matrix. Song *et al*. **[19]** reported similar results, whereby nanocomposites systems consisting of PP/MMT, PP/graphene oxide, and PP/CNTs were investigated. It was reported that all nanocomposites exhibit significantly higher complex viscosities than that of pure PP matrix. The enhancement was attributed to the stiffness of the inorganic filler and better dispersion of the filler within the PP matrix; and as a result, enhancing the viscosity of the system. Moreover, in this current study,

amongst all the clays investigated, halloysite seemed to show better complex viscosity and loss modulus properties, while ZnB seemed to enhance the flexibility in the system; and thereby reducing the complex viscosity. Similar behaviour that was observed in the complex viscosity was also seen in the loss modulus. The PLA/halloysite/ZnB showed better loss modulus properties, followed by the PLA, PLA/kaolin/ZnB, PLA/MMT/ZnB as well as PLA/ZnB (**Figure 5.15**). As expected, halloysite-filled composites reduced flexible component of the PLA; and as a result, enhanced the loss modulus of the system. Meanwhile, the results imply that the poor dispersion of unmodified ZnB within the PLA is responsible for reduced loss modulus in the PLA/ZnB composite. The synergy of the ZnB/MMT therefore provided less modulus due to anti-synergistic behaviour between the two components, agglomeration as well as less interaction between the fillers and organic components in MMT, which might have also contributed to the reduction in loss modulus of the system.

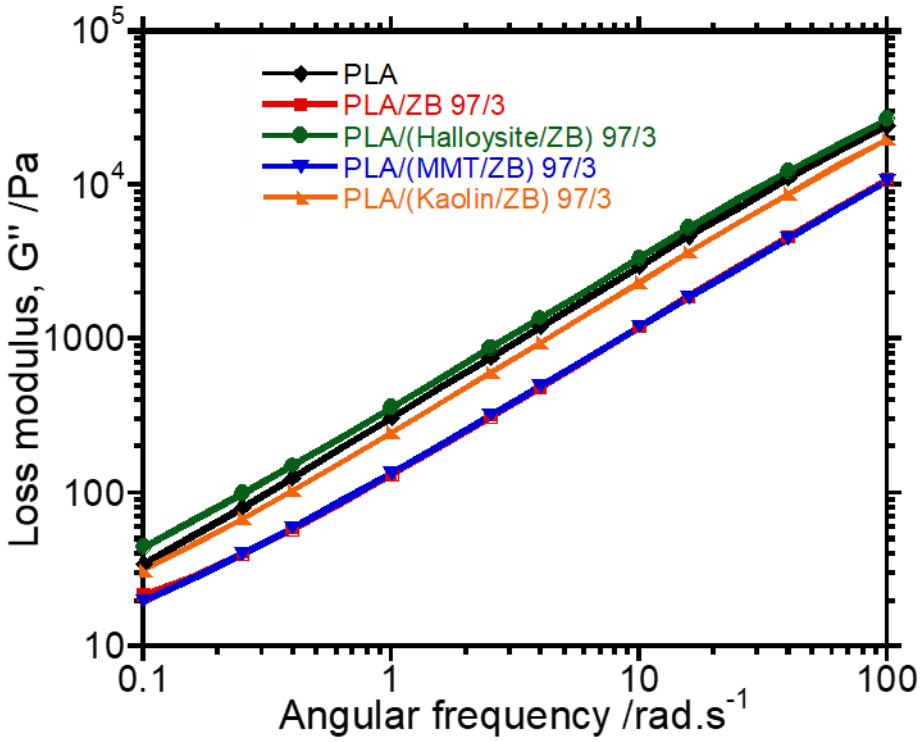

Figure 5.15 The plot of complex viscosity vs angular frequency for PLA, PLA/ZnB, PLA/(Halloysite/ZnB), PLA/(MMT/ZnB) and PLA/(kaolin/ZnB)

5.6 Adsorption studies

In order to evaluate the efficacy of PLA composites as suitable pollutant adsorption, Congo red anionic dye, was used as an organic pollutant model. The adsorption study was carried out by immersing ~50 mg of pelletized PLA composites in a conical flask containing 25 mL of a Congo red solution at 10 mg/L. **Table 5.5** represent the CR removal efficiency of the samples after 12 hours **(Figure A1).** As presented in **Table 5.5**, PLA is PLA/Halloysite and PLA/Halloysite/Kaolin showed no removal of Congo red from the solution, meanwhile other samples exhibited removal of CR below 50%. The limited adsorption efficiency may be attributed to PLA covering the incorporated fillers which are responsible for dye adsorption. PLA is more hydrophobic which limit its interaction with dye **[20]**. The fillers have surface functionalities which serve as active sites for dye adsorption, hence there was limited adsorption showed by these samples. In the case of Halloysite-based composites, PLA had strong interaction with Halloysite which makes these fillers to be well-covered by hydrophobic PLA hence no adsorption has been recorded for these samples. However, the presence of zinc borate improved the overall adsorption efficiency of Halloysite-based composites. This can be explained by segregation of Halloysite and zinc borate within PLA (see **Figure 5.3**). Such morphology offers fillers an opportunity to protrude out to the surface of the host matrix, and hence improves the adsorption efficacy.

Table 5.5 CR Dye adsorption of PLA composites

Sample	**Adsorption (%)**
Neat PLA	0
PLA/Kaolin	22.9 ± 1.9
PLA/MMT	25.9 ± 2.3
PLA/Halloysite	0
PLA/Zinc borate	21.5 ± 2.1
PLA/MMT/Halloysite	0

PLA/MMT/Kaolin	12.3 ± 2.6
PLA/Halloysite/Zinc borate	39.2 ± 3.2
PLA/Halloysite/Zinc borate	24.6 ± 1.3
PLA/MMT/Zinc Borate	16.7 ± 1.6
PLA/Halloysite/Kaolin	0

5.6 References

1. Wang, S., Li, J., Wang, W., Wang, X., Li, H., Sun, J., Fei, B., Gu, X., Zhang, S. **(2020)**. Silicone filled halloysite nanotubes for polypropylene composites: flame retardancy, smoke suppression and mechanical property. *Composites Part A: Applied Science and Manufacturing*,140, 106170(1-27).
2. Zehetmeyer, G., Scheibel, J.M., Soares, R.M.D., Weibel, D.E. **(2013)**. Morphological, optical, and barrier properties of PP/MMT nanocomposites. *Polymer bulletin*, 70(8), 2181–2191.
3. Ba, L.T., Alkurdi, A.Q., Lukács, I.E., Molnár, J., Wongwises, S., Gróf, G., Szilágyi, I.M. **(2020)**. A Novel Experimental Study on the Rheological Properties and Thermal Conductivity of Halloysite Nanofluids. *Nanomaterials*, 10(9), 1834(1-14).
4. Wu, X., Liu, C., Qi, H., Zhang, X., Dai, J., Zhang, Q., Zhang, L., Wu, Y., Peng, X. **(2016)**. Synthesis and adsorption properties of halloysite/carbon nanocomposites and halloysite-derived carbon nanotubes. *Applied Clay Science*, 119, 284-293.
5. Borah, S., Deka, M. **(2021)**. Study of electrical and electrochemical properties of P (VdF-HFP)-MMT based nanocomposite gel polymer electrolytes for application in energy storage devices. *Materials Science and Engineering: B*, 263, 1148229(1-7).
6. Dewi, R., Agusnar, H., Alfian, Z. (**2018**). Characterization of technical kaolin using XRF, SEM, XRD, FTIR and its potentials as industrial raw materials. In *Journal of Physics: Conference Series*, 1116 (4), 0420109(1-6).
7. Vardar, D.S., Senberber, F.T., Kipcak, A.S., Tugrul, N. **(2017).** A green sonochemical synthesis of zinc borates from Zn 5 (CO 3) 2·(OH) 6. *Main Group Chemistry*, 16(2), 163-173.
8. Abareshi, M., Zebarjad, S.M., Goharshadi, E.K. **(2009)**. Crystallinity behavior of MDPE-clay nanocomposites fabricated using ball milling method. *Journal of Composite Materials*, 43(23), 2821-2830.
9. Lee, S.R., Park, H.M., Lim, H., Kang, T., Li, X., Cho, W.J., Ha, C.S. **(2002)**. Microstructure, tensile properties, and biodegradability of aliphatic polyester/clay nanocomposites. *Polymer*, 43(8), 2495-2500.
10. Panda, A. K., Mishra, B. G., Mishra, D. K., Singh, R. K. (2010). Effect of sulphuric acid treatment on the physico-chemical characteristics of kaolin clay. Colloids and Surfaces A: Physicochemical and Engineering Aspects, 363(1-3), 98–104.

11. Mochane, M. J., Luyt, A. S. (2015). Synergistic effect of expanded graphite, diammonium phosphate and Cloisite 15A on flame retardant properties of EVA and EVA/wax phase-change blends. *Journal of Materials Science*, 50(9), 3485–3494.
12. Timochenco, L. (2010). Swelling of organoclays in styrene. Effect on flammability in polystyrene nanocomposites. *eXPRESS Polymer Letters*, 4(8), 500–508.
13. Kouini, B.; Serier, A. **(2017).** Combustion behavior of polypropylene/polyamide66/clay nanocomposites. *Journal of Vinyl and Additive Technology*.23, 68-71.
14. Chow, W.S., Teo, E.L. **(2015)**. Flexible and flame resistant poly(lactic acid)/organomontmorillonite nanocomposites. *Journal of Applied Polymer Science*, 132(2).
15. Li, Z., Fernández-Expósito, D., Jiménez-González, A., Wang, D.-Y. **(2017)**. Natural halloysite nanotube based functionalized nanohybrid assembled via phosphorus-containing slow release method: A highly efficient way to impart flame retardancy to polylactide. *European Polymer Journal*, 93, 458–470.
16. Zhan, J., Wang, L., Hong, N., Hu, W., Wang, J., Song, L., Hu, Y. **(2014)**. Flame-retardant and Anti-dripping Properties of Intumescent Flame-retardant Polylactide with Different Synergists. *Polymer-Plastics Technology and Engineering*, 53(4), 387–394.
17. Cavallaro, G., Lazzara, G., Milioto, S., Palmisano, G., Parisi, F. **(2014)**. Halloysite nanotube with fluorinated lumen: Non-foaming nanocontainer for storage and controlled release of oxygen in aqueous media. *Journal of Colloid and Interface Science*, 417, 66–71.
18. Zdiri, K.; Elamri, A.; Hamdaoui, M.; Harzallah, O.; Khenoussi, N.; Brendlé, J. **(2018)**. Valorization of Post-consumer PP by (Un)modified Tunisian Clay Nanoparticles Incorporation. *Waste and Biomass Valorization*,11, 2285-2296.
19. Song, P.; Yu, Y.; Zhang, T.; Fu, S.; Fang, Z.; Wu, Q. **(2012).** Permeability, Viscoelasticity, and Flammability Performances and Their Relationship to Polymer Nanocomposites. *Industrial & Engineering Chemistry Research*, 51(21), 7255–7263.
20. Schneider, R., Facure, M.H.M., Alvarenga, A.D., Chagas, P.A.M., dos Santos, D.M., Correa, D.S. (**2021**). Dye Adsorption Capacity of MoS2 Nanoflakes Immobilized on Poly(lactic acid) Fibrous Membranes. ACS Applied Nano Materials, 4, 4881-4894.

CHAPTER 6: Conclusion and future recommendations

The effect of various clays (*viz.* MMT, kaolin, and halloysite) together with zinc borate on the properties PLA was reported for advanced application of PLA. Furthermore, the synergy of the clays incorporated into the PLA matrix was also reported in this study. The morphology, crystallinity, thermal stability, rheological and flammability properties are reported in this study. Generally, one can observe that the MMT nanoclay played a key role in improving the morphology of the composites and synergistic composites. The behaviour was associated with the presence of organic modifiers within the MMT-based composites and synergistic composites except in cases where ZnB is involved. The majority of the properties however seemed to have improved in cases where tubular halloysite was involved when compared with the silicate clays. For an example, the flammability properties, thermal stability, and rheological properties were all improved in the presence of halloysite. Generally, the dominance of the halloysite is usually associated with its stiffness and stable tubular nanostructure, which might have contributed to an enhancement in properties. Additionally, the impact of zinc borate can be said to have reduced the flammability of the clay nanocomposites, thus making such instance to be in support of UL-94 results, whereby the majority of the zinc-based samples attained V-1 ratings with dripping in most cases, except when halloysite is employed. For future purposes, especially if one wants to improve the flame resistance of the PLA/clay nanocomposites, it is highly recommended that the carbon-based fillers have to be utilized instead of zinc borate, which failed to form a synergy with clays. The reason for suggesting carbon-based fillers is due to the anticipation that they would form a silicate-carbon based chars, which are well known for preventing heat from entering the substrate and inhibiting the removal of volatiles out of the system. Because the halloysite was found to be more effective in improving the properties, it is suggested that it should be the clay of interest for fabrication of the carbon-based fillers/clay/PLA composites. To further extend the techniques, mechanical properties, and cone calorimetry have to be utilized for future purposes. The pollutants removal efficiency of the composites was very limited due to hydrophobicity of PLA that covered active sites of the incorporated fillers. The change of the processing methods to afford porous materials is recommended to afford the accessibility of the fillers' active sites for pollutants. Further studies should be conducted on the synergy of zinc borate and clays in future.

Appendix

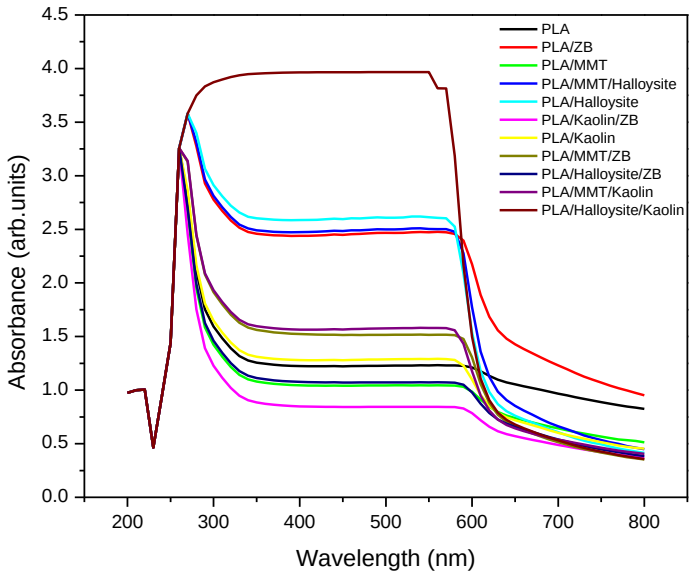

Figure A1 UV-vis of all the investigated samples.